# Assessment of Visual Function and Retinal Histology in a *Snf2h* Knockout Mouse Model

**Skyra Cheng**

Thesis submitted to the University of Ottawa
in partial fulfillment of the requirements for the
MSc. degree in Cellular and Molecular Medicine

Department of Cellular and Molecular Medicine
Faculty of Medicine
University of Ottawa

**ABSTRACT**

Regulation of gene expression is required for embryogenesis and maintenance of the highly specialized and diverse neuron populations of the retina. Chromatin remodelling proteins control gene expression by modifying chromatin structure and are essential for many biological processes including mammalian development. The ATP-dependent chromatin remodelling protein Snf2h is highly expressed in the central nervous system, and pathogenic variants that cause neurodevelopmental abnormalities in the human population have recently been identified. This work aims to characterize the effects of *Snf2h* loss in the retina. *Snf2h* retinal conditional knockout (cKO) mice were generated using *Snf2h*-floxed mice and *Chx10-Cre* retina-specific Cre driver lines to ablate the Snf2h protein from the retina at embryonic day 10.5. Visual function was assessed via optomotor response-based testing and full-field scotopic electroretinography, and histological changes were examined via immunohistochemistry. Disease progression was tracked at one, two, three, and six months of age. *Snf2h* cKO mice showed a significant decline in visual function and exhibited retinal neuron loss compared to wildtype control littermates at all time points assessed. This work shows that the chromatin remodelling protein Snf2h plays an essential role in the structure and function of the retina.

## TABLE OF CONTENTS

## LIST OF TABLES

## LIST OF FIGURES

## ABBREVIATIONS

| | |
|---|---|
| AC | Amacrine cell |
| ACVS | Animal care and veterinary service |
| BC | Bipolar cell |
| bHLH | basic helix-loop-helix |
| bp | base pair |
| BSA | Bovine serum albumin |
| cKO | Conditional knockout |
| DNA | Deoxyribonucleic acid |
| E | Embryonic day |
| ECL | Enhanced chemiluminescence |
| EGFP | Enhanced green fluorescent protein |
| ELM | External limiting membrane |
| ERG | Electroretinography |
| GC | Ganglion cell |
| GCL | Ganglion cell layer |
| GFP | Green fluorescent protein |
| HC | Horizontal cell |
| HRP | Horseradish peroxidase |
| HSS | HAND-SANT-SLIDE |
| IHC | Immunohistochemistry |
| ILM | Inner limiting membrane |
| INL | Inner nuclear layer |

| | |
|---|---|
| IPL | Inner plexiform layer |
| ISWI | Imitation SWItch |
| ISWI-C | ISWI C-terminus |
| ISWI-N | ISWI N-terminus |
| L | Long |
| M | Medium |
| MG | Müller glia |
| NDS | Normal donkey serum |
| NFL | Nerve fiber layer |
| n.s. | Not significant |
| OCT | Optical cutting temperature |
| OKR | Optokinetic response |
| OMR | Optomotor response |
| ONL | Outer nuclear layer |
| OPL | Outer plexiform layer |
| OV | Optic vesicle |
| P | Postnatal day |
| PBS | Phosphate buffered saline |
| PCR | Polymerase chain reaction |
| PI | Protease Inhibitor |
| PRC | Photoreceptor cell |
| RIPA | Radioimmunoprecipitation assay |
| RPC | Retinal progenitor cell |

| | |
|---|---|
| RPE | Retinal pigmented epithelium |
| S | Short |
| SEM | Standard error of the mean |
| Snf2h | Sucrose nonfermenting protein 2 homolog |
| TF | Transcription factor |
| VA | Visual acuity |
| WT | Wildtype |

## ACKNOWLEDGMENTS

I would like to extend my sincerest gratitude towards my supervisor Dr. Catherine Tsilfidis for this opportunity. Thank you very much for your guidance and mentorship throughout the entirety of this project and for making the time I spent in your lab an invaluable experience. You are the best mentor I could have ever hoped to have!

I would also like to warmly thank Dr. Pamela Lagali for her mentorship and advice throughout all aspects of this research project. Your knowledge and commitment to research inspire me and you have been an amazing teacher and friend. Thank you to Adam Baker for technical assistance in the lab, especially with electroretinography.

Thank you to my thesis advisory committee Dr. Pierre Mattar and Dr. David Picketts for their continued feedback and suggestions. Furthermore, I am grateful to all my lab mates and friends I have made throughout this journey. Lastly, thank you to my family for their unwavering support. This research project would not have been possible without the support and encouragement of everyone involved.

# CHAPTER 1. INTRODUCTION

## 1.1. The retina

The retina is the innermost neural tissue layer of the eye and extends anteriorly from the ora serrata, which junctions with the choroid, to the back of the eye (Ledford & Hoffman, 2005; Remington, 2012). Light entering the eye passes through the cornea and lens and is refracted onto the retina where the light signal is converted into a neural impulse through the phototransduction cascade (Remington, 2012). Nerve fibers exit the retina at the optic disc and transmit the electrical signal via the optic nerves to the brain for image processing (Figure 1.1A).

### 1.1.1. Structure of the retina

Structurally, the retina is organized into ten layers consisting of five neuron cell types (photoreceptor cells, bipolar cells, ganglion cells, horizontal cells, and amacrine cells) and three glial cell types (Müller glia, microglial cells, and astrocytes) (Remington, 2012) (Figure 1.1B). The outermost retinal layer is the monocellular retinal pigmented epithelium (RPE) and is derived embryonically from the neural ectoderm along with the rest of the retina. RPE cells contain high amounts of melanin granules that absorb light not absorbed by photoreceptors to prevent interference with image formation (*The Senses*, 2008), as well as peroxisomes that eliminate oxidative stress from free radicals (Brar, 2021; Peters & Schraermeyer, 2001; Remington, 2012). Microvilli extend from the apical surface of RPE cells and associate with the photoreceptor cell layer (Brar, 2021; Remington, 2012).

Photoreceptors cells (PRCs) contain photopigments that absorb light and transmit the signal to the interneurons. Cone and rod cells make up the photoreceptor layer and their cell bodies are found in the outer nuclear layer (ONL). The inner and outer segments of the photoreceptors, which house the organelles and the photopigment containing discs of the photoreceptors,

respectively, are found between the ONL and the RPE. Junctions between Müller glia and photoreceptor cells form the external limiting membrane (ELM), which is found at the junction between the ONL and the inner segments of the photoreceptors (Remington, 2012). Cone nuclei in the ONL are a single layer thick whereas rod layer thickness is dependent on the area of the retina and ranges from approximately 8-10 cell layers thick (Olmsted, 1944; Remington, 2012).

The inner nuclear layer is comprised of horizontal cells, bipolar cells, amacrine cells, and Müller glia. Bipolar cells, named for their morphology (Grünert, 2009), synapse at their dendrites with photoreceptors in the outer plexiform layer (OPL) and at their axons with ganglion cells in the inner plexiform layer (IPL) (Remington, 2012). Ganglion cells (GCs) are the output neurons of the eye and the only retinal neurons to generate action potentials and communicate directly with the brain (Marieb & Hoehn, 2012; *The Senses*, 2008). The unmyelinated axons of GCs form the nerve fiber layer (NFL) and converge at the optic disc. After passing through the lamina cribrosa, they become myelinated and form the optic nerve (Levine, 2011; Remington, 2012). The optic nerve carries electrical impulses to the brain where the majority of these axons terminate at the lateral geniculate nucleus of the thalamus for visual processing (Olmsted, 1944; Remington, 2012; Selhorst et al., 1984).

The phototransduction pathway is tightly regulated through the actions of several other retinal cell types. Horizontal cells (HCs) synapse with each other as well as PRCs and BCs to transmit signals horizontal to the retinal surface (Remington, 2012). These neurons play a role in contrast sensitivity through negative feedback inhibition of PRCs upon light-mediated hyperpolarization of cone photoreceptors (Brar, 2021). Amacrine cells (ACs) are the most diverse type of neurons in the retina and modulate interactions between bipolar cells and ganglion cells (Brar, 2021; Remington, 2012).

**A**

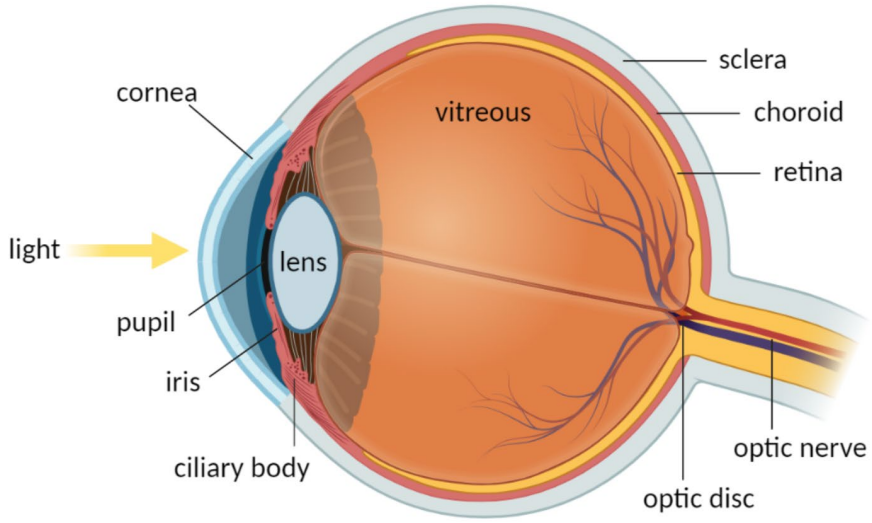
cornea
vitreous
sclera
choroid
retina
light
lens
pupil
iris
ciliary body
optic nerve
optic disc

**B**

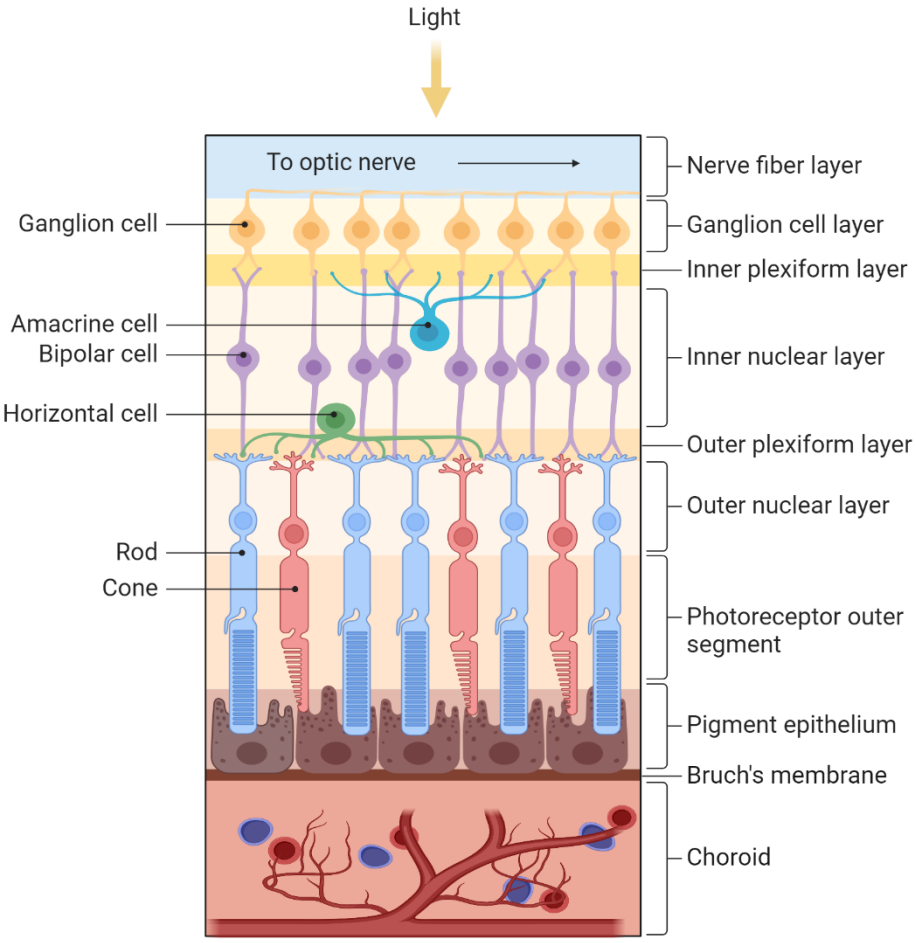
Light
To optic nerve
Nerve fiber layer
Ganglion cell
Ganglion cell layer
Inner plexiform layer
Amacrine cell
Bipolar cell
Inner nuclear layer
Horizontal cell
Outer plexiform layer
Outer nuclear layer
Rod
Cone
Photoreceptor outer segment
Pigment epithelium
Bruch's membrane
Choroid

**Figure 1.1. Anatomy of the eye and retina.** (A) Light passes through the cornea, pupil and lens and is focused onto the retina. The phototransduction pathway initiates at the retina where neurons transform the light signal into an electrical signal. (B) The retina is comprised of neurons and glia cells, which are structurally organized into ten distinct layers. The retinal pigmented epithelium lies posterior to the photoreceptor cell layer. Retinal cell bodies reside in the three neuron layers: cone and rod photoreceptors are located in the outer nuclear layer (ONL), bipolar cells, amacrine cells, and horizontal cells are located in the inner nuclear layer (INL), and ganglion cells are located in the ganglion cell layer (GCL). Neuron synapses form at the outer plexiform layer (OPL) and inner plexiform layer (IPL). Ganglion cell axons form the nerve fiber layer (NFL) and the optic nerve which delivers the signal to the brain. Adapted from "Structure of the Retina", by BioRender.com (2023). Retrieved from https://app.biorender.com/biorender-templates.

The retinal structure is supported by neuroglia cells which do not transmit neural signals but have functions in homeostasis and metabolism of retinal neurons, as well as tissue injury and infection (Reichenbach & Bringmann, 2020; Remington, 2012). Microglia, the resident innate immune cells of the retina, are activated upon homeostatic imbalance to initiate inflammation and mediate the immune response (Brar, 2021; Okunuki et al., 2019). Astrocytes contribute to retinal vascular development and form sheaths around nerve fibers and retinal capillaries (Olmsted, 1944; Reichenbach & Bringmann, 2020). Müller glia cells span almost the entire retina from the photoreceptor layer to the inner limiting membrane, the innermost layer of the retina, where the end-feet processes of these cells terminate (Brar, 2021, p. 2; Reichenbach & Bringmann, 2020; Remington, 2012). These cells aid in maintenance the blood-retinal barrier (Reichenbach & Bringmann, 2020) and contribute to neuron survival through production of neurotrophic factors (Harada et al., 2005; Reichenbach & Bringmann, 2010; M. Wang et al., 2011). The processes of MG ensheath the synapses of retinal neurons and regulate their activity through neurotransmitter recycling (Reichenbach & Bringmann, 2020; Remington, 2012).

### 1.1.2. Photoreceptors

#### 1.1.2.1. Structure of photoreceptors

Photoreceptor cells are functionally conserved across the animal kingdom (*The Senses*, 2008) and initiate the phototransduction signalling cascade in response to light. Photoreceptors are broadly categorized into two types depending on their structure and function: rod and cone cells. Rods and cones are morphologically similar and both consist of an outer segment (OS), inner segment (IS), cell body, and synaptic ending (Remington, 2012) (Figure 1.2).

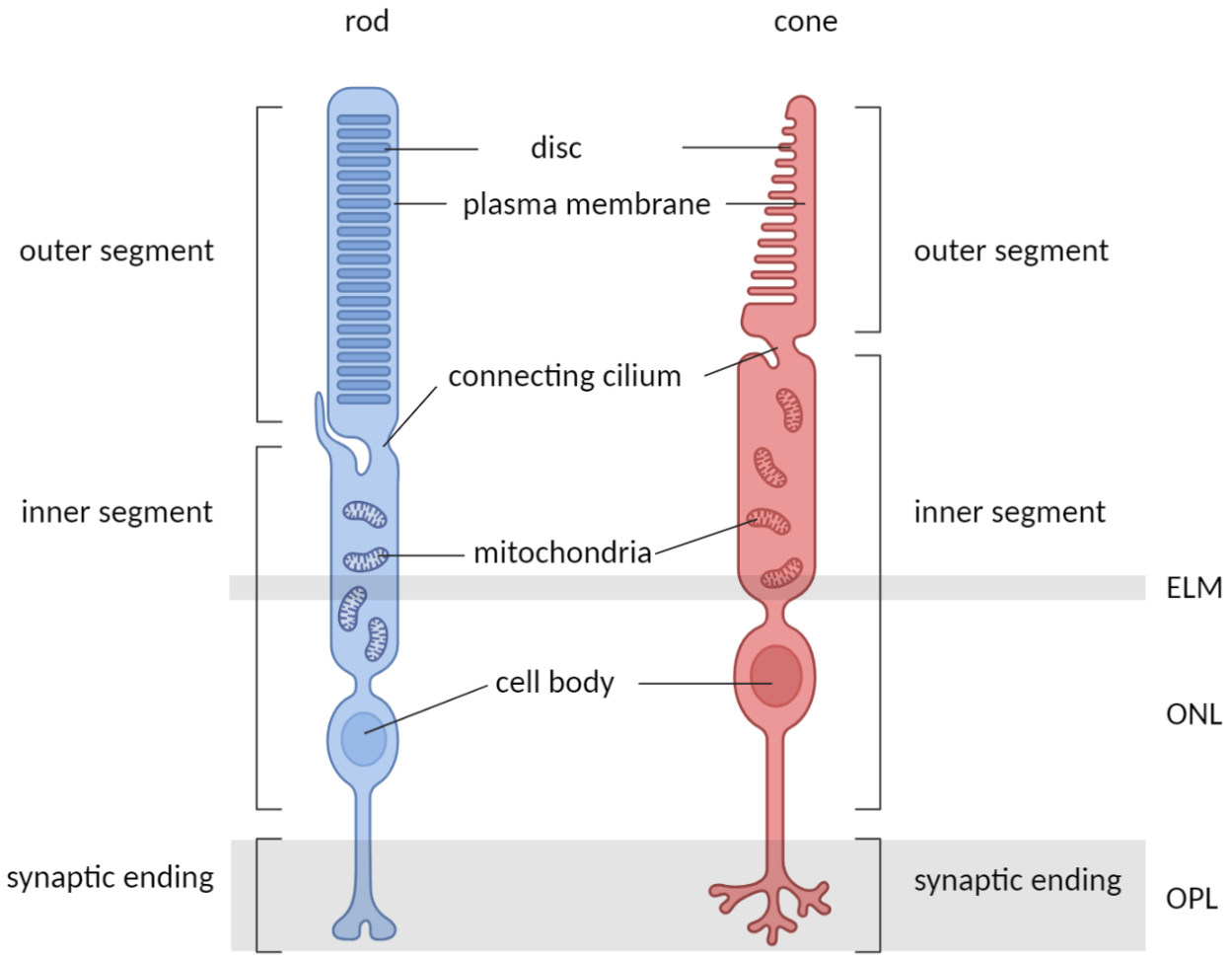


**Figure 1.2. Anatomy of rod and cone photoreceptors.** The outer segment (OS) is comprised of tightly packed discs that contain light-absorbing photopigments in their plasma membrane. Rod OS discs are enclosed within the cell membrane; in contrast, cone OS discs are continuous with the cell membrane. The organelles of the inner segment (IS) synthesize protein and generate energy for biochemical reactions. The synaptic ending transmits the electrical signal. ELM: external limiting membrane, ONL: outer nuclear layer, OPL: outer plexiform layer. Created with BioRender.com.

The naming of rod and cone photoreceptors are derived from their OS cylindrical form and tapered shape, respectively. The OS lies proximal to the RPE and is composed of flattened membranous discs that are stacked on top of each other perpendicular to the long axis. The tight packing of hundreds of discs increases the probability of light absorption as photons transverse the photopigment-rich membranes (Spencer et al., 2020; *The Senses*, 2008). In rod cells, almost all the discs are internalized within the cell membrane whereas in cones, discs are continuous with the cell membrane (*The Senses*, 2008). The membrane of the discs contains photopigments which absorb light. To eliminate photooxidative stress, disc shedding and renewal occurs continuously with a complete turnover rate of approximately ten days (Kocaoglu et al., 2016). New discs are formed in the IS and are shuttled towards the OS tip where they are eventually phagocytosed by RPE cells (Young, 1971; Young & Bok, 1969). This process has been shown to follow a circadian rhythm with peak shedding activity occurring in the morning (LaVail, 1976).

The photoreceptor IS is adjoined to the OS by the cilium, which is structured in a 9+0 axoneme of nine microtubule doublets in a circular arrangement with an absence of a central tubule pair (Wensel et al., 2021). The IS contains the organelles and is the site of protein synthesis. The hyperreflective ellipsoid zone immediately continuous to the cilium is abundant in mitochondria that provide the ATP required to meet the high metabolic demand of photoreceptor functioning (Hoang et al., 2002).

Several mechanisms govern the homeostasis and survival of photoreceptor cells including actions of the RPE cells (Hanna et al., 2022; Stone et al., 1999). In addition to OS disc phagocytosis, RPE cells transport metabolic substrates through diffusion from the choroid vasculature to the photoreceptor cells (*The Senses*, 2008). The tight junctions between RPE cells maintain the blood-retina barrier and selectively filter passage of nutrients and removal of waste

products (Naylor et al., 2019). Loss or dysfunction of RPE cells has been shown to result in rapid subsequent death of photoreceptors (Cideciyan et al., 2004). Additionally, photoreceptor autophagy is essential for mediating cell death and survival; cellular constituents targeted for degradation via lysosomes are recycled for cytoplasmic turnover and regeneration of cellular components[26,27].

#### 1.1.2.2. Rod and cone physiology

The physiological process by which light signals are converted into electrical signals that are then transmitted as nerve impulses is known as phototransduction. Rods and cones are photosensitive and are adapted to function at different light intensities and wavelengths based on their containing photopigment.

The rhodopsin photopigment of rod cells absorb optimally at 500 nm. Rods are active in scotopic conditions and are extremely sensitive up to a single photon (Rieke & Baylor, 1998) but are completely bleached at high light intensities (Cassin, 1995). Dark-adaptation under low lighting levels where rod function is dominant allows for object detection although hue discrimination is diminished (Levin et al., 2011). In contrast, cones are active in photopic conditions and play a role in color and motion detection due to their increased kinetic response (*The Senses*, 2008). There are three types of cones found in the human retina, which are named based on the optimal absorption wavelength of their photopigment: long (L) or red opsin (588 nm), medium (M) or green opsin (531 nm), and short (S) or blue opsin (420-nm) (Remington, 2012).

### 1.1.3. Development of the mouse retina

Upon implantation of the mouse embryo at embryonic (E) day 6.5, gastrulation of the blastula results in the formation of the embryonic plate consisting of the ectoderm, mesoderm, and endoderm primary germ layers (Rossant & Tam, 2002). Subsequent thickening of the ectoderm

gives rise to the neural plate, which invaginates to form the neural tube and neural crest (Gilbert, 2000). Development of the eye begins at E8 at which time two indentations known as the optic pits of the neural tube in the forebrain region form (Heavner & Pevny, 2012; Smith et al., 2001). Expansion of the optic pits results in formation of the optic vesicles (OV), which expand until contact with the surface ectoderm is established at E9 to E10 (Heavner & Pevny, 2012; Pei & Rhodin, 1970; Remington, 2012; Smith et al., 2001) (Fig 1.3). Cells of the OV are comprised of retinal progenitor cells that ultimately give rise to all retinal neurons (Heavner & Pevny, 2012). Invagination of the OV results in the formation of a bilayered cup with the inner layer developing to form the neural retina and the outer layer forming the RPE (Heavner & Pevny, 2012). The optic stalk connects the OV and the forebrain to generate the optic stalk towards which ganglion cell axons eventually grow to form the optic nerve (Deiner et al., 1997; Smith et al., 2001).

Multipotent progenitor cells possess the competency to generate various cell lineages under the effects of regulatory mechanisms. Differentiation of retinal progenitor cells (RPCs) of the retinal neuroepithelium gives rise to all retinal neuron types and Müller glia, and is dependent on the spatiotemporal expression patterns of specific transcription factors (TFs). Numerous studies have shown that dysregulation of TFs in mutant mice result in significant changes in retinal structure and distribution of neuronal populations (Badea & Nathans, 2011; Bramblett et al., 2004; Jiang et al., 2013; S. W. Wang et al., 2000). RPC differentiation occurs in a specific order that is highly conserved among vertebrates (Ohsawa & Kageyama, 2008; X. Zhang et al., 2011) with temporal overlap between cell types such that multiple neuron populations may be simultaneously produced (Ohsawa & Kageyama, 2008) (Figure 1.3A). The following description highlights select key TFs involved in RPC fate specification but should not be taken as an exhaustive list.

**A**

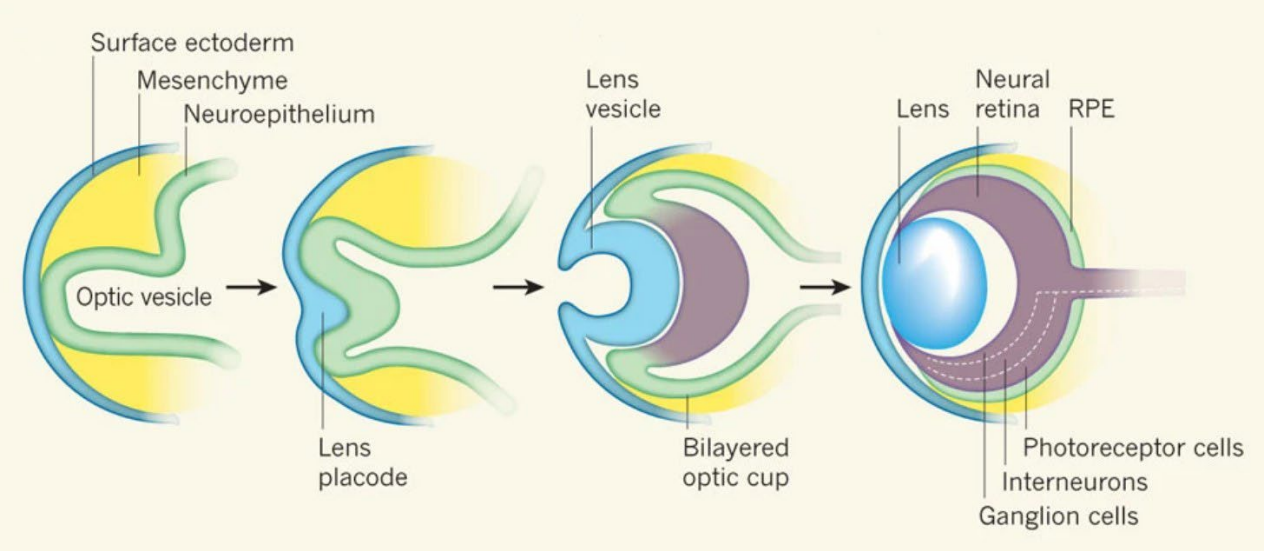


**B**

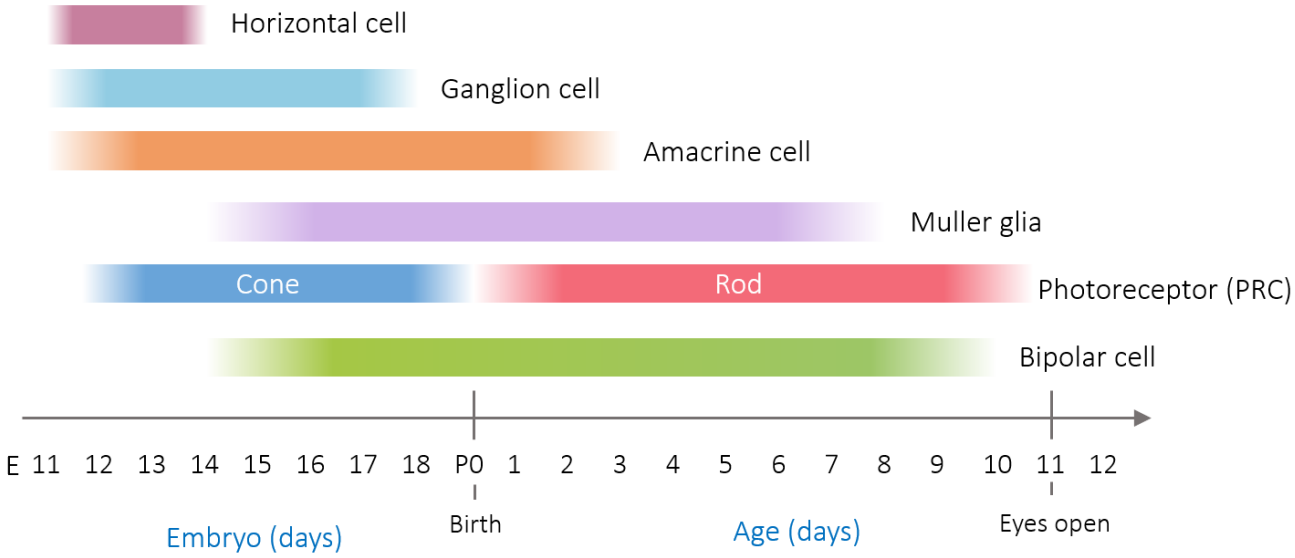


**Figure 1.3. Development of the mouse eye and retina. (**A) The optic vesicle invaginates to form the bilayered optic cup, which then develops to form the neural retina and retinal pigment epithelium (RPE). Reproduced with permission from Springer Nature from Nature, Vol 472, Robin R Ali, Jane C Sowden, DIY eye, Page 43, Copyright 2011. **(**B) Cell differentiation in the retina. All retinal neurons differentiate from a common pool of retinal progenitor cells (RPCs). Cell fate specification begins embryonically and continues postnatally.

Early neurogenesis requires the expression of basic helix-loop-helix (bHLH) transcription factors (Pennesi et al., 2006; Rossant & Tam, 2002; Yan et al., 2005), which have roles in cross-regulation, neuronal subtype specification, and Notch signalling (X. Zhang et al., 2011). Retinal ganglion cells (GCs) are the first cells to be differentiated beginning at around E10.5 and require the transient expression of the bHLH Math5 and its downstream target Brn3b (N. L. Brown et al., 2001; S. W. Wang et al., 2001). Up to 40 subtypes of GCs have been identified with many sharing initial signalling pathways prior to specification by distinct TFs (Ge et al., 2023; Rheaume et al., 2018). GC development is followed by RPC differentiation into horizontal cells, amacrine cells, and cone photoreceptors. Horizontal cell and amacrine cell genesis begin at approximately the same time and are both controlled by the expression of Foxn4 (S. Li et al., 2004), Prox1 (Dyer et al., 2003), and Ptf1a (Fujitani et al., 2006); neuron type specification is determined by co-expression of various other TFs (Inoue et al., 2002). Photoreceptor development occurs throughout most of retinal development. Cone photoreceptor development begins at around E12 prior to rod photoreceptor specification and is complete by the time of birth (Brzezinski et al., 2010). Bipolar cells, Müller glia, and rod photoreceptors are the last to be differentiated and continue postnatally (Reese, 2011). The upregulation of the TF Otx2 as proliferative RPCs exit the mitotic cell cycle is essential for photoreceptor development. In contrast to cone cells, rod cell development starts at around E13.5 and continues until postnatal (P) day 7 (Brzezinski et al., 2010). Expression of the TF Nrl is pivotal in rod differentiation through synergistic interactions with Nr2e3 and Crx to control transcription of rhodopsin (Cheng et al., 2004; Mears et al., 2001; Peng et al., 2005). In addition to photoreceptors, Otx2 is also expressed in bipolar cells and fate determination between either cell type is regulated by additional downstream factors including Chx10, Prdm1, and Vsx1. Upregulation of the homeobox gene *Chx10* promotes bipolar cell differentiation through inhibition

of photoreceptor-specific gene expression (Dorval et al., 2005, 2006; Livne-bar et al., 2006), while transcription of *Vsx1* (Chow et al., 2004) and *Prdm1* (Brzezinski et al., 2013, 2010; Katoh et al., 2010) support photoreceptor cell differentiation and inhibit bipolar cell development.

### 1.1.4. Notable difference between the mouse and human retina

The house mouse (*Mus musculus*) is one of the most common animal models used in the study of human biology due to numerous practical considerations including its small size, low cost, fast breeding times, and short lifespan (Vandamme, 2014). Genetically, the protein-coding regions of the mouse genome are 85% homologous to the human genome (Makałowski et al., 1996) and their amenability to genetic manipulation allows for targeted studies on specific genes and modeling of human diseases (Watts, 2007). Research on the mouse visual system has provided valuable insight on the embryonic development of the eye and the mechanisms underlying various retinal degenerative diseases (Chang, 2013; Fletcher et al., 2011). However, notable differences exist between the mouse and human retina that should be taken into consideration when performing experimentation.

The ratio of rods and cone photoreceptors in the retina is dependent on the species with many mammals having a greater proportion of rods (Szél et al., 1996). Both humans and mice are heavily rod-dominant with rods constituting approximately 95% and 97% of photoreceptors, respectively (Chalupa & Williams, 2008; *The Senses*, 2008). However, the distribution of photoreceptors is not constant across regions of the retina. A unique anatomical feature found in several species is the fovea, a posterior region of the retina that is extremely dense in cone photoreceptors and is specialized in high acuity central vision. Among mammals, primates are the only order in which the fovea is present. Mice lack a fovea and instead, cone density across the entire mouse retina is comparable to that of the peripheral retina of primates (Huberman & Niell,

2011; Jeon et al., 1998). This results in an extended visual field of uniform optical focus (Sundin, 2005), which is evolutionarily adapted to the nocturnal prey nature of mice.

Additionally, mice differ from humans in the optimal absorption spectra of their photopigments. Mouse rod photoreceptors have a rhodopsin photopigment while cone photoreceptors express only two photopigments: M-opsin (508 nm) and S-opsin (360nm) (Geng et al., 2011; Nikonov et al., 2006). Notably, S- and M-cone photopigments are commonly co-expressed within the same cone photoreceptor, which increases the detectable spectral sensitivity of these cells. M-opsin is constitutively expressed in all cone photoreceptors although levels within individual cells vary from the dorsal to ventral regions of the retina. In contrast, S-opsin protein levels remain relatively constant in individual photoreceptors but are not expressed in select cones of the far dorsal region (Applebury et al., 2000).

## 1.2. Chromatin

### 1.2.1 Chromatin structure

Packaging of the approximately 3.2 billion base pairs (bp, haploid number) of DNA into a human nucleus with a 10 μm diameter necessitates an efficient and precise method of organization that condenses genetic material while also allowing transcription of genes (T. A. Brown, 2002; Sun et al., 2000). DNA compaction is primarily mediated by histone proteins, which interact with each other and other chromosomal proteins (Wolffe, 2012). Within the nucleus of a eukaryotic cell, nucleosomes form the basic structural unit and consist of 147 bp of DNA wrapped 1.65 turns around an octameric histone core of two subunits each of H2A, H2B, H3, and H4 (Grigoryev, 2012). Linker histones such as histones H1 and H5 bind with DNA to stabilize and link the nucleosomes together (Brockers & Schneider, 2019; Fan & Roberts, 2006; Hergeth & Schneider, 2015) to form higher order structure chromatin. Histone proteins are lysine and arginine rich and

their key role in processes in the nucleus is highlighted by their high degree of conservation (Wolffe, 2012). The basic structures of all four histone core proteins are similar. The C-terminus histone-fold domain consists of three alpha helices through which histone dimerization and histone-DNA binding can occur. The lysine-rich charged N-terminus possesses a crucial structure that interacts with other chromatin-regulating proteins and is often the target of posttranslational modifications (Wolffe, 2012).

The degree of DNA packing within chromatin is correlated with gene expression and may be structurally distinguished into two types. Euchromatin constitutes the majority of the human genome (International Human Genome Sequencing Consortium, 2004) and is defined by its loosely packaged structure. Since this less condensed form of chromatin enables binding of regulatory factors and RNA polymerase, euchromatin is often associated with active gene transcription (Morrison & Thakur, 2021). In contrast, the structure of heterochromatin is more compact, which prevents binding of transcriptional machinery, and gene expression is therefore repressed. This structural state associated with gene silencing is observed in the repetitive DNA sequences of centromere and telomere regions (Achrem et al., 2020), as well as the inactive X chromosome (Barr body) of mammalian female somatic cells (Priyadharscini & Sabarinath, 2013).

### 1.2.2. Chromatin remodelling

Chromatin is not static but rather a highly dynamic structure that interchanges between transcriptionally active and repressed states (Wolffe, 2012). The process of altering the compaction states of chromatin structure allows for precise spatiotemporal regulation of gene expression and is known as chromatin remodelling. Regulation of DNA accessibility to transcriptional binding factors is primarily achieved through two processes (Manelyte et al., 2013). The first is changes in nucleosome conformation through post-translational covalent histone modifications such as

phosphorylation, ubiquitination, and methylation (Strahl & Allis, 2000; Struhl, 1998; Wolffe & Hayes, 1999). Acetylation of specific lysine residues in nucleosome histone tails lowers the protein's positive charge and subsequently decreases their affinity to negatively charged DNA. The weaker nucleosome-DNA interactions results in a less compact structure of DNA and allows for recruitment of effector proteins to chromatin (Struhl, 1998). The second is through a shift in position or removal of nucleosomes from DNA by chromatin remodellers to reveal the underlying sequence and allow binding of transcriptional factors (Becker & Workman, 2013; Gutiérrez et al., 2007). Chromatin remodellers are dependent on ATP and generally perform one of three processes: nucleosome assembly, modification of nucleosomes through exchange of histone variants, and alterations in chromatin accessibility (Clapier et al., 2017). There are several proposed theories on the mechanisms of action underlying catalysis of nucleosome mobilization by chromatin remodelling complexes (Clapier et al., 2017). The two strands of DNA are wrapped around nucleosomes in different lengths and unwinding results in a 10 bp difference. The twist diffusion theory suggests that if the DNA is bound to a core histone protein at a specific region, DNA unwinding from the nucleosome by an action of a remodelling complex creates torsion that could result in DNA sliding. An alternate theory suggests that the bulge created by superhelical stress may mechanically dislocate DNA from the nucleosome surface (Flaus & Owen-Hughes, 2001).

The essential function of chromatin remodelling proteins has been demonstrated in many physiological processes including mammalian development, DNA replication, and epigenetic inheritance. Chromatin remodelling continues to be an extensively studied area of research due to the numerous diseases arising from the dysfunction of chromatin remodellers. Mutations in chromatin remodelling genes may lead to dysregulation of a spectrum of other genes that manifest

in physiological symptoms including neurodegeneration and cancer (Hendrich & Bickmore, 2001). Chromatin remodelling proteins and their associated diseases are extensively documented in existing literary reviews (Cho et al., 2004; Huang et al., 2003; Mirabella et al., 2016). Select notable diseases resulting from dysfunction of chromatin remodelling complexes include ATRX syndrome resulting from mutations in the *ATRX* gene (Gibbons et al., 2008; Wu et al., 2022), and CHARGE syndrome caused by mutations in the *CHD7* gene (Vissers et al., 2004).

### 1.2.3. ISWI family of chromatin remodellers

In humans, there are at least 53 different chromatin remodellers categorized into four families based on the catalytic subunit of the complex: CHD, INO80, SWI/SNF, and ISWI. The diversity of chromatin remodellers allows for a broad range of specialized activities via nucleosome repositioning, which is in part dependent on binding preferences to DNA (Rippe et al., 2007).

The imitation switch (ISWI) enzyme was first discovered for its role in *Drosophila* development from purification studies of embryo extracts (Tsukiyama et al., 1995; Tsukiyama & Wu, 1995). ISWI is evolutionarily conserved and homologous proteins have since been identified in other species such as yeast, mice, and humans (Yadon & Tsukiyama, 2011). The structure of the ISWI protein has been elucidated by imaging techniques including a combination of mass spectrometry, X-ray crystallography, small X-ray scattering, and computational modelling (Grüne et al., 2003; Harrer et al., 2018). The catalytic core of ISWI proteins is composed of several domains with specialized activities. The N-terminus forms the ATPase domain and is involved in DNA interactions. The ISWI C-terminus (ISWI-C) is composed of 12 a-helices that form the HAND-SANT-SLIDE (HSS) domains. These domains are structurally rigid due to tight packing of helices and move in relation to each other (Grüne et al., 2003). The ISWI-C binds to DNA

proximal to nucleosomes, then releases binding and undergoes an ATP-catalyzed conformational change before then binding to the histone H4 in the nucleosome core (Harrer et al., 2018; Klinker et al., 2014). This conformational shift of ISWI plays a role in regulating separation so that nucleosome spacing is consistent independent of nucleosome density (Hota et al., 2013; Lieleg et al., 2015). The HAND domain is named for its four helices arranged in a conformation resembling a hand and is connected to the SANT domain, which has an overall negative charge and appears to be involved in histone tail interaction but not DNA binding (Boyer et al., 2002). In contrast, the SLIDE domain possesses a overall positive charge and is essential for DNA binding (Grüne et al., 2003). It further functions in nucleosome recognition by interacting directly with histone H4 tails at a $R_{17}H_{18}R_{18}$ amino acid sequence (D. F. V. Corona & Tamkun, 2004; Grüne et al., 2003).

ISWI proteins are involved in a variety of roles that include both repressing and activating DNA transcription (Mellor, 2006).. In addition to the control of gene expression, ISWI complexes have also been shown to play a role in DNA replication through the recruitment of transcription factors (Mellor, 2006). During replication, ISWI remodellers utilize histone H3-H4 tetramers and H2A-H2B dimers recruited by histone chaperones to form the nucleosome octamer as well as evenly space nucleosomes apart to form the nucleosome array (Clapier et al., 2017).

### 1.2.4. *Snf2h* and *Snf2l*

The two mammalian ISWI homologues Snf2h (*Smarca5*) and Snf2l (*Smarca1*) share 86% peptide sequence identity (Aihara et al., 1998) and function as the ATPase catalytic domain in multiple chromatin remodelling complexes involved in processes such as transcriptional regulation, maintenance of chromatin structure, development, cell differentiation, and DNA replication and repair (Yadon & Tsukiyama, 2011) (Figure 1.4). The enzymatic units Snf2h and

Snf2l can function independently or can complex with other protein subunits, which confer the complexes with differing properties and functions (Manelyte et al., 2013).

*Snfh2* and *Snf2l* mRNA temporal expression patterns were examined in embryonic and adult mice. Whole embryonic analysis of E9.5-15.5 mice showed transcripts of both genes at all timepoints; *Snf2h* expression decreased slightly over this period whereas *Snf2l* expression increased. Further localization experiments using RNA *in situ* hybridization were conducted to examine tissue-specific expression patterns. Both genes were found to be expressed throughout the embryo during this developmental phase. However, *Snf2h* was expressed at much higher levels in the brain which then decreased postnatally while *Snf2l* levels increased. In adult mice, *Snf2h* expression was detected in all tissues examined (cortex, cerebellum, heart, lung, spleen, kidney, skeletal muscle, uterus, ovary, placenta, testes) with expression levels peaking in the testes. *Snf2l* expression in adult mice was mainly detected in the brain (cortex and cerebellum) and reproductive organs (ovaries, uterus, testes and placenta) (Lazzaro & Picketts, 2001).

Complete knockout of *Snf2h* in mice is embryonic lethal, which demonstrates its essential in embryonic development (Stopka & Skoultchi, 2003). A double heterozygous cross of $Snf2h^{+/-}$ lines showed that *Snf2h* knockout (KO) embryos were observed in E3.5 litters at Mendelian ratios and the size of the decidua was normal at E5.5. However, *Snf2h* KO embryos were absent at E7.5 and approximately a quarter of uterine horn nodules were empty. E3.5 blastocysts isolated from *Snf2h* KO mouse lines and cultured *ex vivo* were initially viable and showed normal inner cell mass and trophectoderm morphology. At 12 h, all blastocysts adhered to the culture dish and were rapidly proliferating. However, the cell cycle of *Snf2h* KO blastocysts began to arrest at 2 days post culture and shortly after, underwent apoptosis at days 3 to 6. This suggests that *Snf2h* is required for embryonic development by promoting cell proliferation and survival. Ablation of

*Snf2h* results in embryos that die post implantation and subsequently undergo fetal resorption (Stopka & Skoultchi, 2003). In contrast, *Snf2l* KO mice are viable but exhibit delayed neurogenesis (Yip et al., 2012). *Snf2l*$^{f/f}$ mice crossed with *GATA1-Cre* mice, which express Cre recombinase activity ubiquitously beginning at E10.5, were born at Mendelian ratios with no difference in body weight between genotypes. *Snf2l* KO mice performed on par with WT mice in behavioral tests and an increased brain size was the only noted phenotype. This was hypothesized to be due to *Snf2l*'s role in neuronal differentiation as dysregulation may have led to loss of proliferation control during development. Overall, these results appear to be consistent with *Snf2h* and *Snf2l* expression patterns during brain development, in which *Snf2h* is predominantly expressed in progenitor cells, while *Snf2l* is predominantly involved in neuron terminal differentiation (Yip et al., 2012).

Recently, pathogenic variants of *SMARCA5* were identified in the human population. Nine different *SMARCA5* heterozygous variants were found across 10 families by exome sequencing; these included one splice-altering variant, one in-frame deletion, and seven missense variants. Eight of these mutations were *de novo* including the in-frame deletion, which was present in two individuals with no family relation, and one missense variant which was also identified in the individual's mother and maternal grandmother. Bioinformatics algorithm software predicted all missense variants to be deleterious; this was confirmed in one individual by Sanger sequencing of fibroblasts which revealed a 52 amino acid in-frame deletion in the helicase ATP-binding domain. Other variants were mapped at or proximal to the ATPase domain, helicase C-terminal, or HSS domain (D. Li et al., 2021). Notably, all variants were mapped to protein locations that were predicted to be non viable upon mutation.

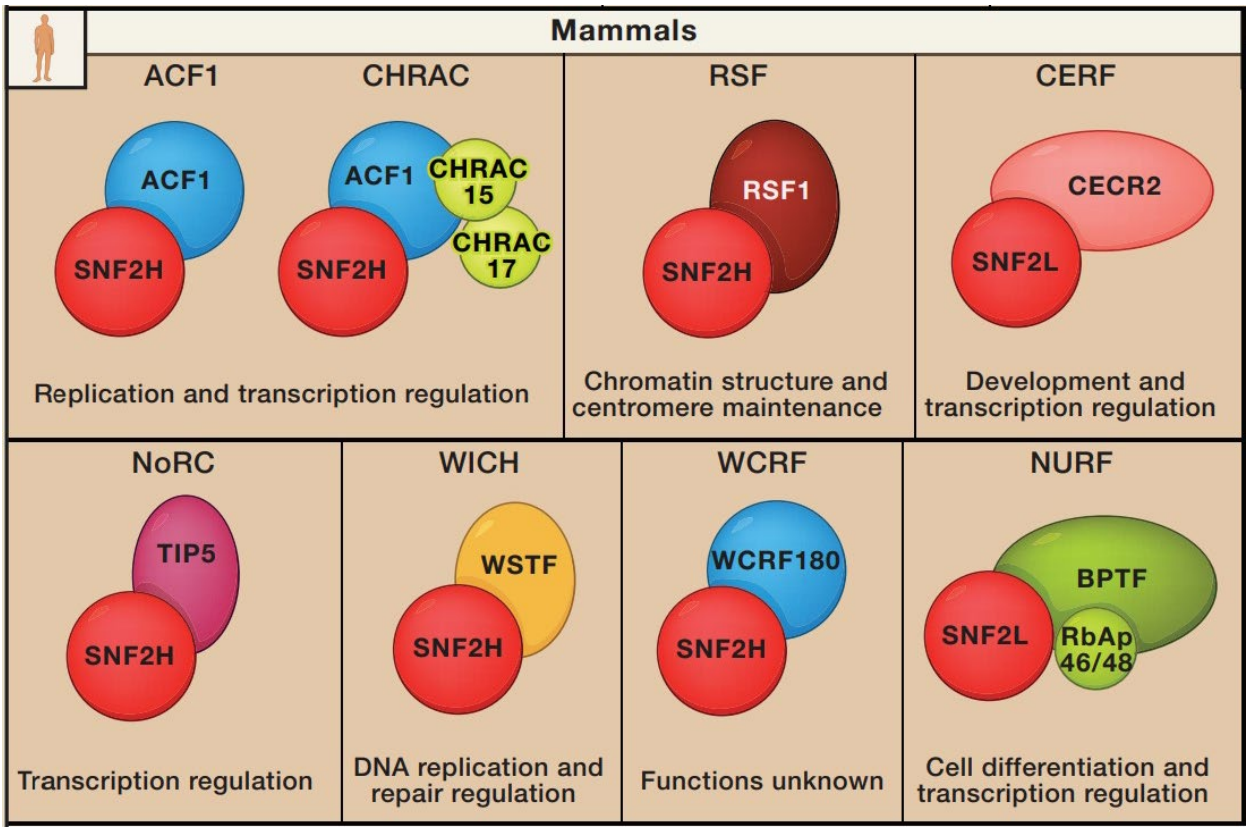


**Figure 1.4. Mammalian ISWI complexes and their physiological functions.** Snf2h and Snf2l act as the ATPase catalytic domains of ISWI complexes. Reprinted from Cell, Vol 144, Adam N. Yadon, Toshio Tsukiyama, SnapShot: Chromatin Remodeling: ISWI, Page 453, Copyright 2011, with permission from Elsevier.

### 1.3. Vision testing

Vision testing is performed to examine the physiological health of the eye and its ability to perceive light from the visible spectrum (Casper & Cioffi, 2019; de-Wit & Wagemans, 2012). This is important not only for direct studies of the visual system but also for animal research where a vision phenotype may be expected. Many commonly employed rodent behavioral tests are in part dependent on visual ability and failure to consider the animals' baseline visual performance may lead to inaccurate conclusions (Leinonen & Tanila, 2018). Screening of 1000 strains at The Jackson Laboratory (JAX) found that 204 strains carried mutations in one of three genes (*Pde6b*, *Crb1*, and *Gnat2*) implicated with retinal diseases (Chang et al., 2013).

Numerous tests have been developed for laboratory use to assess components of the visual system including behavior-based tests, electrophysiological tests and anatomical examination. Factors to consider when selecting a method of assessment include cost, reproducibility between animals, time requirement in order to facilitate testing of large numbers of animals, and ability of the test to provide quantitative results (Pinto & Enroth-Cugell, 2000). Employing a combination of these tests is an effective method for evaluating the relative contribution of different retinal cell types and components of the visual system in causing visual dysfunction (Chalupa & Williams, 2008).

#### 1.3.1. Optomotor response-based testing

The optomotor response (OMR) is an innate head tracking behavior evoked in response to the visual perception of a moving stimulus in order to maintain the focus of a formed image on the retina. This stabilization response prevents dissociation of the vestibular system by visual cues during locomotion (Cullen, 2016; Kretschmer et al., 2015). A normal OMR is comprised of an initial slow tracking phase where the head tracks a moving object followed by a rapid return to its

initial position in the opposing direction (Kretschmer et al., 2017). Related to the OMR is the optokinetic response (OKR) which functions in a similar manner but refers to compensatory eye movements while the head is stationary. These reflexes are conserved among both invertebrates and vertebrates (van der Zouwen & Ryczko, 2020) and emerge during different stages of development depending on the species (Veselov et al., 1998, 1998). In humans, significant developments in communication between the eye muscles and the cerebellum occur after two months of age (Goodkin, 1980) and the OKR response is acquired within the first six months of infancy (Dobson & Teller, 1978). In rodents, development of this behavior varies depending on the strain and is observed in wildtype C57BL/6 mice at P15 once the eyes have opened. Visual performance increases until P24 after which there is no discernable change throughout adulthood (Prusky et al., 2004).

An optomotor response-based test is commonly used in laboratory research to determine visual acuity (VA), a measure of the ability of the eyes to precisely resolve details. VA assessment is a frequently employed standard for monitoring progression of vision loss and treatment outcomes (Kiser et al., 2005) and relies on coordinated function between the optical and neural systems (de-Wit & Wagemans, 2012). As such, abnormal VA values may be indicative of vision

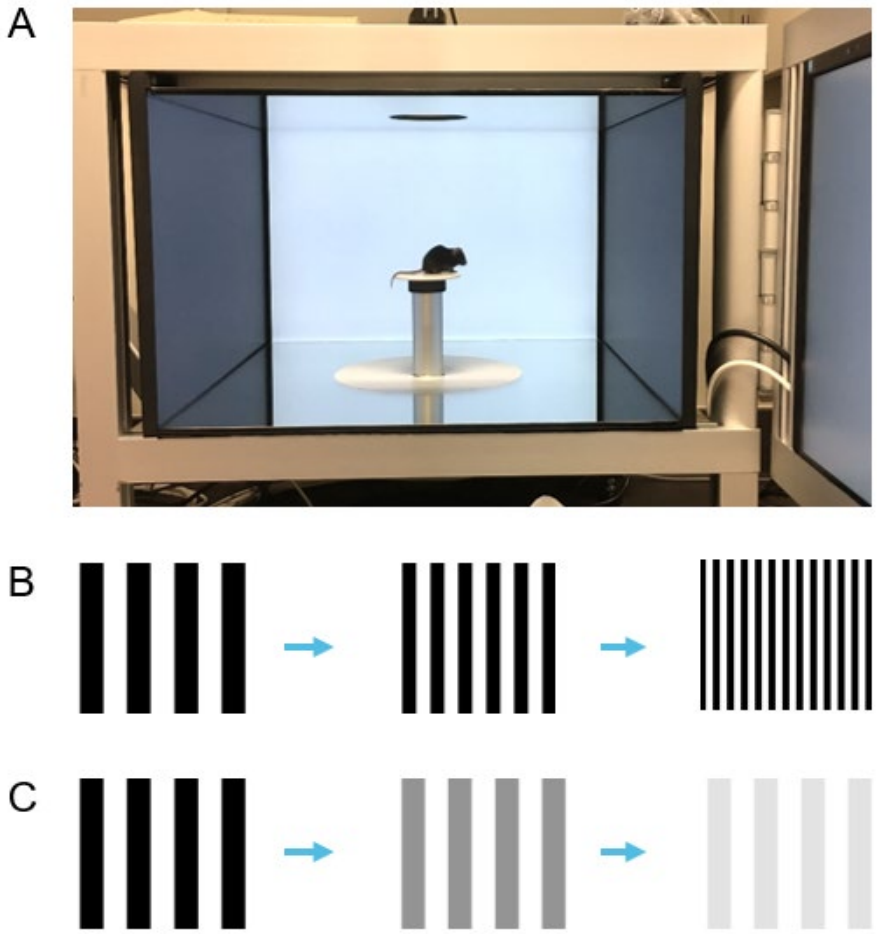


**Figure 1.5. Optomotor response test setup and variations in stimuli testing parameters.** (A) A mouse is placed on the platform of the Striatech OptoDrum system. Variables that may be changed include (B) spatial frequency and (C) contrast.

problems caused by refractive error, retina health, optic nerve transmission of signals, and visual processing in the brain.

Setup of the OMR testing system is achieved by placing the test subject on a raised platform and surrounding it laterally with a display of a vertical striped pattern that rotates horizontally (Figure 1.5). The pattern may be displayed through the use of a mechanical drum or electronical monitors, such as the Striatech Optodrum system used in this thesis (Benkner et al., 2013). A camera situated above the test subject captures its head movement in response to the stimulus and the results are evaluated by the experimenter or an automated software. Parameters which can be tested include stimulus rotation direction, rotation speed, contrast, and stripe colors (Abdeljalil et al., 2005). In cases where bilateral symmetry of eyes is expected, rotation direction may be alternated in order to test eyes simultaneously and to prevent motion habituation (Barnatan et al., 2019; Brandt et al., 1974). To assess the VA, the spatial frequency, inversely proportional to thickness of the stripes, is progressively increased until the no response is observed. For mice, studies have shown that the OMR is optimally elicited at 100% contrast and a rotation speed of 12 $^{o}$/sec.

OMR-based tests boast several advantages including the lack of anesthesia or animal training required prior to data collection as it relies on an innate behavioral reflex. Furthermore, advances in technology have resulted in the development of machine head tracking software and automated scoring of trials to eliminate experimenter bias (Benkner et al., 2013). This non-invasive method of assessment is ideal for longitudinal studies and may act as a first-line screening of function deficits in the visual system.

### 1.3.2. Electroretinography

The electroretinogram (ERG) is another *in vivo* test frequently used as a measure of visual performance and is an assessment of the electrophysiological response of cell types in the retina. There are several types of ERG tests that quantitatively measure different components of the phototransduction pathway. The multifocal ERG displays a hexagonal flickering stimulus that detects focal damage to the inner retina (Hood, 2000) while the pattern ERG presents a checkerboard pattern that assesses ganglion cell activity and is primarily used in studies of optic nerve disorders (Asanad & Karanjia, 2023b). The full-field ERG (ffERG) is a measure of overall retina function and is the technique used in this research project (Asanad & Karanjia, 2023a).

In the ffERG, mice are dark-adapted and the iris is dilated topically. Electrodes positioned on the surface of the cornea present a light stimulus and record the response of the electrical potential generated by retinal neurons (Figure 1.6A). The resulting waveform is displayed as a function of amplitude (μV) over latency (ms) and is comprised of several components. The initial a-wave is measured from the pre-stimulus baseline to the negative a-wave trough and reflects photoreceptor cell function (Figure 1.6B). In the absence of light, photoreceptors remain in a depolarized state. The cell membrane is permeable to $Na^+$ through cGMP-gated channels and the neurotransmitter glutamate is continuously released. Light activation stimulates a signalling cascade that depletes cGMP and prevents permeability of $Na^+$, thereby resulting in the hyperpolarization of the photoreceptors that is detected as the a-wave (Remington, 2012). This is followed by the b-wave, measured from the trough of the a-wave to the peak of the b-wave, and is an assessment of bipolar cell and Müller glia activity (Figure 1.6B). Bipolar cells may be categorized as ON or OFF cells depending on the lighting conditions that trigger a depolarized state. ON cells depolarize with an increase in light intensity while OFF cells depolarize with a

decrease in light intensity (Nelson & Connaughton, 1995). When mice are in the dark-adapted state, glutamate released from photoreceptors binds to the ionotropic receptors of OFF bipolar cells, which maintain a depolarized state of the bipolar cells as they also release glutamate. Upon light-induced hyperpolarization of photoreceptors, the glutamate-gated ion channels of the bipolar cell membrane close and the bipolar cells hyperpolarize giving rise to the b-wave (Remington, 2012). Additionally, wavelets of the oscillatory potentials (OPs) overlap the ascending b-wave and may be graphically separated and quantified (Figure 1.6C). OPs reflect amacrine cell activity, which modulate the phototransduction signal (Asanad & Karanjia, 2023a; Creel, 2019). Changes in any aspect of the various components of the waveform can be used to identify specific cell defects in the visual pathway.

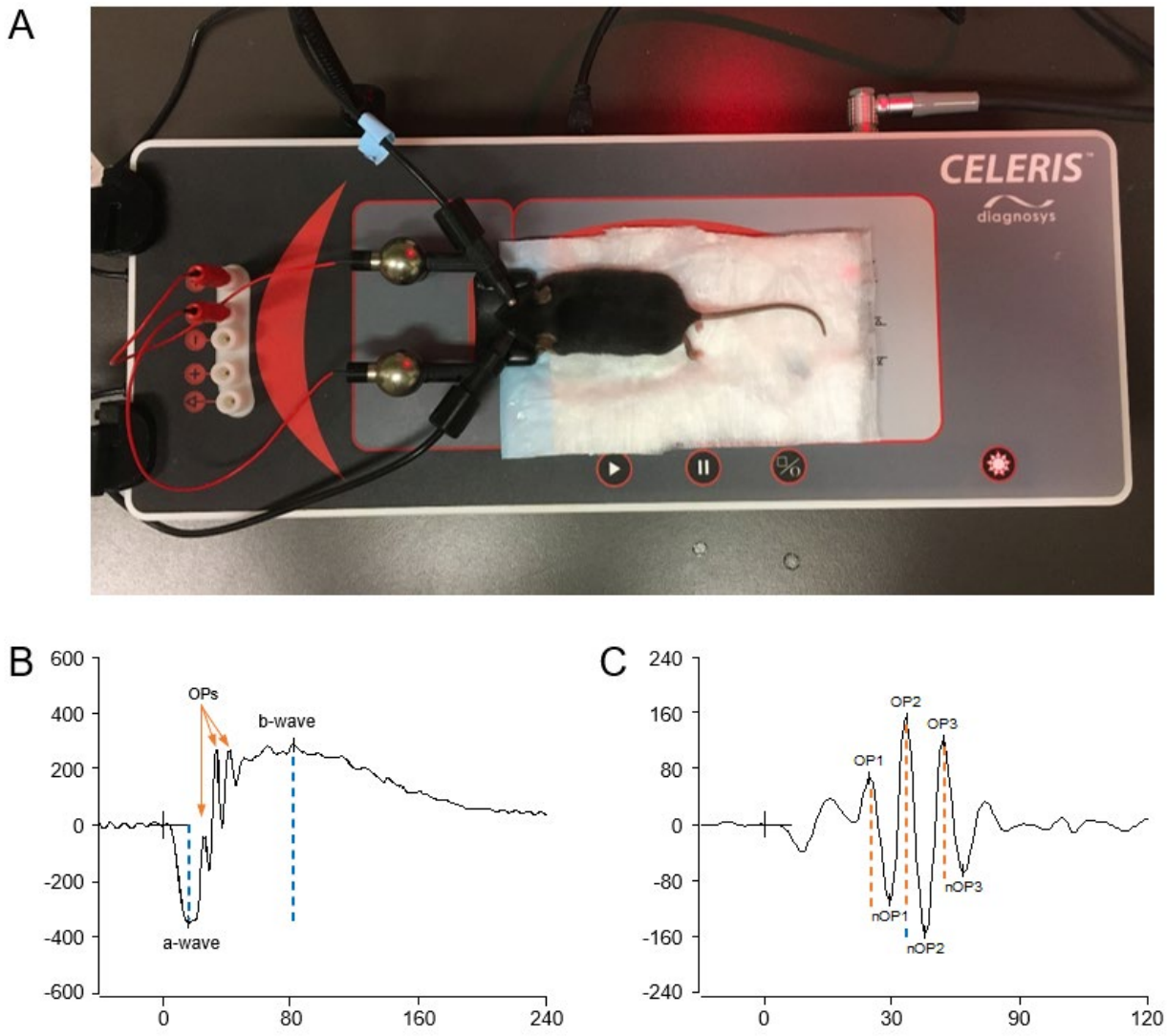


**Figure 1.6. Electroretinography test setup and resulting waveforms.** (A) A wildtype mouse is anaesthetized and electrodes are positioned on the surface of its corneas to elicit a stimulus and record the results using the Diagnosys Celeris system. (B,C) The normal waveform of a wildtype mouse consists of an initial negative deflection (a-wave) followed by a positive deflection (b-wave) during which multiple oscillatory potential (OP) waveforms are also observed.

### 1.4. *Snf2h* cKO mouse model

Since the chromatin remodelling protein Snf2h is expressed ubiquitously in tissues of the mouse embryo and is essential during neurodevelopment, complete knockout of the *Snf2h* gene is embryonic lethal at the peri-implantation stage (Stopka & Skoultchi, 2003). To examine the role of *Snf2h* in the visual system and its effects in maintaining visual function and retinal neurogenesis, a retina-specific conditional knockout mouse model was employed.

The Cre-Lox recombination system is a genetic editing tool used for site specific recombination to implement nucleotide changes at targeted loci of DNA (Figure 1.7). Cre recombinase is a 38 kDa enzyme that recognizes the loxP sequence and catalyzes a recombination reaction. The loxP site is a 34 bp sequence consisting of an 8 bp central spacer sequence flanked by two 13 bp palindromic sequences. The spacer sequence confers orientation to the loxP sequence and to allow for DNA modifications such as insertions, deletions, inversions, and translocations (Nagy, 2000). *Snf2h* retinal cKO mice were generated using the cross of two mouse lines. Mice with LoxP sequences flanking exon 5 of the *Snf2h* gene were bred with mice expressing Cre recombinase under the Chx10 promoter using methods previously described (Alvarez-Saavedra et al., 2014). *Snf2h* exon 5 transcribes the ATPase catalytic domain and its deletion results in complete loss of function (D. F. V. Corona & Tamkun, 2004; Kokavec et al., 2010). Cre expression begins at E10.5 and is localized in progenitor cells of the retina shortly after the start of cell differentiation (details in methods section 2.1).

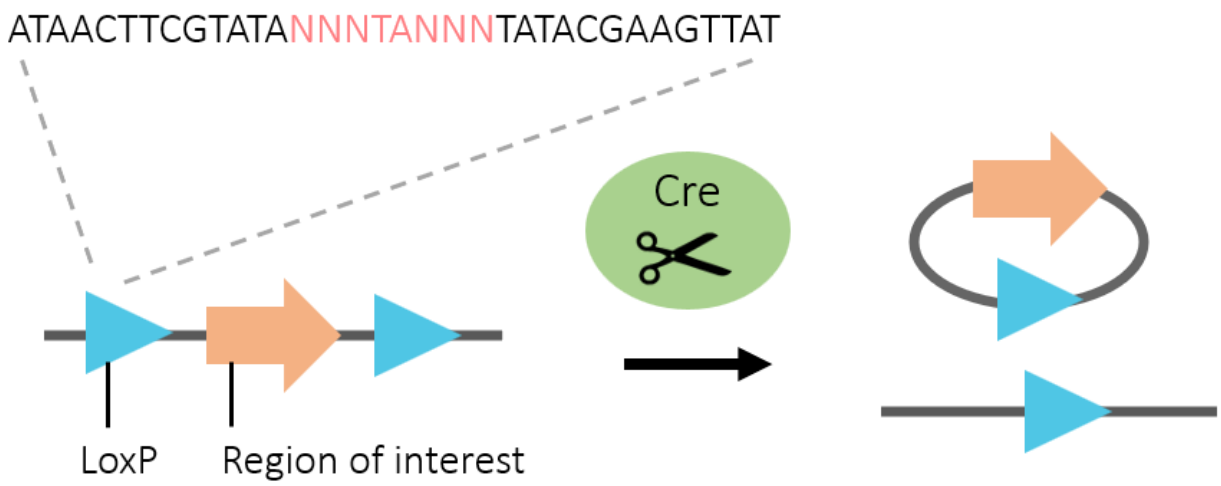


**Figure 1.7. Cre-lox recombination mechanism of action.** Cre recombinase recognizes and excises the region flanked by LoxP sequences, which consist of a spacer sequence (pink) flanked by two palindromic sequences (black).

### 1.5. Rationale, aims, and hypothesis

Mutations in chromatin remodelling genes have been identified in various human diseases. Neurodevelopmental and vision abnormalities were observed in individuals with pathogenic variants of the chromatin remodelling protein Snf2h. Characterizing the morphological and functional changes of a *Snf2h* retinal conditional knockout (cKO) mouse model will provide insights into the role of *Snf2h* in the visual system. We hypothesize that Snf2h loss leads to retinal neuron loss and impaired visual function.

# CHAPTER 2. MATERIALS AND METHODS

## 2.1. Animals

All animal experimental procedures were performed with prior approval from the University of Ottawa Animal Care and Veterinary Service (ACVS). Mice were housed in standard 12-hour light/dark conditions and were fed *ad libitum* on a diet of standard 2018 Tekland Global 18% protein diet and water.

Since *Snf2h* germline knockout mice are embryonic lethal, a retina-specific conditional knockout (cKO) mouse model was generated using *Snf2h* floxed and *Chx10-Cre* mouse lines. Using methods previously described (Alvarez-Saavedra et al., 2014), LoxP sites were introduced to flank exon 5 of the *Snf2h* gene, which encodes the ATP-binding catalytic domain for chromatin remodelling. Deletion of this domain results in complete loss of Snf2h function (D. F. Corona et al., 1999; Kokavec et al., 2010). The retina-specific transgenic *Chx10-Cre* mouse line was generated as previously described (Rowan & Cepko, 2004). Two successive generations of breedings were required to generate *Snf2h* cKO mice. Homozygous *Chx10-Cre*$^{+/+}$ mice were crossed with heterozygous *Snf2h*$^{+/-}$ mice to obtain *Chx10-Cre*$^{+/-}$ ; *Snf2h*$^{+/-}$ mice. The *Chx10-Cre*$^{+/-}$ ; *Snf2h*$^{+/-}$ mice were subsequently crossed with homozygous *Snf2h*$^{f/f}$ mice, which resulted in four possible genotypes (Table 1).

The Cre recombinase expressed in the *Chx10-Cre* mouse line is fused to enhanced green fluorescent protein (EGFP). Furthermore, *Chx10-Cre*$^{+/+}$ mice were crossed with *Ai14*$^{+/+}$ mice to examine functionality of Cre recombinase. *Ai14*$^{+/+}$ mice encode the red fluorescent protein tdTomato at the *Gt(ROSA)26Sor* locus, which is expressed upon Cre-mediated removal of a STOP cassette flanked by loxP sites (Madisen et al., 2010). Therefore, direct fluorescence imaging of *Chx10*$^{+/-}$; *Ai14*$^{+/-}$ retinas is used to investigate both the location of Cre expression by examining

GFP expression and ensure the functionality of Cre-mediated recombination by examining tdTomato expression.

**Table 2.1.** Mouse genotypes and abbreviations

| **Genotype** | **Genotype (abbreviation)** |
|---|---|
| Chx10-Cre$^{-/-}$ ; Snf2h$^{+/f}$ | Wildtype (WT) |
| Chx10-Cre$^{+/-}$ ; Snf2h$^{+/f}$ | Snf2h retinal conditional heterozygote (Snf2h cond. het.) |
| Chx10-Cre$^{-/-}$ ; Snf2h$^{-/f}$ | Snf2h constitutive heterozygote (Snf2h const. het.) |
| Chx10-Cre$^{+/-}$ ; Snf2h$^{-/f}$ | Snf2h retinal conditional knockout (Snf2h cKO) |

## 2.2. Genotyping

Ear clipping biopsies were obtained from mice and genomic DNA was extracted from samples by lysis in 75 µL of 25 nM NaOH, 0.2 mM EDTA for 1 h at 95 ºC followed by subsequent neutralization with 40 mM Tris-HCl, pH 8.0 using the Hot Sodium Hydroxide and Tris (HotSHOT) protocol as previously described (Truett et al., 2000). Genomic DNA was amplified by PCR reaction using Snf2h and Cre primers (Table 2.2) in a thermocycler (Eppendorf Mastercycler Pro S 6325).

Each *Snf2h* and *Chx10-Cre* genotyping reaction consisted of 2.5 µL of 10X PCR buffer (200 mM Tris-HCl, 500 mM KCl, pH 8.4), 2.5 µL of 2.5 mM dNTP, 0.75 µL of 50 mM $MgCl_2$, 0.25 µL of Taq polymerase, 0.5 µL of 10 µM of each primer, and 1.5 µL of extracted DNA (variable concentration) in $dH_2O$ for a total volume of 25 µL. Snf2h PCR amplification cycles were as follows: initial denaturation for 4 min at 94 ºC, followed by 35 cycles each consisting of denaturation for 30 s at 94 ºC, annealing at 30 s for 58 ºC, extension for 1 min at 72 ºC, and a final

extension of 10 min at 72 ºC. Chx10-Cre PCR amplification cycles were as follows: initial denaturation for 2 min at 95 ºC, followed by 35 cycles each consisting of denaturation for 20 s at 95 ºC, annealing at 20 s for 60 ºC, extension for 30 s at 72 ºC, and a final extension of 5 min at 72 ºC.

Agarose gel electrophoresis was performed by loading a mixture of PCR products and gel loading dye on a gel consisting of 1.67 % agarose and 0.15 ng/mL ethidium. The gel was run at 100 µV in 1X TAE buffer (40 mM Tris base, 29 mM acetic acid, 1 mM EDTA disodium salt dihydrate) and visualized on a UV Transilluminator. The *Snf2h* wildtype and knockout alleles resulted in band lengths of 188 and 486 bp respectively (Fig. 2.1). The *Chx10-Cre* allele resulted in a single band, whereas the absence of a band indicated a wildtype allele.

**Table 2.2.** PCR genotyping primer sequences

| **Primer** | **Sequence (5' - 3')** |
|---|---|
| *Snf2h* forward | GATTTCTGATAGGGTTAGAAGC |
| *Snf2h* wildtype reverse | TGTAAGGCAAGGGAGAACTG |
| *Snf2h* knockout reverse | CCTCCTATCCCCTACATATTACCCTAGCC |
| *Cre* forward | ATGCTTCTGTCCGTTTGCCG |
| *Cre* reverse | CCTGTTTTGCACGTTCACCG |

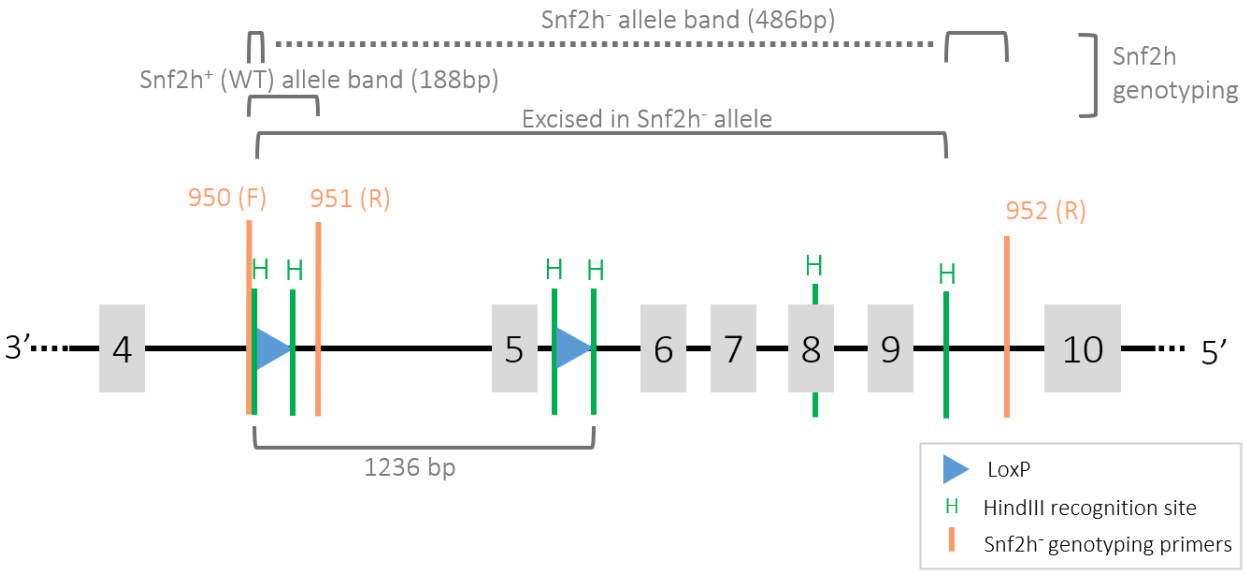


**Figure 2.1. *Snf2h* allele primer binding locations and expected band length results.** Figure not to size.

### 2.3. Optomotor response-based testing

Visual acuity was examined by optomotor response testing using the Striatech OptoDrum system and software. Setup of the OptoDrum consists of a 54 x 54 x 30 cm rectangular prism with mirrors composing the floor and ceiling and four 23.8-inch LCD monitor on the lateral faces of the system. Mice at one, two, three, and six months of age were placed individually in the centre of the OptoDrum system on a 9 cm diameter circular white platform elevated at 14.5 cm. A vertical black and white striped pattern was rotated horizontally on the screens to trigger the innate optomotor response of the mouse. The threshold of spatial frequency was determined by varying the spatial frequency (cycles/degree) at a fixed maximum contrast of 99.72 % and optimal rotation speed of 12 °/sec (Abdeljalil et al., 2005). Stimulus rotation direction was alternated clockwise-counterclockwise. A camera (Matrix Vision Bluefox IGC200w, 752 x 480 pixel resolution, F1.6 focal length) fixed centrally at the ceiling directly above the mouse recorded its response and the OptoDrum software objectively analyzed its behavior by corresponding the angular velocity of the mouse's head rotation to the track quality in response to the stimulus. The mouse was determined to have passed a trial if the spatial frequency displayed triggered the optomotor response and to have failed if insufficient head movement was evoked. Tracking was automatically halted by the software when excessive body movement of the mouse was detected and manually paused by the experimenter when grooming behavior was observed. The threshold of spatial frequency was determined when a mouse had passed a trial once and failed an increased spatial frequency twice. Experimentation was conducted in technical triplicates for each mouse and the values were averaged to determine the visual acuity.

## 2.4 Electroretinography

Electroretinography testing was performed using the Celeris system (Diagnosys) and Espion software (Diagnosys). Mice at one, two, three, and six months of age were dark-adapted overnight and experimentation was conducted in a dark room under 660 nm red light. Mice were anaesthetized by intraperitoneal injection of a mixture of 1 mg/kg medetomidine and 50 mg/kg ketamine. The pupils were dilated by topical administration of 2.5% w/v phenylephrine hydrochloride (Mydfrin) and 1% w/v tropicamide (Mydriacyl) eye drops. The topical analgesic 0.5% proparacaine hydrochloride (Alcaine) was applied to the corneal surface of each eye and eyes were hydrated with 0.3 % hypromellose lubricant eye gel (Systane). Ag/AgCl contact-lens type electrodes were positioned on the surface of both corneas to present the stimulus and record the retinal signals from both eyes. Mice were presented with full-field white single-flash stimuli at five increasing light intensities of 0.01, 0.1, 1.0, 4.0, and 10.0 $cd \cdot s/m^2$. Upon completion of ERG assessment, mice were hydrated with a subcutaneous injection of approximately 1 mL of saline and the anaesthetic was reversed by intraperitoneal injection of 0.5 mg/kg atipamezole. Mice were kept on a 37 $^oC$ heating pad throughout experimentation and recovery to maintain body temperature.

The a-wave peak amplitude was measured relative to the baseline. The b-wave amplitude was measured from the base of the a-wave trough to the maximum positive deflection between 40 and 80 ms post-stimulus. For each light intensity, ERG waveforms were recorded in technical triplicates and the values were averaged to determine the peak amplitudes for each eye; subsequently, the values between both eyes were averaged to calculate a single biological replicate for each mouse.

## 2.5. Histology

### 2.5.1. Retinal whole mount

Mice aged P0 were euthanized by rapid decapitation and eyes were removed from the head. The cornea, lens and retinal pigmented epithelial layer was removed in PBS to isolate the retina. The whole retina was placed on a slide and imaged by fluorescence microscopy to examine EGFP and tdTomato expression at excitation wavelengths of 488 nm and 555 nm, respectively.

### 2.5.1. Retinal tissue collection for immunohistochemistry

Embryonic and P0 aged mice were euthanized by rapid decapitation and the entire head containing intact eyes were fixed in 4% paraformaldehyde for 16 h at 4 ºC. Mice aged P14 and older were euthanized by intraperitoneal injection of sodium pentobarbital at 120mg/kg and manually perfused by transcardiac injection of approximately 10 mL of 4 % paraformaldehyde in PBS, pH 7.4. Mice were decapitated and the corneas and lens were removed from the eyes. The eyecups retained within the surrounding head tissue were fixed in 4 % paraformaldehyde for 30 min at room temperature.

Following fixation, tissues of mice at all ages were washed twice with 1X PBS on a shaker at room temperature for 1 hour each time. The head tissues were immersed in 30% sucrose in PBS overnight and subsequently incubated with a 1:1 solution of 30% sucrose in PBS and OCT overnight. Head tissues were frozen on dry ice in a 1:1 solution of 30% sucrose in PBS and OCT and stored at -80 ºC until sectioning. The tissues were sectioned at 12 µm thickness along the sagittal plane using a cryostat (Leica CM1860) set at -22 ºC and mounted on Superfrost slides (Fisher Scientific). Slides were dried at room temperature for one hour then stored at -80 ºC.

### 2.5.2. Immunohistochemistry

Slides used for retinal immunohistochemistry were thawed at room temperature for 30 min then fixed in 70 % ethanol for 5 min on a shaker. Slides were washed with 1X PBS three times for 10 min each time on a shaker then blocked for 1 h with a solution of 10% normal donkey serum (NDS), 0.1% Triton X-100 in TBLS (1M Tris pH 7.4, 145 mM NaCl, 1% BSA, 62mM L-lysine, 0.1% sodium azide). The blocking solution was removed and slides were incubated with solutions containing primary antibodies (Table 2.3) in 10% NDS, 0.1% Triton X-100 in TBLS overnight at 4 ºC in a humidified chamber. The slides were rinsed with 1X PBS three times for 10 min each time on a shaker and were incubated with solutions containing fluorophore-conjugated secondary antibodies in 0.1 % Triton X-100 in TBLS in the dark for 2 h at room temperature. The slides were washed with 1X PBS three times for 10 min each time on a shaker and incubated in the dark in a solution of 5 µg/ml DAPI in PBS for 20 minutes on a shaker. The slides were rinsed with 1X PBS three times for 10 min each time on a shaker and coverslips were applied along with Fluorescent Mounting Medium (DAKO, Ref# S3023).

Secondary antibodies used were donkey anti-mouse IgG conjugated to Alexa Fluor 488 (Invitrogen, Ref# A21202), donkey anti-mouse IgG conjugated to Alexa Fluor 594 (Invitrogen, Ref# A21203), donkey anti-rabbit IgG conjugated to Alexa Fluor 488 (Invitrogen, Ref# A21206), donkey anti-rabbit IgG conjugated to Alexa Fluor 594 (Invitrogen, Ref# A21207), donkey anti-goat IgG conjugated to Alexa Fluor 488 (Invitrogen, Ref# SA5-10086), and donkey anti-goat IgG conjugated to Alexa Fluor 594 (Invitrogen, Ref# SA5-10088), each at a concentration of 1:1000.

**Table 2.3.** Immunohistochemistry primary antibodies

| Antibody | Dilution | Host | Target | Manufacturer (Reference #) |
|---|---|---|---|---|
| Calbindin | 1:500 | Rabbit | Horizontal cells | Sigma-Aldrich (ABN2192) |
| Cone-Arrestin | 1:300 | Rabbit | Cone photoreceptors | Sigma-Aldrich (AB15282) |
| GFP | 1:1000 | Chicken | GFP | Abcam (ab13970) |
| Otx2 | 1:100 | Goat | Bipolar cells | R&D (AF1979) |
| RBPMS | 1:200 | Rabbit | Ganglion | PhosphoSolutions (1830-RBPMS) |
| Snf2h | 1:200 | Rabbit | Snf2h | Bethyl Laboratories (A301-017A) |
| Sox2 | 1:50 | Goat | Müller glia | R&D (AF2018) |
| Tfap2a (serum) | 1:10 | Mouse | Amacrine | Jackson ImmunoResearch (017-000-121) |

### 2.5.3. Microscopy and histological analysis

All fluorescent images were taken using the Zeiss Axio Imager M2 epifluorescence microscope and AxioVision camera. Excitation wavelengths were at 365 nm for DAPI, 470 nm for AlexaFluor 488, and 590 nm for AlexaFluor 594. Image analysis was performed using the Adobe Photoshop CC 2018 software. Retinal neuron populations were quantified by manually counting fluorescently labelled cells from a 400 μm linear area of central retina for all cell types except for DAPI labelled cells in the outer nuclear layer, which were quantified from a 100 μm linear area of central retina. Cell counts were quantified for both the right and left eyes of two adjacent sections, and the value of the four sections averaged to represent one biological replicate. The number of rod photoreceptor cells were determined by the difference between DAPI stained cells and cone-Arrestin stained cells in the outer nuclear layer.

### 2.6. Statistical analysis

Statistical analysis was performed using GraphPad Prism 8.0.1 using two-wave ANOVA and Bonferroni post-hoc analysis to compare between mice of different genotypes and ages. All data is presented as mean ± standard error of the mean. Significance is defined as a p-value of $<0.05$ and asterisks represent significant values as follows: *$p<0.05$, **$p<0.01$, ***$p<0.001$, ****$p<0.0001$.

## CHAPTER 3: RESULTS

*Snf2h* was knocked out conditionally in the mouse retina using *Snf2h* floxed and *Chx10-Cre* transgenic lines. Using the Chx10 reporter, Cre expression begins at E10.5 and is localized in progenitor cells of the retina shortly after the start of cell differentiation. Snf2h protein expression levels were examined in retina whole mounts by fluorescence imaging and quantified by Western blot. *In vivo* functional testing and histological analysis were performed on *Snf2h* cKO mice to determine the extent of visual dysfunction and changes in retinal pathology. Mice were examined from embryonic stages to adulthood to track disease progression over time.

### 3.1. Cre recombinase expression is mosaic in the mouse retina

To assess the expression levels of Cre recombinase in the *Chx10-Cre* line, *Chx10-Cre*$^{+/+}$ mice were breed with *Ai14*$^{+/+}$ mice to generate double heterozygotes. In *Chx10-Cre* positive mice, Cre recombinase fused with enhanced green fluorescent protein (EGFP) is expressed under the *Chx10* promoter. *Ai14* mice encode the fluorescent protein tdTomato downstream of a STOP cassette flanked by LoxP sites, which is removed by the action of Cre recombination. Fluorescence imaging of EGFP and tdTomato of whole *Chx10-Cre*$^{+/-}$; *Ai14*$^{+/-}$ P0 retinas were used to examine both the Cre expression pattern and to ensure its functionality. Cre recombinase showed mosaic expression even within pups of the same litter (Figure 3.1). EGFP expression corresponded with tdTomato expression indicating functional Cre recombinase expression wherever expressed.

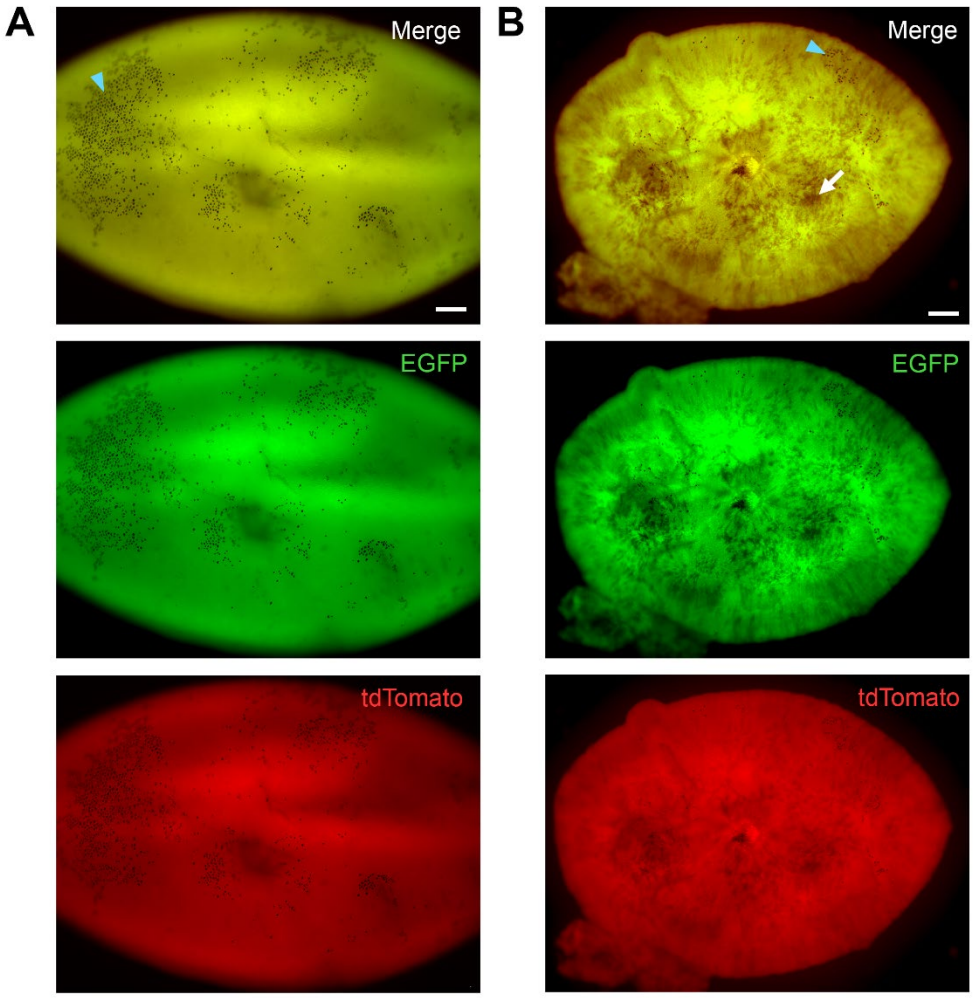


**Figure 3.1. Fluorescence imaging of *Chx10-Cre*$^{+/-}$; *Ai14*$^{+/-}$ P0 retinas.** Cre-EGFP in *Chx10-Cre* positive mice is expressed under the *Chx10* promoter (green). Cre recombinase excises the STOP cassette upstream of tdTomato (red) in *Ai14* positive mice. (A) One mouse shows complete Cre recombinase expression throughout the entire retina. (B) Another mouse shows mosaicism of Cre expression with an area lacking fluorescence indicated by the white arrow. Turquoise arrowhead indicates RPE cells.

### 3.2. *Snf2h* cKO mice show a decline in visual acuity as measured by optomotor response testing

*Snf2h* loss in the retina has the potential to cause visual deficits in mice. Visual function of *Snf2h* cKO mice and their control wildtype and heterozygous littermates were assessed by a succession of *in vivo* tests designed to examine various components of the visual pathway. Testing began in juvenile mice at one month of age shortly after their eyes had opened (around P12) and continued for adult mice until six months of age to examine age-related effects of *Snf2h* loss on visual performance. To determine visual acuity, an optomotor response-based assay was utilized to assess the ability of mice to precisely resolve small details. For all genotypes, the OMR was evoked at lower spatial frequencies, which demonstrated a detectable level of visual function in the *Snf2h* cKO mice (Figure 3.2A). The spatial frequency was progressively increased until mice failed to respond to the stimulus and this was determined as the threshold of observable spatial frequency (Figure 3.2B).

Retinal *Snf2h* deletion was shown to compromise visual performance in mice at all ages assessed. Compared to wildtype mice, *Snf2h* cKO mice displayed a significant decrease in VA at all timepoints assessed with a 9.6% reduction at one month (WT: 0.460±0.006 cyc/deg, cKO: 0.416±0.006, $p<0.0001$), 10.2% reduction at two months (WT: 0.454±0.005 cyc/deg, cKO: 0.408±0.006 cyc/deg, $p<0.0001$), 9.9% reduction at three months (WT: 0.450±0.007 cyc/deg, cKO: 0.405±0.007 cyc/deg, $p<0.0001$), and 15.5% reduction at six (WT: 0.413±0.010, cKO: 0.349±0.022 cyc/deg, $p<0.0001$) months of age (Figure 3.3). The *Snf2h* gene is haplosufficient for visual acuity as no significant difference was observed between wildtype and heterozygous genotypes. Sex-disaggregated data showed minor differences in p-value at various timepoints; however, there was no significant difference between female and male mice of the same genotype for each timepoint. Overall, these results indicate that *Snf2h* is required for visual acuity from

juvenile to mature mice. Embryonic knockout of *Snf2h* in the retina results in early pathological changes that persist throughout adulthood.

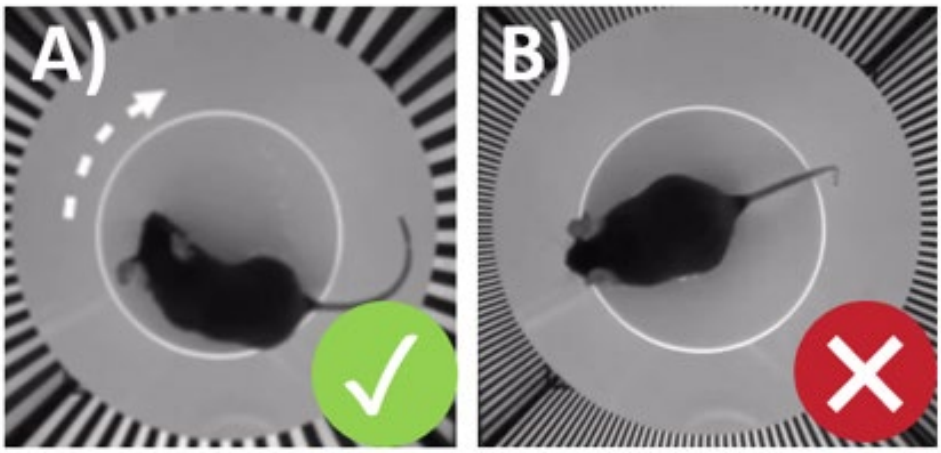


**Figure 3.2. Optomotor response of mouse.** The mouse responds to the stimulus displayed at the spatial frequency shown until the observable threshold is reached. (A) The optomotor response of a *Snf2h* cKO mouse is triggered and it turns its head in the direction of the rotating strips displayed at the spatial frequency shown. (B) An increased spatial frequency does not evoke a response from the mouse.

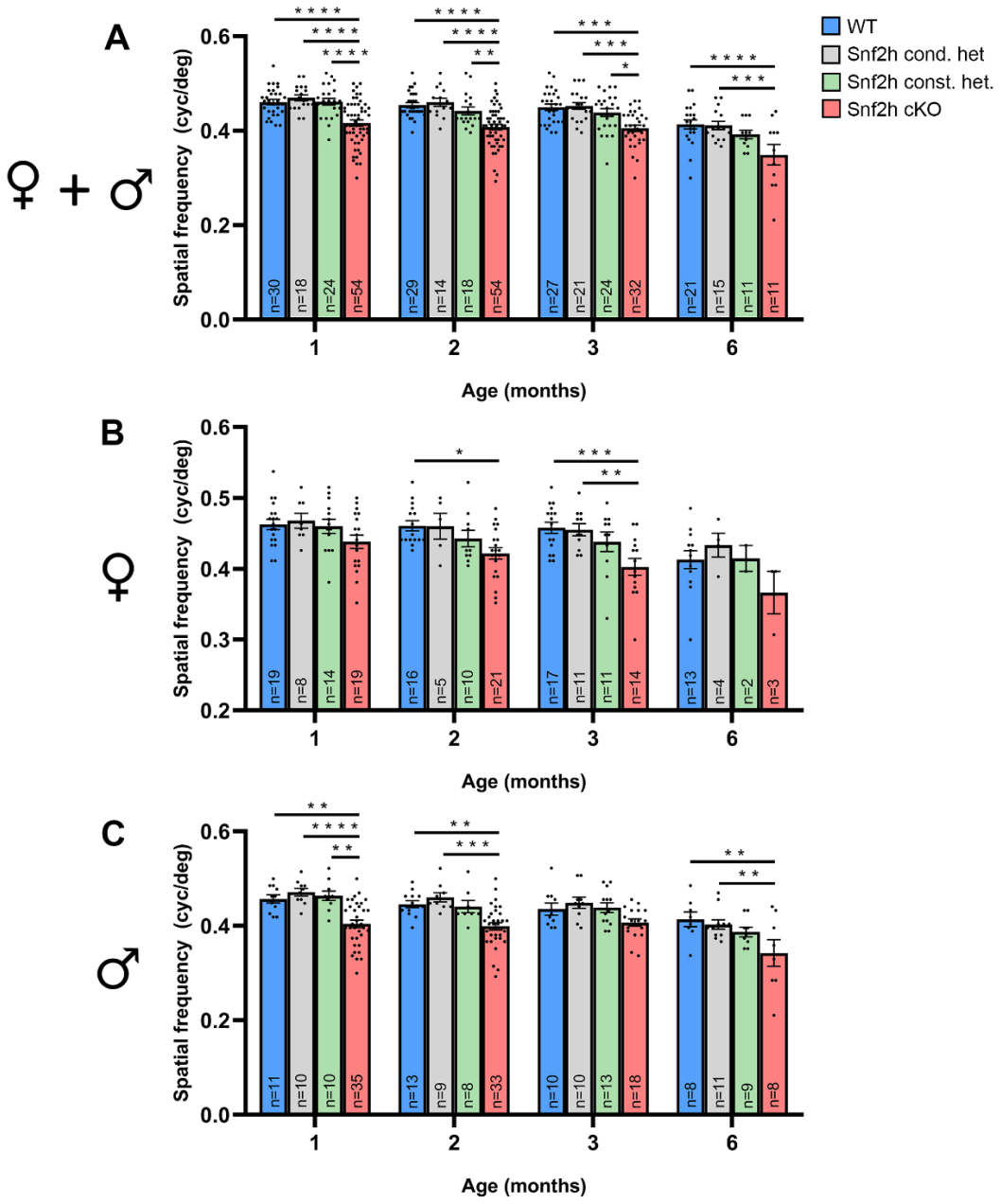


**Figure 3.3. Visual acuity as measured by optomotor response-based testing of *Snf2h* cKO is significantly decreased compared to WT and heterozygous mice at all timepoints.** Individual and average values are shown for (A) all mice, (B) female mice, (C) and male mice. (A-C) No significant difference was observed between Snf2h heterozygous mice and WT littermates. N values represent biological replicates. *p<0.05, **p<0.01, ***p<0.001, ****p<0.0001.

### 3.3. *Snf2h* cKO mice show a decline in the electroretinogram response

The next series of *in vivo* testing was conducted to examine retinal cell-type specific responses in the phototransduction pathway. Dark-adapted electroretinography (ERG) was performed and the waveform response consisted of three components: 1) the initial a-wave negative deflection, which is a function of photoreceptor cell activity, 2) followed by the b-wave, which measures bipolar cell and Müller glia activity and 3) oscillatory potentials (OPs) descending the b-wave, which measure amacrine cell activity. The full-field white stimulus was tested at five light intensities: 0.01, 0.1, 1.0, 4.0, and 10.0 cd·s/$m^2$. An increase in light intensity generally corresponded to an increase in a-wave and b-wave peak amplitudes for all genotypes at lower light intensities. However, increases in both peak amplitudes plateaued for light intensities greater than 1.0 cd·s/$m^2$ with either a minimal increase or a decline in peak amplitudes at 4.0, and 10.0 cd·s/$m^2$ light intensity (Figure 3.4). Due to the maximal a-wave and b-wave peak amplitudes response at 1.0 cd·s/$m^2$ stimulus intensity, results presented in this thesis thereafter are at this light intensity. Representative waveforms are shown in Figure 3.5.

When a-wave and b-wave peak amplitudes were graphed as a function of age, an analysis of recordings showed that retinal *Snf2h* deletion resulted in a significant decline in the retinal electrophysiological response in mice at all ages assessed. At a 1.0 cd·s/$m^2$ light intensity, *Snf2h* cKO mice displayed a significant decrease in a-wave peak amplitudes compared to WT mice at all timepoints assessed with a 60% reduction at one month (WT: 377±8 μV, cKO: 149±15 μV, $p<0.0001$), 58% reduction at two months (WT: 306±9 μV, cKO: 129±11 μV, $p<0.0001$), 62% reduction at three months (WT: 292±10 μV, cKO: 112±14 μV, $p<0.0001$), and 63% reduction at six (WT: 276±8 μV, cKO: 103±26 μV, $p<0.0001$) months of age (Figure 3.6). Similarly, b-wave peak amplitudes of *Snf2h* KO mice at a 1.0 cd·s/$m^2$ light intensity significantly declined compared

to WT mice with a 63% reduction at one month (WT: 680±21 μV, cKO: 255±24 μV, $p<0.0001$), 61% reduction at two months (WT: 533±17 μV, cKO: 205±18 μV, $p<0.0001$), 68% reduction at three months (WT: 513±18 μV, cKO: 163±22 μV, $p<0.0001$), and 70% reduction at six (WT: 450±14 μV, cKO: 137±39 μV, $p<0.0001$) months of age (Figure 3.7). For both the a-wave and b-wave peak amplitudes, the *Snf2h* gene is haplosufficient for the ERG response as no significant differences were observed between wildtype and heterozygous genotypes. Sex-disaggregated data showed differences in p-value at various timepoints; however, there was no significant difference between female and male mice of the same genotype for each timepoint.

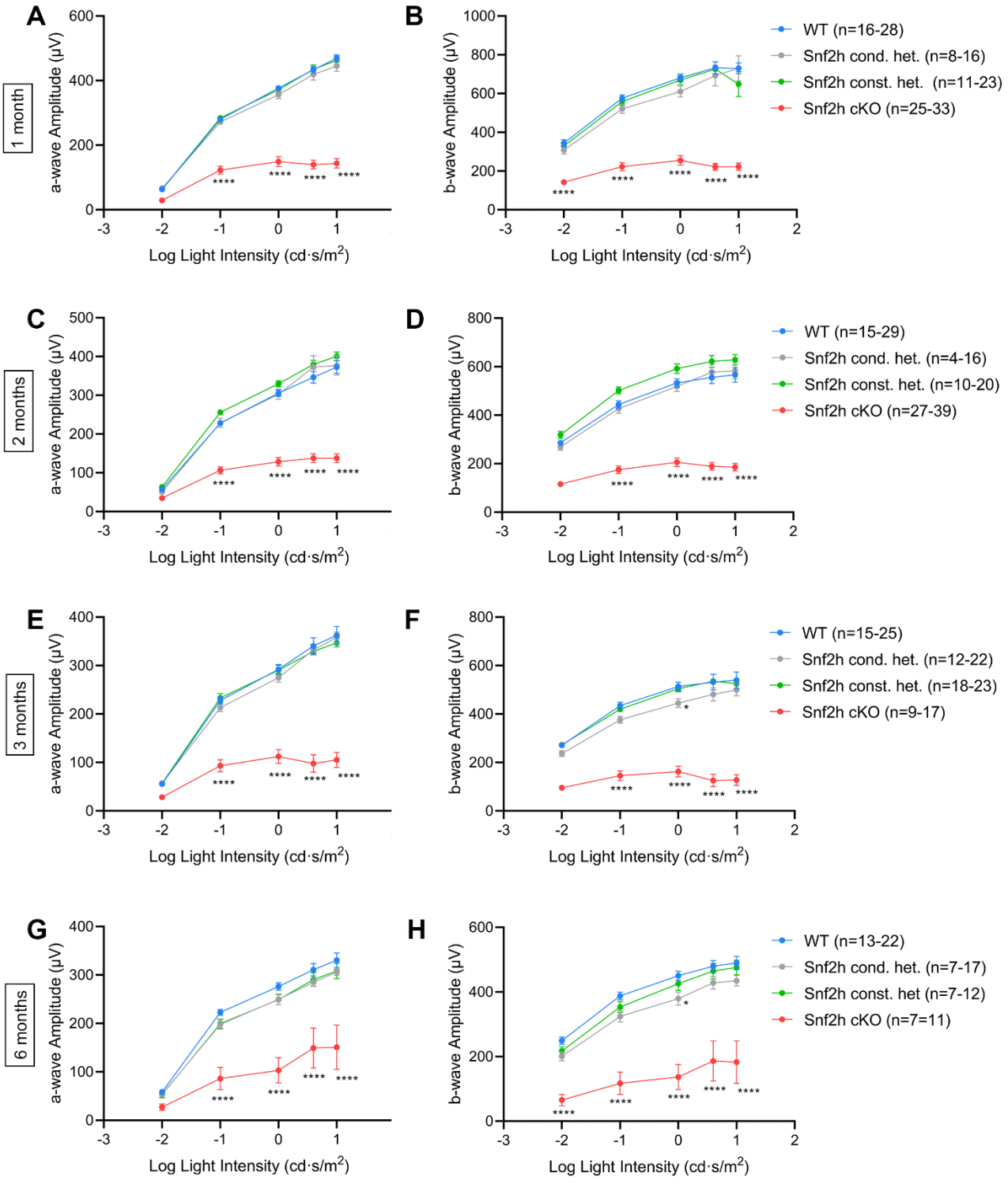


**Figure 3.4. A-wave and b-wave amplitudes at various light intensities for *Snf2h* cKO mice and littermates.** All asterisks represent significant difference between indicated genotype and WT mice. *p<0.05, **p<0.01, ***p<0.001, ****p<0.0001.

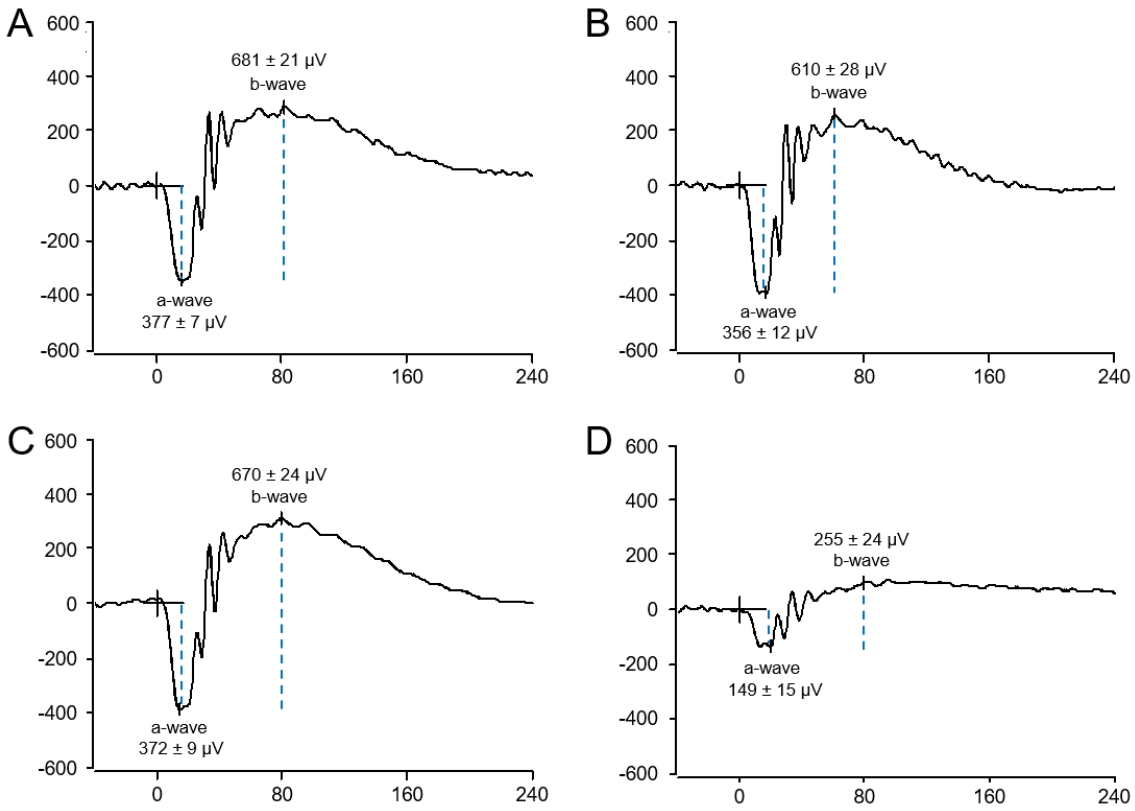


**Figure 3.5. Representative ERG waveforms at an optimized stimulus intensity of 1.0 cd·s/m$^2$ for individual mice of each genotype at 1 month of age.** Average a-wave and b-wave peak amplitudes are indicated for (A) WT, (B) *Snf2h* conditional heterozygous, (C) *Snf2h* constitutive heterozygous and (D) *Snf2h* cKO mice.

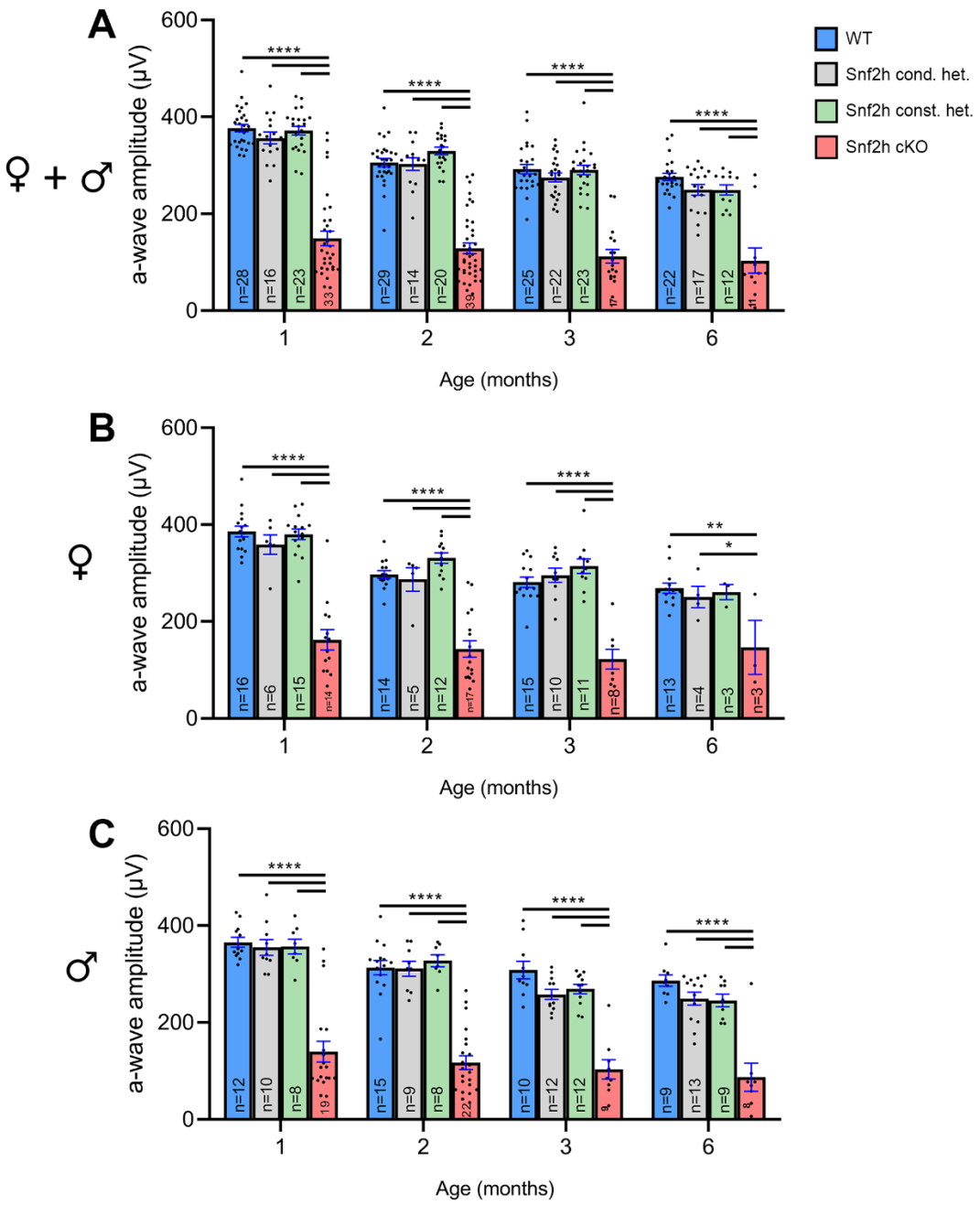


**Figure 3.6. A-wave peak amplitudes of *Snf2h* cKO mice are significantly decreased compared to WT and heterozygous mice at all timepoints at 1.0 cd·s/m$^2$ light intensity.** (A) Individual and average values are shown for (A) all mice, (B) female mice, (C) and male mice. (A-C) No significant difference was observed in Snf2h heterozygous mice compared to WT littermates. N values represent biological replicates. *p<0.05, **p<0.01, ****p<0.0001.

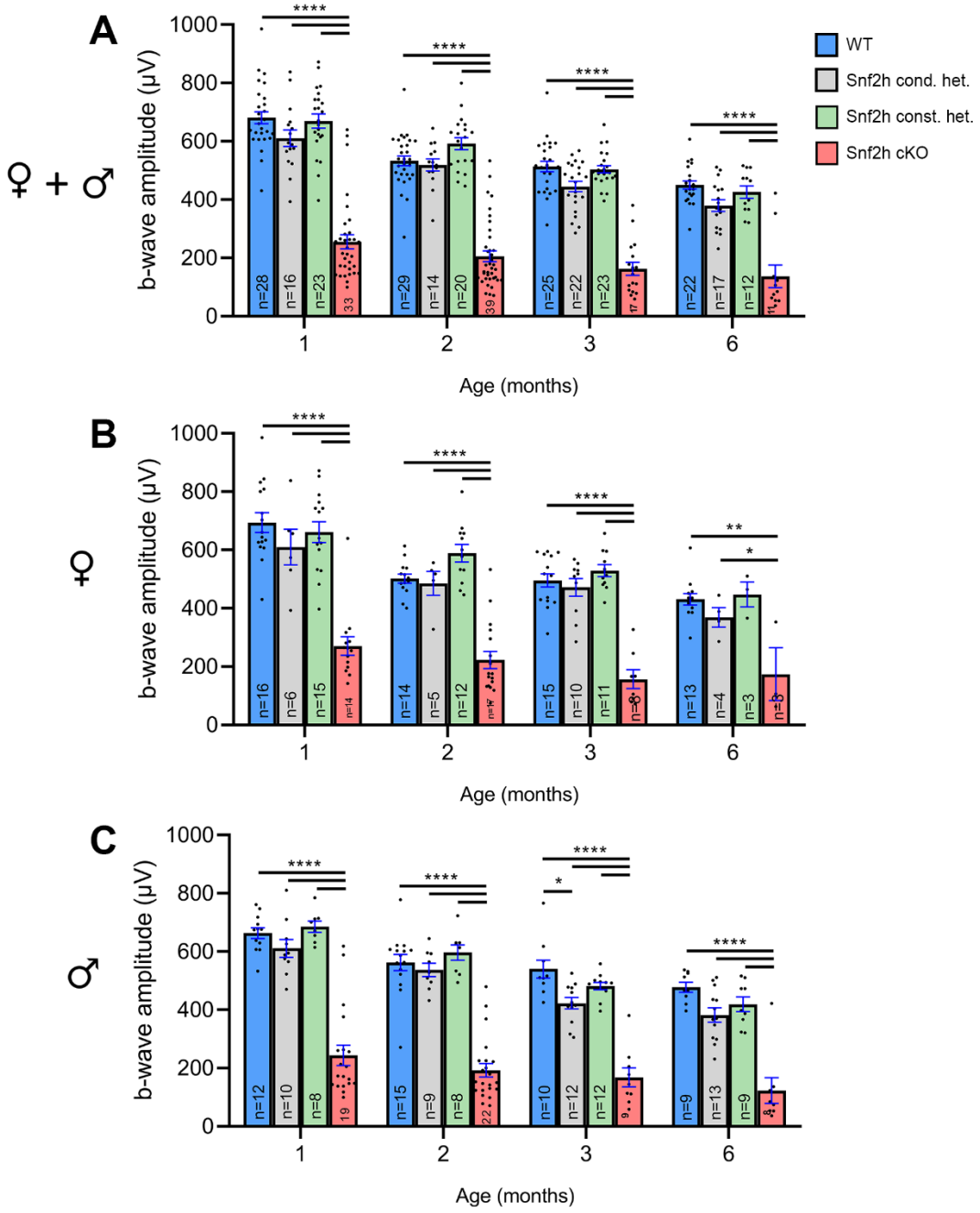


**Figure 3.7. B-wave peak amplitudes of *Snf2h* cKO mice are significantly decreased compared to WT and heterozygous mice at all timepoints at 1.0 cd·s/m$^2$ light intensity.** (A) Individual and average values are shown for (A) all mice, (B) female mice, (C) and male mice. (A-C) No significant difference was observed in Snf2h heterozygous mice compared to WT littermates. N values represent biological replicates. *p<0.05, **p<0.01, ****p<0.0001.

When OP amplitudes were graphed as a function of age, analysis of recordings showed that retinal *Snf2h* deletion resulted in a decline in the retinal electrophysiological response in mice at all ages assessed and at virtually all intensities of light (Figure 3.8). Representative waveforms are shown in Figure 3.9. At a 1.0 cd·s/$m^2$ light intensity, *Snf2h* cKO mice displayed a significant decrease in [OP1; OP2; OP3] compared to wildtype mice at all timepoints assessed with a [47 %, $p<0.0001$; 53 %, $p<0.0001$; 49 %, $p<0.0001$] reduction at one month, [44 %, $p<0.0001$; 48 %, $p<0.0001$; 47 %, $p<0.001$] reduction at two months, [48 %, $p<0.0001$; 49 %, $p<0.0001$; 42%, $p<0.01$] reduction at three months, and [50 %, $p<0.01$; 56 %, $p<0.0001$; 53 %, $p<0.0001$] reduction at six months of age (Figure 3.10).

For the OP peak amplitudes, the *Snf2h* gene is haplosufficient for the ERG response as no significant differences were observed between WT and heterozygous genotypes. Sex-disaggregated data showed minor differences in p-value at various timepoints; however, there was no significant difference between female and male mice of the same genotype for each timepoint.

Taken together, these results show that Snf2h expression is required for the ERG response of juvenile and adult mice. Knockout of *Snf2h* in the developing retina resulted in decreased a-wave, b-wave, and oscillatory potential amplitudes, which indicate photoreceptor cell (a-wave), bipolar cell and Müller glia (b-wave), and amacrine cell (OP) dysfunction..

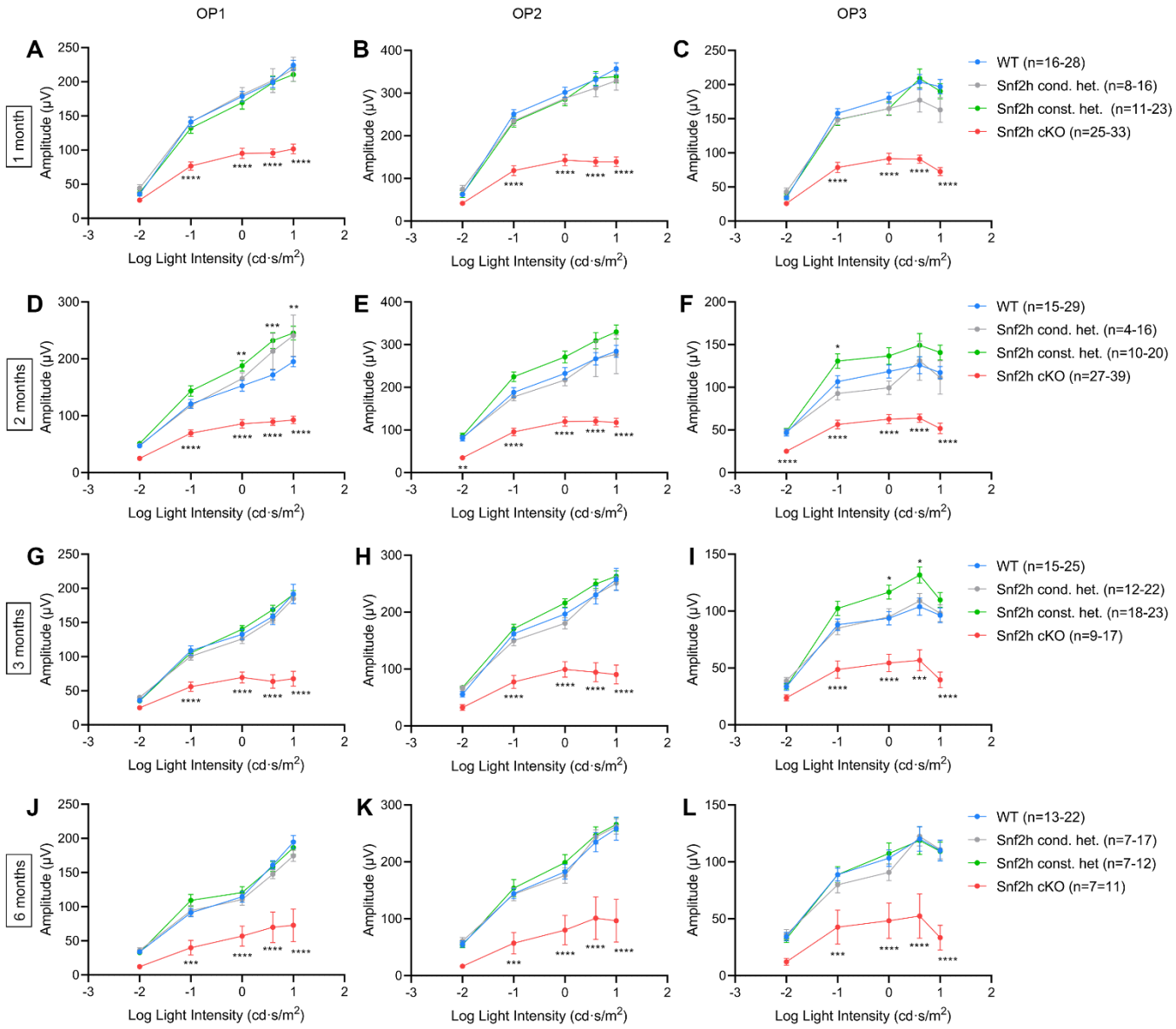


**Figure 3.8. OP amplitudes at various light intensities for *Snf2h* cKO mice and littermates.** Data shown is at (A-C) 1 month, (D-F) 2 months, (G-I) 3 months, (J-L) and 6 months of age. All asterisks represent significant difference between indicated genotype and WT mice. *p<0.05, **p<0.01, ***p<0.001, ****p<0.0001.

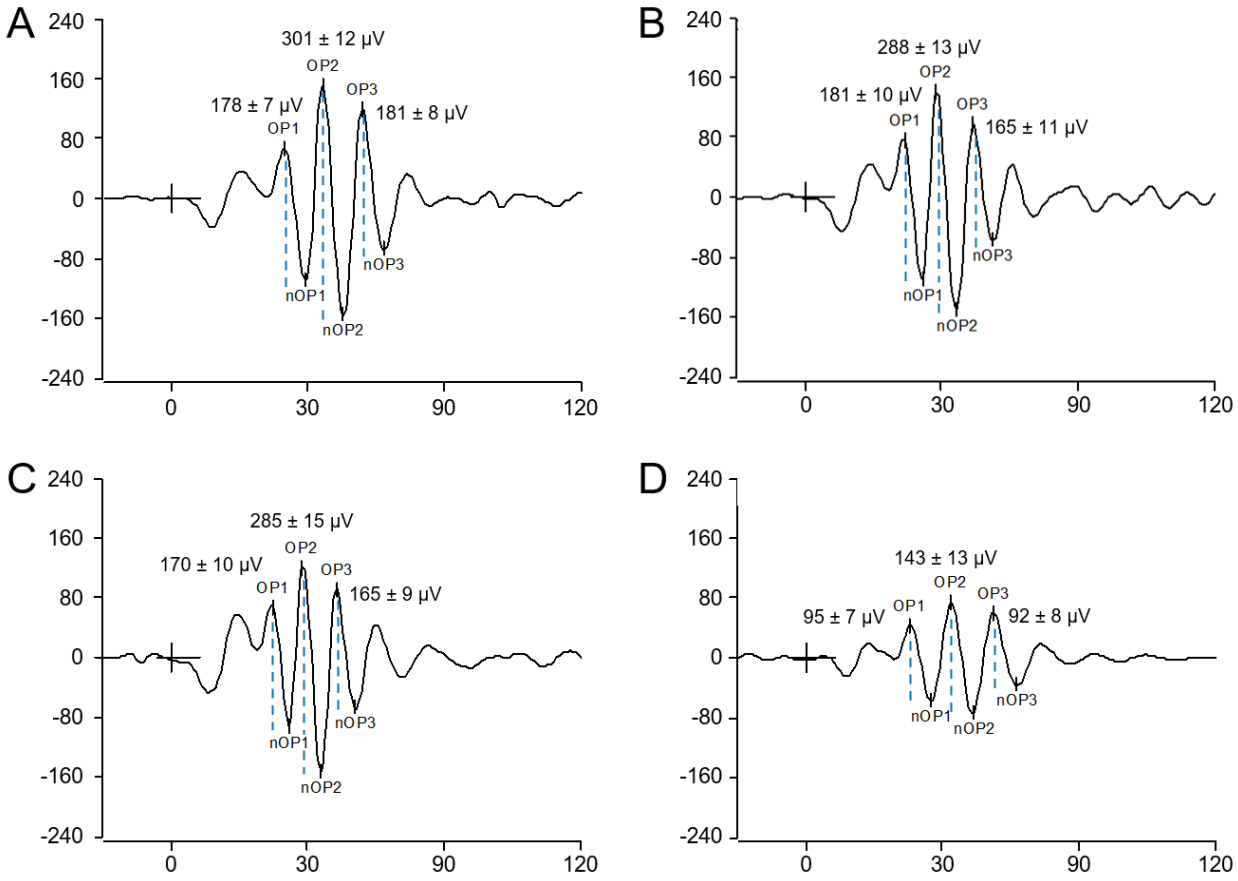


**Figure 3.9. Representative OP waveforms at an optimized stimulus intensity of 1.0 cd·s/m$^2$ for individual mice of each genotype at 1 month of age.** OP1, OP2, and OP3 mean amplitudes are indicated for (A) WT, (B) *Snf2h* conditional heterozygous, (C) *Snf2h* constitutive heterozygous and (D) *Snf2h* cKO mice.

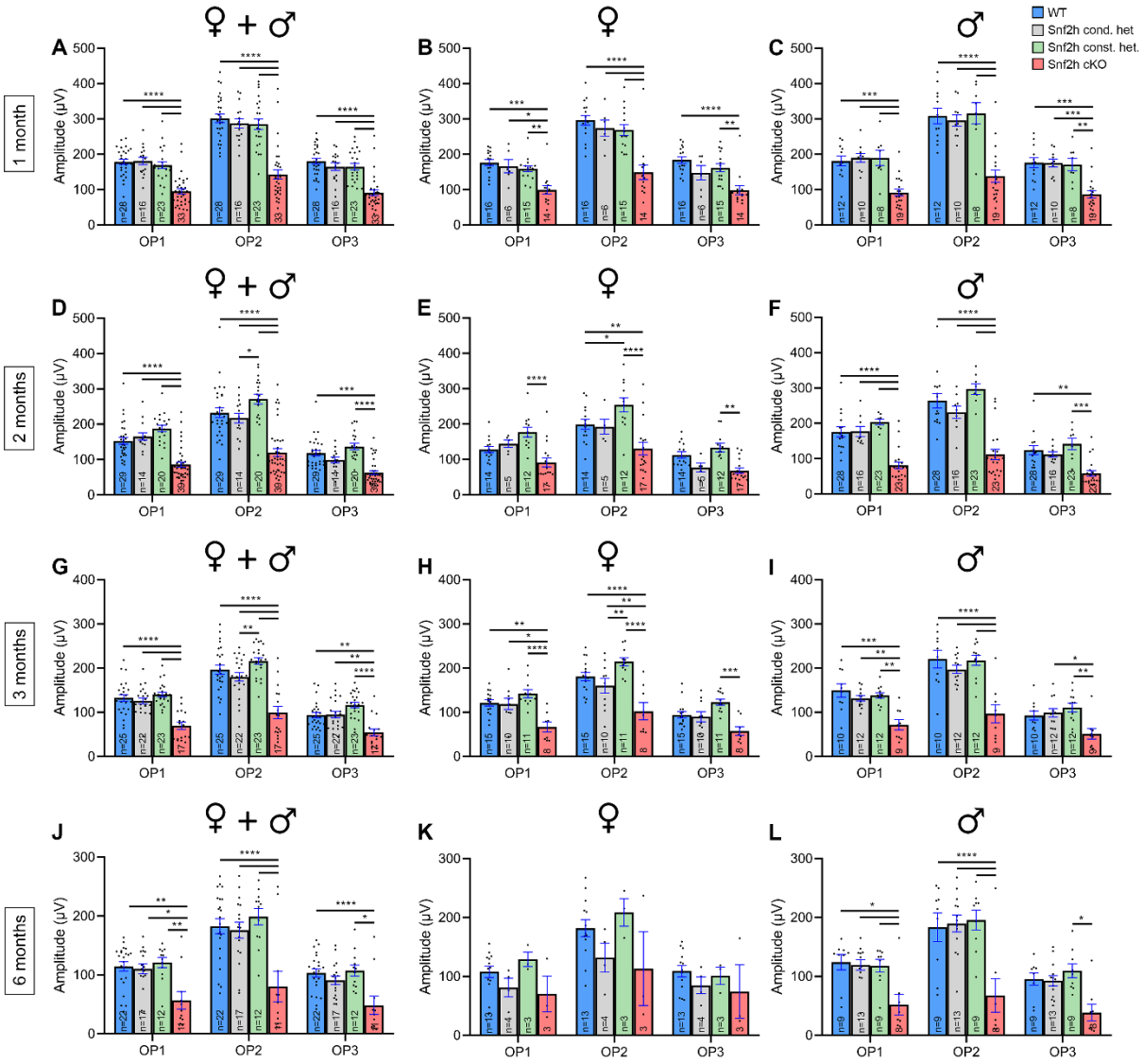


**Figure 3.10. OP peak amplitudes at of *Snf2h* cKO mice is significantly decreased compared to WT and heterozygous mice at all timepoints at 1.0 cd·s/m$^2$ light intensity.** (A) Individual and average values are shown for (A, D, G, J) all mice, (B, E, H, K) female mice, (C, F, I, L) and male mice. N values represent biological replicates. *p<0.05, **p<0.01, ***p<0.001, ****p<0.0001.

### 3.4. Loss of retinal Snf2h results in decreased retinal cells

WT and *Snf2h* cKO embryonic (E13.5, E15.5, E17.5) and postnatal (P0, P14, 1 month, 2 months, 3 months, 6 months) retinal tissues were stained to examine Snf2h protein expression (Figure 3.11). The earliest embryonic time point assessed, E13.5, was chosen to examine *Snf2h* expression shortly after the onset of Cre expression at E10.5. Subsequent embryonic and early postnatal timepoints examined *Snf2h* expression throughout retinal development. In both WT and *Snf2h* cKO mice, intense Snf2h staining was initially observed at E13.5 and E15.5 but decreased towards P0. *Snf2h* expression was detected throughout the retina and in the ONL, INL, and GCL cell body layers once retinal structure had formed in mice aged P14 and older. A trend towards reduction in the number of Snf2h+ cells was observed in the *Snf2h* cKO mice compared to the WT mice.

Upon complete retinal cell differentiation, cell-type specific antibody staining was performed against the five neuron types and Müller glia in retinal tissues at one, two, three, and six months of age (Figure 3.12). Since no significant differences were observed between *Snf2h* retinal conditional heterozygotes and *Snf2h* constitutive heterozygotes at any time point for the functional vision tests, only WT, *Snf2h* constitutive heterozygote, and *Snf2h* cKO mice were examined for this experiment. Fluorophore-labelled cells were quantified by manual cell counting and the results showed a significant decrease in almost all cell types with the exception of bipolar cells. *Snf2h* cKO mice showed a significant decrease in cone photoreceptor cells compared to wildtype mice at all timepoints assessed with a 50 % ($p<0.0001$), 54 % ($p<0.0001$), 62 % ($p<0.0001$), and 70 % ($p<0.0001$) reduction at one month, two months, three months, and six months of age, respectively (Figure 3.13A). *Snf2h* cKO mice showed a significant decrease in rod photoreceptor cells compared to wildtype mice at all timepoints assessed with a 59 % ($p<0.0001$),

58 % ($p<0.0001$), 64 % ($p<0.0001$), and 76 % ($p<0.0001$) reduction at one month, two months, three months, and six months of age, respectively (Figure 3.13B). *Snf2h* cKO mice showed an equal or decreased number of bipolar cells compared to wildtype mice with a 27% ($p<0.05$), 0 % (n.s), 22 % (n.s), and 21 % (n.s.) reduction at one month, two months, three months, and six months of age, respectively (Figure 3.13C). *Snf2h* cKO mice showed a significant decrease in horizontal cells compared to wildtype mice at all timepoints assessed with a 32 % ($p<0.01$), 35 % ($p<0.01$), 33 % ($p<0.05$), and 33 % ($p<0.05$) reduction at one month, two months, three months, and six months of age, respectively (Figure 3.13D). *Snf2h* cKO mice showed a significant decrease in amacrine cells compared to wildtype mice at all timepoints assessed with a 36 % ($p<0.001$), 29 % ($p<0.01$), 32 % ($p<0.01$), and 56 % ($p<0.0001$) reduction at one month, two months, three months, and six months of age, respectively (Figure 3.13E). *Snf2h* cKO mice showed a significant decrease in ganglion cells compared to wildtype mice at all timepoints assessed with a 29 % ($p<0.01$), 25 % ($p<0.01$), 25 % ($p<0.05$), and 21 % ($p<0.05$) reduction at one month, two months, three months, and six months of age, respectively (Figure 3.13F). *Snf2h* cKO mice showed a decrease in Müller glia compared to wildtype mice at all timepoints assessed with a 19 % (n.s.), 22 % ($p<0.05$), 32 % ($p<0.001$), and 45 % ($p<0.0001$) reduction at one month, two months, three months, and six months of age, respectively (Figure 3.13G).

Furthermore, thickness of the retina ONL and INL were measured (Figure 3.14). *Snf2h* cKO mice showed a decrease in ONL thickness compared to wildtype mice at all timepoints assessed with a 58 % ($p<0.0001$), 58 % ($p<0.0001$), 61 % ($p<0.0001$), and 78 % ($p<0.0001$) reduction at one month, two months, three months, and six months of age, respectively (Figure 3.14A). *Snf2h* cKO mice showed a decrease in INL thickness compared to wildtype mice at all timepoints assessed with a 35 % ($p<0.0001$), 29 % ($p<0.0001$), 38 % ($p<0.0001$), and 54 %

($p<0.0001$) reduction at one month, two months, three months, and six months of age, respectively (Figure 3.14B). The observed significant decreases in the thickness of both layers in the *Snf2h* cKO mice compared to WT and *Snf2h* constitutive littermates correlate to the decrease in cell numbers in the retinal cell populations found in these layers.

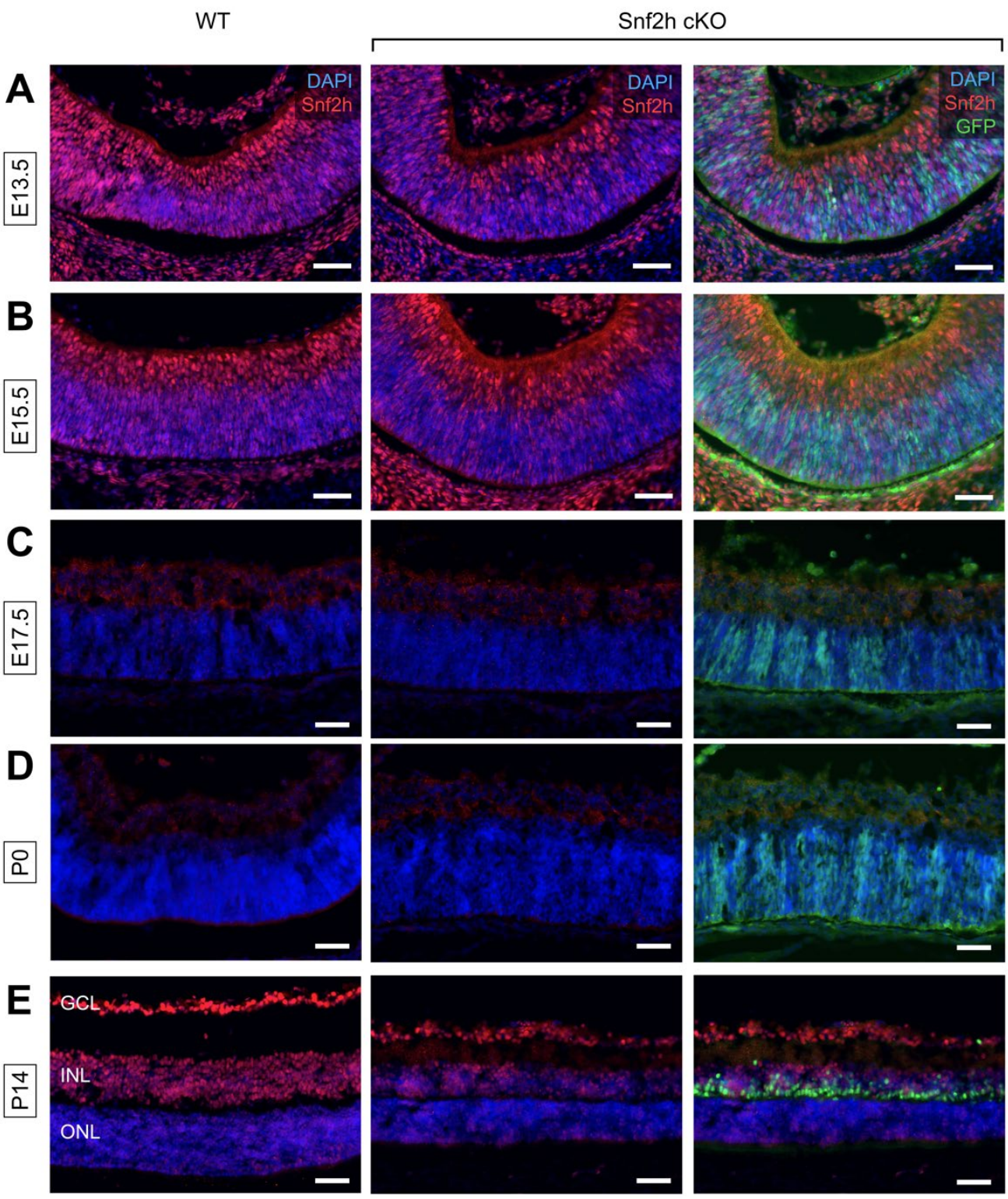
WT
Snf2h cKO
A
E13.5
DAPI
Snf2h
DAPI
Snf2h
DAPI
Snf2h
GFP
B
E15.5
C
E17.5
D
P0
E
P14
GCL
INL
ONL

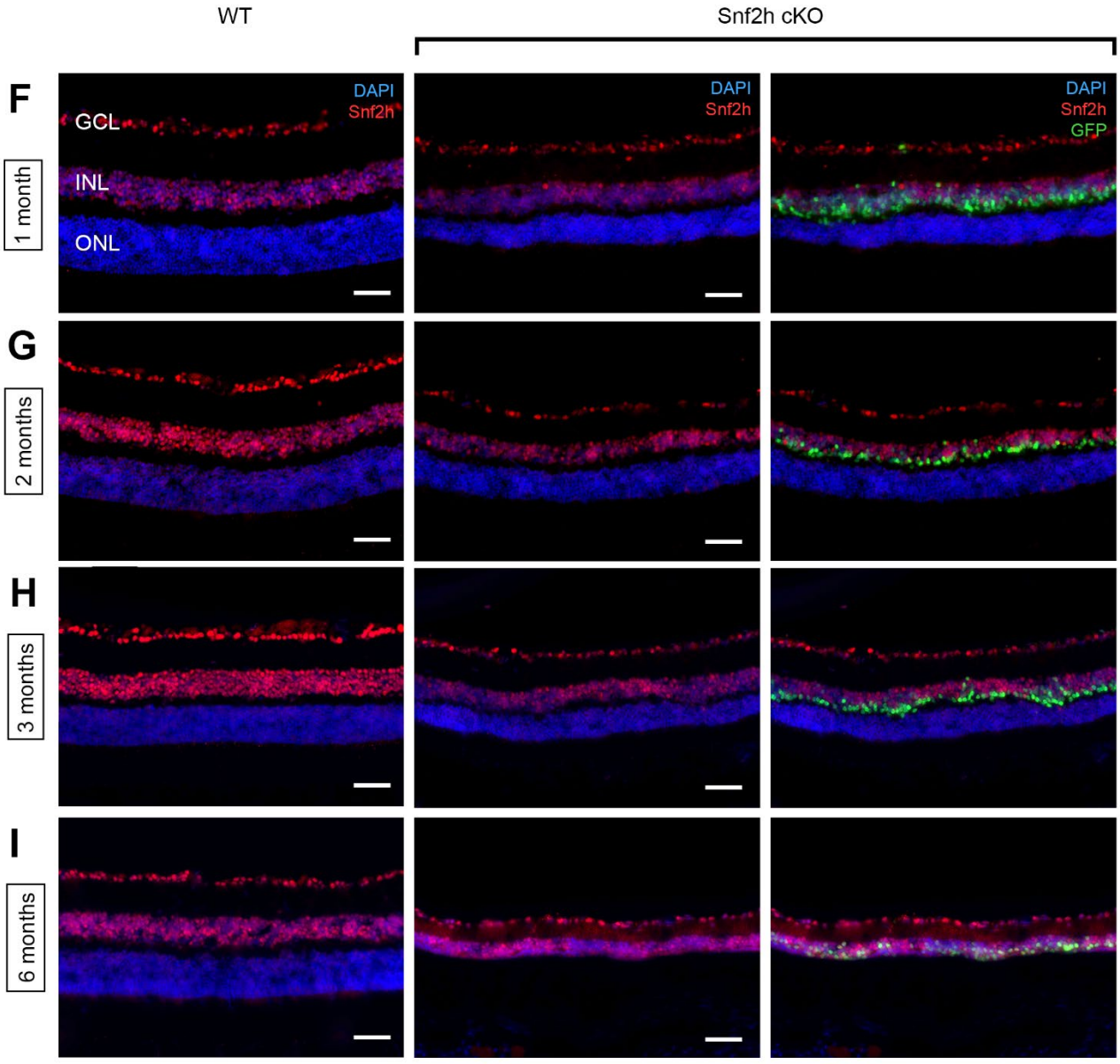


**Figure 3.11. Snf2h expression in the retina of representative WT and *Snf2h* cKO mice**. *Snf2h* cKO mice were additionally stained against GFP to track expression of the Cre construct. Mouse retinal tissues at (A) E13.5, (B) E15.7, (C) E17.5, (D) P0 (E) P14, (F) 1 month, (G) 2 months, (H) 3 months, and (I) 6 months of age. GCL: Ganglion cell layer, INL: inner nuclear layer, ONL: outer nuclear layer. Scale bar, 50 µm.

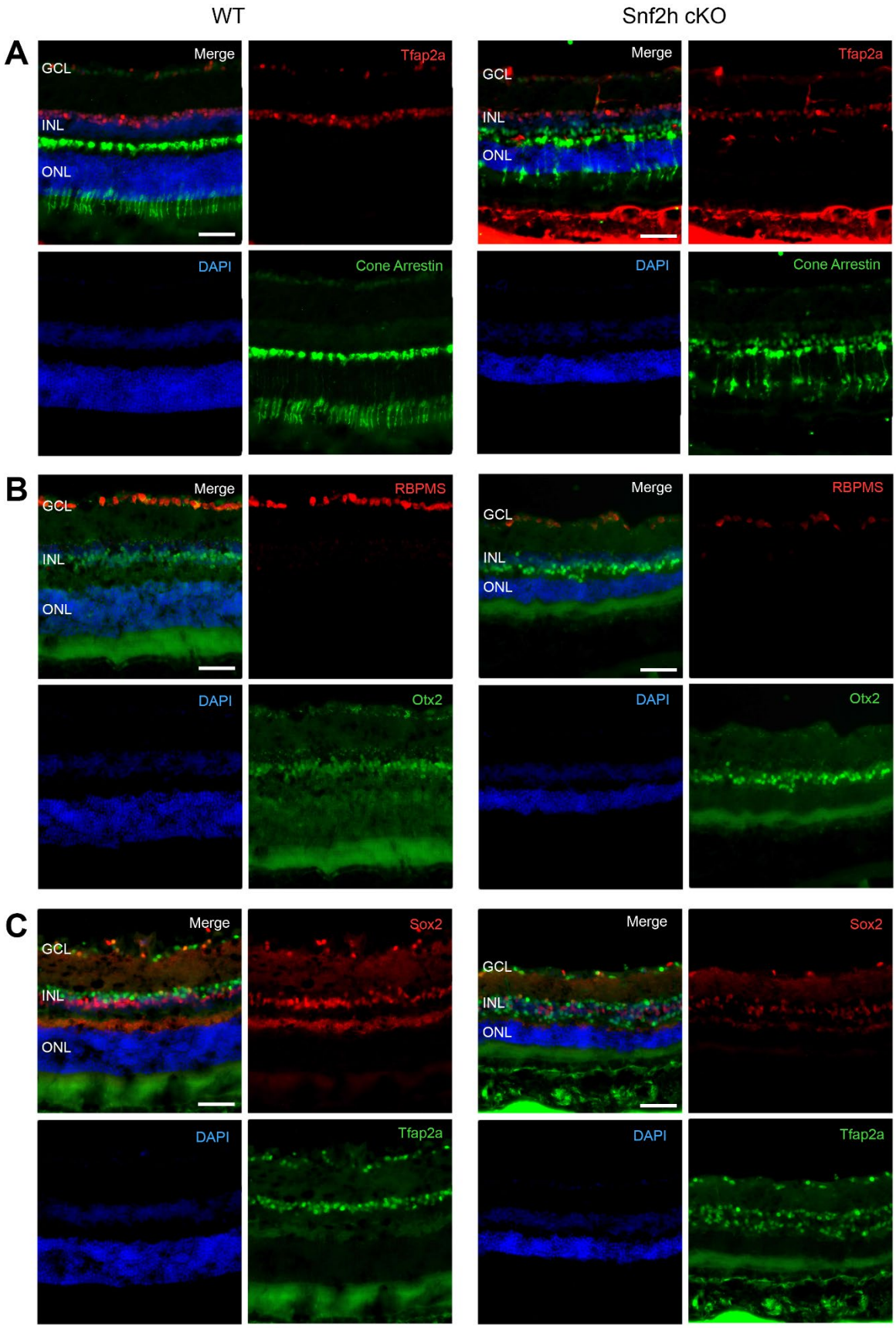
WT
Snf2h cKO
A
Merge
Tfap2a
GCL
INL
ONL
DAPI
Cone Arrestin
B
RBPMS
Otx2
C
Sox2

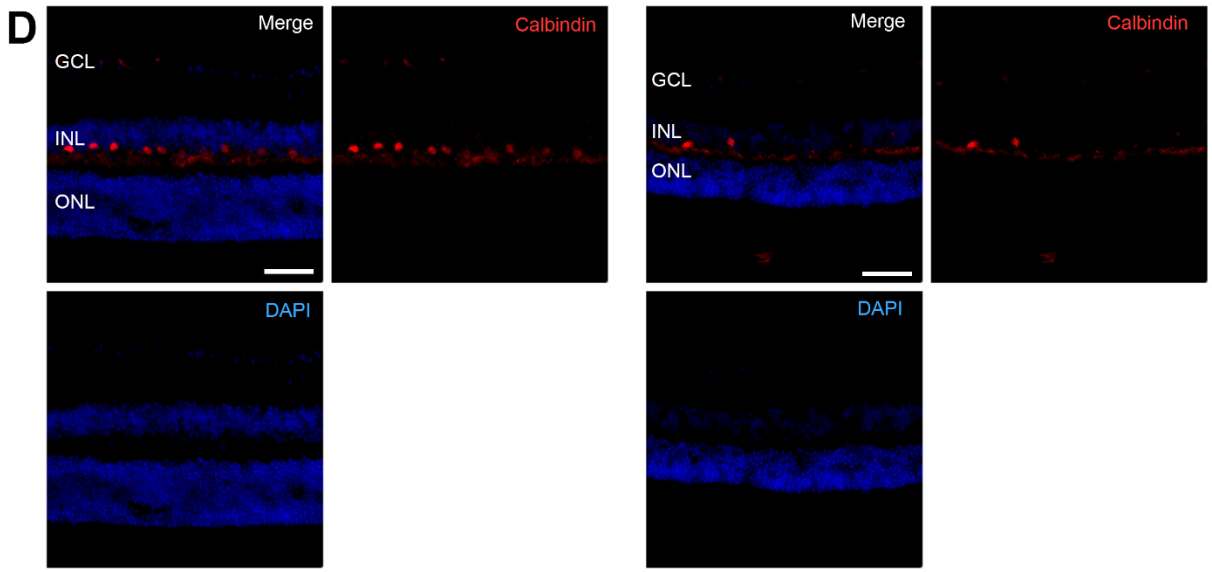


**Figure 3.12. Cell type specific staining in the retina of WT and *Snf2h* cKO mice at 2 months of age.** Cell-type specific antibodies used were (A) Tfap2a (amacrine cells) and cone arrestin (cone photoreceptors) (B) RBPMS (ganglion cells) and Otx2 (bipolar cells), (C) Tfap2a (amacrine cells) and Sox2 (Müller glia) and (D) Calbindin (horizontal cells). GCL: Ganglion cell layer, INL: inner nuclear layer, ONL: outer nuclear layer. Scale bar, 50 µm.

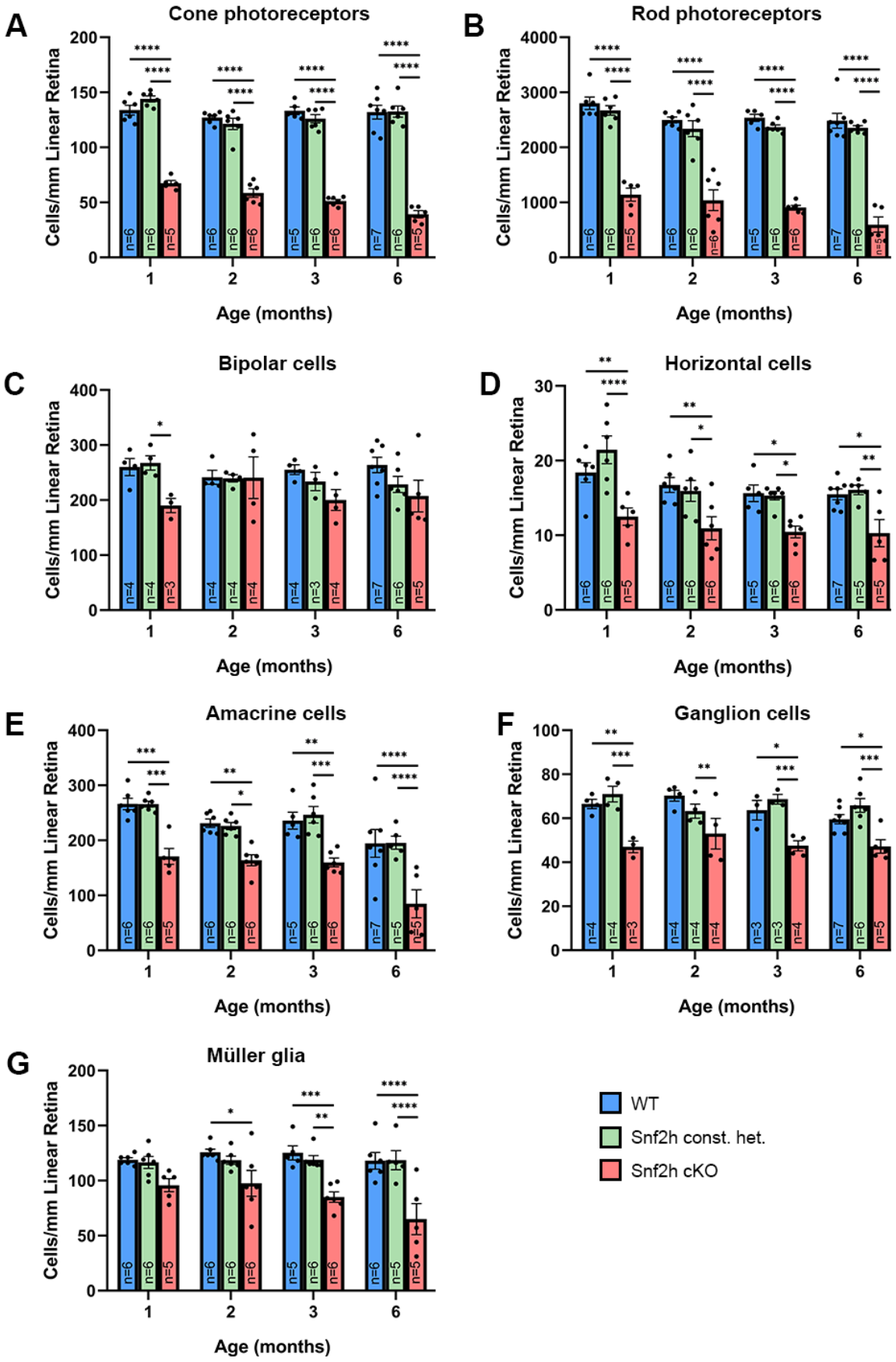
A
Cone photoreceptors
Cells/mm Linear Retina
Age (months)
B
Rod photoreceptors
C
Bipolar cells
D
Horizontal cells
E
Amacrine cells
F
Ganglion cells
G
Müller glia
WT
Snf2h const. het.
Snf2h cKO

**Figure 3.13. Cell counts in the retina of WT, constitutive heterozygote, and *Snf2h* cKO mice.** Cells were stained with fluorophore-conjugated antibodies against specific cell types and manually counted from a central area of the retina. The number of retinal cells were quantified for (A) cone photoreceptors, (B) rod photoreceptors, (C) bipolar cells, (D) horizontal cells, (E) amacrine cells, (F) ganglion cells, and (G) Müller glia. (A-G) Significant decrease in cell numbers were observed in for all cell types with the exception of bipolar cells. N values represent biological replicates. *p<0.05, **p<0.01, ***p<0.001, ****p<0.0001.

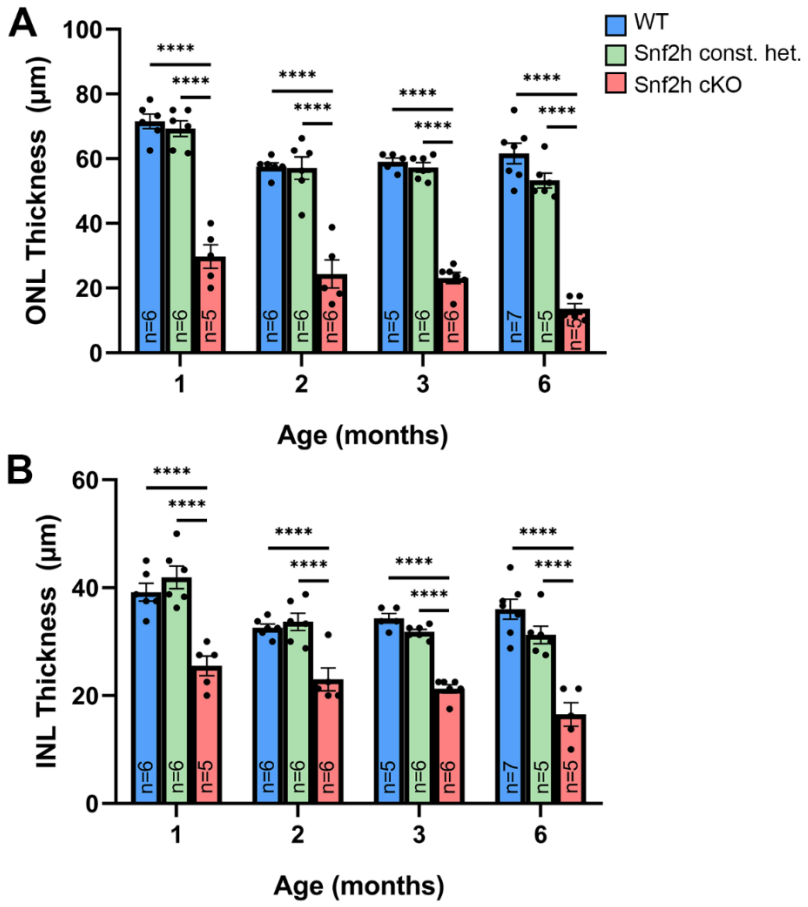


**Figure 3.14. (A) ONL and (B) INL thickness is decreased in *Snf2h* cKO mice compared to WT and *Snf2h* constitutive heterozygous littermates at various ages.** N values represent biological replicates. ONL: outer nuclear layer, INL: inner nuclear layer. ****p<0.0001.

# CHAPTER 4. DISCUSSION

The purpose of this research project was to examine the role of the Snf2h chromatin remodelling protein in the visual system. Chromatin remodelling proteins are essential for many cellular processes including embryonic development and gene regulation, and mutations in chromatin remodelling genes have been implicated in many diseases. As an ATPase catalytic subunit of the ISWI family of chromatin remodellers, Snf2h interacts with a variety of other protein subunits to form complexes with numerous biological properties and functions. Unsurprisingly, mutations in the *Snf2h* gene have been linked to neurodevelopmental delays and vision abnormalities in the human population. In mice, *Snf2h* has been extensively studied in the brain using knockout models. However, studies on the role of *Snf2h* in the visual system remain relatively limited currently. A histological study on *Snf2h* retinal cKO mice showed a reduced thickness of the ONL compared to control mice (Kuzelova et al., 2023). Our research seeks to further explore the visual deficits and to quantify retinal cell-type specific changes associated with *Snf2h* loss. Elucidating the mechanisms underlying chromatin remodellers is essential in understanding their disease pathogenesis and provides insights into retinal diseases linked to gene dysregulation.

A *Snf2h* retinal cKO mouse model was generated using the Cre-Lox recombination system by breeding a *Snf2h* floxed mouse line with a *Chx10-Cre* retina-specific Cre driver line, which had an onset of Cre expression at E10.5 to knockout Snf2h in retinal progenitor cells. The phenotype of this mouse model was characterized by assessing visual function and examining histological changes in the retina. Disease progression was tracked from embryonic development to adulthood. *Snf2h* cKO mice exhibited loss in retinal neurons which corresponded with visual deficits in visual

acuity and electroretinograms. Significant histological and functional changes were observed at all time points assessed (one, two, three, and six months of age).

### 4.1. Mosaic Cre expression in the retina and implications in subsequent experiments

Fluorescence imaging of Cre-EGFP in whole retinas of *Chx10-Cre*$^{+/-}$; *Ai14*$^{+/-}$ P0 mice showed that the Cre recombinase expression pattern was mosaic. Since Cre recombinase is required to excise the floxed catalytic domain of *Snf2h*, retinal cells devoid of Cre are unaffected and functional Snf2h is expressed normally. Mice within the same litter exhibited varying levels of Cre expression with some mice showing complete Cre-EGFP expression throughout the retina while others displayed patchy areas of the retina absent of Cre. The mosaic expression pattern of Cre recombinase in the retina under the Chx10-Cre promotor has been previously documented in the literature (Rowan & Cepko, 2004). Consequently, incomplete knockout of Snf2h may have contributed to variability in functional and histological experiments among *Snf2h* cKO biological replicates.

### 4.2. Visual dysfunction is observed in Snf2h cKO mice

Functional vision testing is a component of a complete eye examination and is performed to assess the ability of the subject to visually perceive the surrounding environment (Bennett et al., 2019). Detection of visual impairment can then lead to identification of appropriate accommodations and assistive technologies to improve visual function.

Visual acuity measures the resolving ability of the eye and is a commonly assessed parameter in many vision tests that is used as a first line screening of visual function (Bennett et al., 2019). VA testing is highly advantageous owing to its low cost, rapid testing time, and sensitivity in detecting abnormalities of the visual system (Levenson & Kozarsky, 1990). Furthermore, the accuracy of select home testing methods have shown to be as reliable as the

Snellen chart commonly used in the clinic (Samanta et al., 2023), which make this a convenient method for self screening of visual dysfunction that overcomes common barriers to eye care such as financial and accessibility limitations (Chheda et al., 2019).

VA was measured in the *Snf2h* cKO mice to assess their overall visual performance using the OMR-based test. This long-established method of visual testing for laboratory use is sensitive, reliable and non-invasive, which allows for repeated testing in longitudinal studies. Since testing relies on the innate OMR head tracking behavior of the mouse, minimal to no training is required for both the test subject and the evaluator (Shi et al., 2018). The Striatech OptoDrum software used in this study automatically tracks and scores mice to minimize evaluator bias (Benkner et al., 2013). WT and *Snf2h* cKO mice were tested shortly after eyes were open with the earliest time point at one month of age and subsequently followed up to six months of age. The VA values of WT mice are consistent with observations in previous literature which range from 0.4 cyc/deg (Xiao et al., 2019) to 0.53 cyc/deg (Cha et al., 2022) for mice at six weeks of age. VA for *Snf2h* cKO mice have not previously been tested in existing literature as a novel mouse model was employed in this study. *Snf2h* cKO mice exhibited a significant decrease in VA compared to WT mice at all timepoints, which suggests *Snf2h* expression is essential for development of the visual system. Notably, the range of individual biological replicates for *Snf2h* cKO mice were greater than WT mice at all timepoints. This variability could be a consequence of the mosaicism observed in *Chx10-Cre* expression which led to variable levels of *Snf2h* expression in mice. VA measurements rely on multiple components of the visual pathway functioning in conjunction and a decrease in value could arise from defects in any of these components including refractive error, retinal degeneration, and neurotransmitter deficiency in the brain. As such, additional vision

testing was performed to determine the possible contribution of specific retinal cell types in this decline in visual ability.

Since Snf2h ablation is localized to the retina during embryonic development and a significant decrease in VA was observed, dysfunction in retinal neurons was expected. Electroretinography was performed to measure the electrophysiological response of select retinal cell types. Significant decrease in average a-wave peak amplitudes for WT and Snf2h mice were observed with a 60% reduction at one month, 58% reduction at two months, 62% reduction at three months , and 63% reduction at six months of age. Similarly, b-wave peak amplitudes of Snf2h KO mice significantly declined compared to wildtype mice with a 63% reduction at one month, 61% reduction at two months, 68% reduction at three months, and 70% reduction at six months of age. Reductions were similar for both a-wave (58-63%) and b-wave (61-70%). While the b-wave is a measure of bipolar cell and Müller glia function, the elicitation of this positive deflection response is in part dependent on photoreceptor cell function which synapse and transmit the phototransduction cascade to the bipolar cells (Perlman, 1983; Salmon, 2019). The specific contributions of bipolar cells and Müller glia to the dampened b-wave response in the current *Snf2h* cKO mice used in this research project are unknown and could, in the future, be explored in a mouse model that ablates *Snf2h* in only photoreceptor cells, bipolar cells, or Müller glia. As with the OMR tests, variability was observed among biological replicates of the *Snf2h* cKO genotype with some mice displaying equivalent a-wave and-b-wave peak amplitudes to WT mice. Since some degree of visual function was detected in the *Snf2h* cKO mice using both of these tests, this suggests incomplete retinal cell loss and that the remaining cells are able to transmit the light signal. One study showed that despite the cell loss observed in a retinal degeneration model, surviving cells exhibited a normal molecular profile (Jones et al., 2003). Similarly, it is likely that

a subset of cells of each neuron population in the *Snf2h* cKO mice have normal function as the OMR and ERG response would not otherwise have been able to be evoked.

### 4.3. *Snf2h* loss results in changes to retinal structure

IHC experiments showed Snf2h protein expression throughout the retina during the critical embryonic development phase of cell fate specification. It was hypothesized that loss of *Snf2h* would inhibit retinal progenitor cell differentiation and result in structural changes to the retina. Fluorescence imaging of *Snf2h* cKO retinal tissues stained with cell-type specific antibodies showed significant loss of Müller glia and all retinal neurons except for bipolar cells. The greatest loss was observed in photoreceptor cells with at least half of these neurons missing at all ages assessed. Compared to WT mice, *Snf2h* cKO mouse retinas had 50%, 54%, 62%, and 70% less cone photoreceptors on average at one, two, three, and six months of ages, respectively. Due to difficulties with staining only rod photoreceptors, these cells were quantified by subtracting the number of cone photoreceptors from the total number of DAPI positive cells in the ONL. *Snf2h* cKO mice had 59%, 58%, 64%, and 76% less rod photoreceptors on average than WT mice average at one, two, three, and six months of ages, respectively. These results correlate with the dysfunction observed in VA and ERG a-wave peak amplitudes and demonstrate the essential function of *Snf2h* in photoreceptor development during retinal embryogenesis. Assessment of the b-wave was used to examine bipolar cell and Müller glia function. Since the b-wave relies in part on the function of photoreceptor cells and dysfunction was shown in these cells by the decreased a-wave, the subsequent dampened b-wave response was unsurprising. The Müller glia cell population was shown to be decreased in retinal histology. Interestingly, bipolar cell counts decreased in the *Snf2h* cKO mice compared to WT littermates at one month of age but not at later timepoints. Various studies have debated whether structural or functional changes are detected

first in retinal degenerative diseases. One study on glaucoma suggested that functional changes may precede observable structural changes as dead cells may still reside in their normal location. These cells lack function but contribute to the appearance of a normal structure (Gardiner et al., 2020). This may explain why no bipolar cell loss was observed despite the dysfunctional ERG response. RNA-seq experiments on bipolar cells may provide more information on transcriptomic changes.

Studies have shown that neural plasticity occurs in retinal degenerative diseases (Jones & Marc, 2005; Marc et al., 2003; Pfeiffer et al., 2020). Following photoreceptor cell death, drastic structural changes in the retina occur, which include deafferentation, relocation of other neuronal types to anomalous locations, and invasion of the RPE into the neural retina (Jones & Marc, 2005). Although this plasticity is generally considered a negative consequence of degenerative diseases due to the disruption in retinal structure and function, cellular changes that promote cell survival have also been identified. Single cell transcriptomic changes arising from modification of the epigenetic and chromatin structure were observed to occur in a *Spata7* knockout mouse model of retinal degeneration. Remaining cells initiated a stress response that enabled their prolonged survival (Dharmat et al., 2019). Retinal neurons have also been shown to display resilience to physical injury by expressing neuroprotective genes (Tran et al., 2019). Overall, the elastic nature of the retina signifies it could be amenable to conditioning stimuli which protect against injury and degeneration (Gidday, 2018). Exploring transcriptomic changes and conditions which prevent and rescue cell loss in *Snf2h* cKO may be a topic of future research.

### 4.4. Comparison between the role of *Snf2h* in the retina and the brain

The essential role of *Snf2h* in the brain has been documented in existing literature, which links *Snf2h* loss to neurodevelopment. *Snf2h*$^{f/f}$ mice crossed with the *PCP2-Cre* driver line

produced *Snf2h* cKO mice that aged into adulthood and behaved normally (Alvarez-Saavedra et al., 2014). *Pcp2* expression is restricted to Purkinje cells and examination of its mRNA levels by Northern blot are first detected at P1 (X.-M. Zhang et al., 2004). However, *Snf2h* cKO mice generated by breeding *Snf2h*$^{f/f}$ mice with a *Nestin-Cre*$^{+/-}$ driver line exhibited motor defects and had significantly smaller brains and decreased body weights (Alvarez-Saavedra et al., 2014). Cre is expressed in neural progenitors beginning at approximately E11 and continues early postnatally in these mice (Alvarez-Saavedra et al., 2014; Giusti et al., 2014). When a running wheel was added to the cage of these mice at the time of weaning at approximately P21-23, the severity of the disease phenotype of the *Snf2h* cKO mice was significantly reduced and these mice improved in motor function and had a longer lifespan. Voluntary exercise was shown to increase myelination of cerebella neurons, which induced a neuroprotective effect that resulted in enhanced neuronal function in the *Snf2h* cKO mice(Alvarez-Saavedra et al., 2016).

To investigate the role of Snf2h in the retina, the *Chx10-Cre*$^{+/-}$ *; Snf2h*$^{-/f}$ (*Snf2h* retinal cKO) mouse model was generated by Dr. Pamela Lagali, who conducted preliminary histological experiments that showed that cell loss resulted from retinal cell death rather than defects in retinal progenitor cell proliferation. Voluntary exercise was also shown to ameliorate the disease phenotype and resulted in a less dampened ERG response compared to *Snf2h* cKO mice without a cage running wheel. In contrast to the brain, neurons within the retina are unmyelinated. Myelination is found only in ganglion cells after the axons exit the retina through the lamina cribrosa (Salmon, 2019), which suggests that changes to the retina structure and function resulting from loss of *Snf2h* occur via a distinct mechanism than the one in the brain.

The changes in cell morphology observed in this study may be compared with a recent publication that examines the role of *Snf2h* in proliferation and maintenance of retinal cells using

a different Cre driver line than the one used in this thesis. The authors ablated *Snf2h* in the retina by crossing *Snf2h*$^{f/f}$ mice with *mRx-Cre* mice (Kuzelova et al., 2023). In contrast to the *Chx10-Cre* driver line which begins Cre expression at approximately E10.5, *mRx-Cre* expression begins at E9.0 in retinal progenitor cells (Klimova et al., 2013). *Snf2h*$^{f/f}$; *mRx-Cre* mice displayed significantly decreased ONL and overall retinal thickness. *Snf2h* expression was diminished across the retina throughout all cell types, although all retinal neuron populations were still able to be generated early postnatally. These histological findings align with those in this thesis. However, *in vivo* vision testing in *Snf2h* cKO mice has not previously been examined and thus, this thesis provides valuable information on the functional deficits resulting from *Snf2h* retinal loss.

### 4.5. Future directions

This study focused on the visual function tests and histological analysis. Further insights on the mechanisms underlying the reduction of retinal neurons in *Snf2h* cKO mouse could be elucidated by examining embryonic tissues during the time course of retinal development. Cre expression under the *Chx10* promoter begins at approximately E10.5 and as such, cell proliferation and death assays beginning at E10.5 to P14 once retinal cell development is complete could provide insights and confirm whether retinal cell loss is a result of cell death or deficits in progenitor cell differentiation in *Snf2h* cKO mice. Furthermore, molecular analysis including CUT&RUN and RNA-Seq could be performed to examine Snf2h binding targets and changes in the transcriptome throughout embryonic development and in juvenile and adult mice. This may lead to the identification of pathways through which Snf2h complexes regulate gene expression. Ultimately, elucidating the mechanisms underlying control of gene expression in the eye is an essential first step that furthers existing knowledge of the role of chromatin remodeller protein

dysfunction in eye diseases and has the potential to lead to the development of therapeutics that prevent and mitigate the effects of vision loss in patients.

## REFERENCES


Abdeljalil, J., Hamid, M., Abdel-Mouttalib, O., Stéphane, R., Raymond, R., Johan, A., José, S., Pierre, C., & Serge, P. (2005). The optomotor response: A robust first-line visual screening method for mice. *Vision Research*, *45*(11), 1439–1446.

Achrem, M., Szućko, I., & Kalinka, A. (2020). The epigenetic regulation of centromeres and telomeres in plants and animals. *Comparative Cytogenetics*, *14*(2), 265–311. https://doi.org/10.3897/CompCytogen.v14i2.51895

Aihara, T., Miyoshi, Y., Koyama, K., Suzuki, M., Takahashi, E., Monden, M., & Nakamura, Y. (1998). Cloning and mapping of SMARCA5 encoding hSNF2H, a novel human homologue of Drosophila ISWI. *Cytogenetic and Genome Research*, *81*(3–4), 191–193.

Alvarez-Saavedra, M., De Repentigny, Y., Lagali, P. S., Ram, E. V. R., Yan, K., Hashem, E., Ivanochko, D., Huh, M. S., Yang, D., & Mears, A. J. (2014). Snf2h-mediated chromatin organization and histone H1 dynamics govern cerebellar morphogenesis and neural maturation. *Nature Communications*, *5*(1), 1–18.

Alvarez-Saavedra, M., De Repentigny, Y., Yang, D., O'Meara, R. W., Yan, K., Hashem, L. E., Racacho, L., Ioshikhes, I., Bulman, D. E., Parks, R. J., Kothary, R., & Picketts, D. J. (2016). Voluntary Running Triggers VGF-Mediated Oligodendrogenesis to Prolong the Lifespan of Snf2h-Null Ataxic Mice. *Cell Reports*, *17*(3), 862–875. https://doi.org/10.1016/j.celrep.2016.09.030

Applebury, M. L., Antoch, M. P., Baxter, L. C., Chun, L. L. Y., Falk, J. D., Farhangfar, F., Kage, K., Krzystolik, M. G., Lyass, L. A., & Robbins, J. T. (2000). The Murine Cone Photoreceptor: A Single Cone Type Expresses Both S and M Opsins with Retinal Spatial Patterning. *Neuron*, *27*(3), 513–523. https://doi.org/10.1016/S0896-6273(00)00062-3

Asanad, S., & Karanjia, R. (2023a). Full-Field Electroretinogram. In *StatPearls*. StatPearls Publishing. http://www.ncbi.nlm.nih.gov/books/NBK557483/

Asanad, S., & Karanjia, R. (2023b). Pattern Electroretinogram. In *StatPearls*. StatPearls Publishing. http://www.ncbi.nlm.nih.gov/books/NBK560641/

Badea, T. C., & Nathans, J. (2011). Morphologies of mouse retinal ganglion cells expressing transcription factors Brn3a, Brn3b, and Brn3c: Analysis of wild type and mutant cells using genetically-directed sparse labeling. *Vision Research*, *51*(2), 269–279. https://doi.org/10.1016/j.visres.2010.08.039

Barnatan, Y., Tomsic, D., & Sztarker, J. (2019). Unidirectional Optomotor Responses and Eye Dominance in Two Species of Crabs. *Frontiers in Physiology*, *10*. https://www.frontiersin.org/articles/10.3389/fphys.2019.00586

Becker, P. B., & Workman, J. L. (2013). Nucleosome Remodeling and Epigenetics. *Cold Spring Harbor Perspectives in Biology*, *5*(9), a017905. https://doi.org/10.1101/cshperspect.a017905

Benkner, B., Mutter, M., Ecke, G., & Münch, T. A. (2013). Characterizing visual performance in mice: An objective and automated system based on the optokinetic reflex. *Behavioral Neuroscience*, *127*(5), 788.

Bennett, C. R., Bex, P. J., Bauer, C. M., & Merabet, L. B. (2019). The Assessment of Visual Function and Functional Vision. *Seminars in Pediatric Neurology*, *31*, 30–40. https://doi.org/10.1016/j.spen.2019.05.006

Boyer, L. A., Langer, M. R., Crowley, K. A., Tan, S., Denu, J. M., & Peterson, C. L. (2002). Essential role for the SANT domain in the functioning of multiple chromatin remodeling

enzymes. *Molecular Cell*, *10*(4), 935–942. https://doi.org/10.1016/s1097-2765(02)00634-2

Bramblett, D. E., Pennesi, M. E., Wu, S. M., & Tsai, M.-J. (2004). The transcription factor Bhlhb4 is required for rod bipolar cell maturation. *Neuron*, *43*(6), 779–793. https://doi.org/10.1016/j.neuron.2004.08.032

Brandt, Th., Dichgans, J., & Büchele, W. (1974). Motion habituation: Inverted self-motion perception and optokinetic after-nystagmus. *Experimental Brain Research*, *21*(4), 337–352. https://doi.org/10.1007/BF00237897

Brar, V. S. (2021). *2021-2022 Basic and Clinical Science Course, Section 02: Fundamentals and Principles of Ophthalmology*. American Academy of Ophthalmology.

Brockers, K., & Schneider, R. (2019). Histone H1, the forgotten histone. *Epigenomics*, *11*(4), 363–366. https://doi.org/10.2217/epi-2019-0018

Brown, N. L., Patel, S., Brzezinski, J., & Glaser, T. (2001). Math5 is required for retinal ganglion cell and optic nerve formation. *Development*, *128*(13), 2497–2508. https://doi.org/10.1242/dev.128.13.2497

Brown, T. A. (2002). The Human Genome. In *Genomes. 2nd edition*. Wiley-Liss. https://www.ncbi.nlm.nih.gov/books/NBK21134/

Brzezinski, J. A., IV, Lamba, D. A., & Reh, T. A. (2010). Blimp1 controls photoreceptor versus bipolar cell fate choice during retinal development. *Development*, *137*(4), 619–629. https://doi.org/10.1242/dev.043968

Brzezinski, J. A., Uoon Park, K., & Reh, T. A. (2013). Blimp1 (Prdm1) prevents re-specification of photoreceptors into retinal bipolar cells by restricting competence. *Developmental Biology*, *384*(2), 194–204. https://doi.org/10.1016/j.ydbio.2013.10.006

Casper, D. S., & Cioffi, G. A. (2019). *The Columbia Guide to Basic Elements of Eye Care: A Manual for Healthcare Professionals*. Springer.

Cassin, B. (1995). *Fundamentals for Ophthalmic Technical Personnel*. Saunders.

Cha, S., Ahn, J., Jeong, Y., Lee, Y. H., Kim, H. K., Lee, D., Yoo, Y., & Goo, Y. S. (2022). Stage-Dependent Changes of Visual Function and Electrical Response of the Retina in the rd10 Mouse Model. *Frontiers in Cellular Neuroscience*, *16*. https://www.frontiersin.org/articles/10.3389/fncel.2022.926096

Chalupa, L. M., & Williams, R. W. (2008). *Eye, Retina, and Visual System of the Mouse*. MIT Press.

Chang, B. (2013). Mouse models for studies of retinal degeneration and diseases. *Methods in Molecular Biology (Clifton, N.J.)*, *935*, 10.1007/978-1-62703-080-9_2. https://doi.org/10.1007/978-1-62703-080-9_2

Chang, B., Hurd, R., Wang, J., & Nishina, P. (2013). Survey of Common Eye Diseases in Laboratory Mouse Strains. *Investigative Ophthalmology & Visual Science*, *54*(7), 4974–4981. https://doi.org/10.1167/iovs.13-12289

Cheng, H., Khanna, H., Oh, E. C. T., Hicks, D., Mitton, K. P., & Swaroop, A. (2004). Photoreceptor-specific nuclear receptor NR2E3 functions as a transcriptional activator in rod photoreceptors. *Human Molecular Genetics*, *13*(15), 1563–1575. https://doi.org/10.1093/hmg/ddh173

Chheda, K., Wu, R., Zaback, T., & Brinks, M. V. (2019). Barriers to eye care among participants of a mobile eye clinic. *Cogent Medicine*, *6*(1), 1650693. https://doi.org/10.1080/2331205X.2019.1650693

Cho, K. S., Elizondo, L. I., & Boerkoel, C. F. (2004). Advances in chromatin remodeling and human disease. *Current Opinion in Genetics & Development*, *14*(3), 308–315. https://doi.org/10.1016/j.gde.2004.04.015

Chow, R. L., Volgyi, B., Szilard, R. K., Ng, D., McKerlie, C., Bloomfield, S. A., Birch, D. G., & McInnes, R. R. (2004). Control of late off-center cone bipolar cell differentiation and visual signaling by the homeobox gene Vsx1. *Proceedings of the National Academy of Sciences*, *101*(6), 1754–1759. https://doi.org/10.1073/pnas.0306520101

Cideciyan, A. V., Aleman, T. S., Swider, M., Schwartz, S. B., Steinberg, J. D., Brucker, A. J., Maguire, A. M., Bennett, J., Stone, E. M., & Jacobson, S. G. (2004). Mutations in ABCA4 result in accumulation of lipofuscin before slowing of the retinoid cycle: A reappraisal of the human disease sequence. *Human Molecular Genetics*, *13*(5), 525–534. https://doi.org/10.1093/hmg/ddh048

Clapier, C. R., Iwasa, J., Cairns, B. R., & Peterson, C. L. (2017). Mechanisms of action and regulation of ATP-dependent chromatin-remodelling complexes. *Nature Reviews Molecular Cell Biology*, *18*(7), Article 7. https://doi.org/10.1038/nrm.2017.26

Corona, D. F., Längst, G., Clapier, C. R., Bonte, E. J., Ferrari, S., Tamkun, J. W., & Becker, P. B. (1999). ISWI is an ATP-dependent nucleosome remodeling factor. *Molecular Cell*, *3*(2), 239–245.

Corona, D. F. V., & Tamkun, J. W. (2004). Multiple roles for ISWI in transcription, chromosome organization and DNA replication. *Biochimica et Biophysica Acta (BBA) - Gene Structure and Expression*, *1677*(1), 113–119. https://doi.org/10.1016/j.bbaexp.2003.09.018

Creel, D. J. (2019). Chapter 32—Electroretinograms. In K. H. Levin & P. Chauvel (Eds.), *Handbook of Clinical Neurology* (Vol. 160, pp. 481–493). Elsevier. https://doi.org/10.1016/B978-0-444-64032-1.00032-1

Cullen, K. E. (2016). Chapter 2—Physiology of central pathways. In J. M. Furman & T. Lempert (Eds.), *Handbook of Clinical Neurology* (Vol. 137, pp. 17–40). Elsevier. https://doi.org/10.1016/B978-0-444-63437-5.00002-9

de-Wit, L., & Wagemans, J. (2012). Visual Perception. In V. S. Ramachandran (Ed.), *Encyclopedia of Human Behavior (Second Edition)* (pp. 665–671). Academic Press. https://doi.org/10.1016/B978-0-12-375000-6.00371-2

Deiner, M. S., Kennedy, T. E., Fazeli, A., Serafini, T., Tessier-Lavigne, M., & Sretavan, D. W. (1997). Netrin-1 and DCC mediate axon guidance locally at the optic disc: Loss of function leads to optic nerve hypoplasia. *Neuron*, *19*(3), 575–589. https://doi.org/10.1016/s0896-6273(00)80373-6

Dharmat, R., Kim, S., Liu, H., Fu, S., Li, Y., & Chen, R. (2019). *Epigenetic adaptation prolongs photoreceptor survival during retinal degeneration* (p. 774950). bioRxiv. https://doi.org/10.1101/774950

Dobson, V., & Teller, D. Y. (1978). Visual acuity in human infants: A review and comparison of behavioral and electrophysiological studies. *Vision Research*, *18*(11), 1469–1483. https://doi.org/10.1016/0042-6989(78)90001-9

Dorval, K. M., Bobechko, B. P., Ahmad, K. F., & Bremner, R. (2005). Transcriptional Activity of the Paired-like Homeodomain Proteins CHX10 and VSX1 *. *Journal of Biological Chemistry*, *280*(11), 10100–10108. https://doi.org/10.1074/jbc.M412676200

Dorval, K. M., Bobechko, B. P., Fujieda, H., Chen, S., Zack, D. J., & Bremner, R. (2006). CHX10 Targets a Subset of Photoreceptor Genes *. *Journal of Biological Chemistry*, *281*(2), 744–751. https://doi.org/10.1074/jbc.M509470200

Dyer, M. A., Livesey, F. J., Cepko, C. L., & Oliver, G. (2003). Prox1 function controls progenitor cell proliferation and horizontal cell genesis in the mammalian retina. *Nature Genetics*, *34*(1), Article 1. https://doi.org/10.1038/ng1144

Fan, L., & Roberts, V. A. (2006). Complex of linker histone H5 with the nucleosome and its implications for chromatin packing. *Proceedings of the National Academy of Sciences*, *103*(22), 8384–8389. https://doi.org/10.1073/pnas.0508951103

Flaus, A., & Owen-Hughes, T. (2001). Mechanisms for ATP-dependent chromatin remodelling. *Current Opinion in Genetics & Development*, *11*(2), 148–154. https://doi.org/10.1016/S0959-437X(00)00172-6

Fletcher, E. L., Jobling, A. I., Vessey, K. A., Luu, C., Guymer, R. H., & Baird, P. N. (2011). Chapter 6—Animal Models of Retinal Disease. In K. T. Chang & K.-T. Min (Eds.), *Progress in Molecular Biology and Translational Science* (Vol. 100, pp. 211–286). Academic Press. https://doi.org/10.1016/B978-0-12-384878-9.00006-6

Fujitani, Y., Fujitani, S., Luo, H., Qiu, F., Burlison, J., Long, Q., Kawaguchi, Y., Edlund, H., MacDonald, R. J., Furukawa, T., Fujikado, T., Magnuson, M. A., Xiang, M., & Wright, C. V. E. (2006). Ptf1a determines horizontal and amacrine cell fates during mouse retinal development. *Development*, *133*(22), 4439–4450. https://doi.org/10.1242/dev.02598

Gardiner, S. K., Mansberger, S. L., & Fortune, B. (2020). Time Lag Between Functional Change and Loss of Retinal Nerve Fiber Layer in Glaucoma. *Investigative Ophthalmology & Visual Science*, *61*(13), 5. https://doi.org/10.1167/iovs.61.13.5

Ge, Y., Chen, X., Nan, N., Bard, J., Wu, F., Yergeau, D., Liu, T., Wang, J., & Mu, X. (2023). Key transcription factors influence the epigenetic landscape to regulate retinal cell differentiation. *Nucleic Acids Research*, *51*(5), 2151–2176. https://doi.org/10.1093/nar/gkad026

Geng, Y., Schery, L. A., Sharma, R., Dubra, A., Ahmad, K., Libby, R. T., & Williams, D. R. (2011). Optical properties of the mouse eye. *Biomedical Optics Express*, *2*(4), 717–738. https://doi.org/10.1364/BOE.2.000717

Gibbons, R. J., Wada, T., Fisher, C. A., Malik, N., Mitson, M. J., Steensma, D. P., Fryer, A., Goudie, D. R., Krantz, I. D., & Traeger-Synodinos, J. (2008). Mutations in the chromatin-associated protein ATRX. *Human Mutation*, *29*(6), 796–802. https://doi.org/10.1002/humu.20734

Gidday, J. M. (2018). Adaptive Plasticity in the Retina: Protection Against Acute Injury and Neurodegenerative Disease by Conditioning Stimuli. *Conditioning Medicine*, *1*(2), 85–97.

Gilbert, S. F. (2000). Formation of the Neural Tube. In *Developmental Biology. 6th edition*. Sinauer Associates. https://www.ncbi.nlm.nih.gov/books/NBK10080/

Giusti, S. A., Vercelli, C. A., Vogl, A. M., Kolarz, A. W., Pino, N. S., Deussing, J. M., & Refojo, D. (2014). Behavioral phenotyping of Nestin-Cre mice: Implications for genetic mouse models of psychiatric disorders. *Journal of Psychiatric Research*, *55*, 87–95. https://doi.org/10.1016/j.jpsychires.2014.04.002

Goodkin, F. (1980). The development of mature patterns of head-eye coordination in the human infant. *Early Human Development*, *4*(4), 373–386. https://doi.org/10.1016/0378-3782(80)90042-0

Grigoryev, S. A. (2012). Nucleosome spacing and chromatin higher-order folding. *Nucleus*, *3*(6), 493–499. https://doi.org/10.4161/nucl.22168

Grüne, T., Brzeski, J., Eberharter, A., Clapier, C. R., Corona, D. F. V., Becker, P. B., & Müller, C. W. (2003). Crystal Structure and Functional Analysis of a Nucleosome Recognition Module of the Remodeling Factor ISWI. *Molecular Cell*, *12*(2), 449–460. https://doi.org/10.1016/S1097-2765(03)00273-9

Grünert, U. (2009). Retinal Bipolar Cells. In M. D. Binder, N. Hirokawa, & U. Windhorst (Eds.), *Encyclopedia of Neuroscience* (pp. 3492–3497). Springer. https://doi.org/10.1007/978-3-540-29678-2_5102

Gutiérrez, J. L., Chandy, M., Carrozza, M. J., & Workman, J. L. (2007). Activation domains drive nucleosome eviction by SWI/SNF. *The EMBO Journal*, *26*(3), 730–740. https://doi.org/10.1038/sj.emboj.7601524

Hanna, J., David, L. A., Touahri, Y., Fleming, T., Screaton, R. A., & Schuurmans, C. (2022). Beyond Genetics: The Role of Metabolism in Photoreceptor Survival, Development and Repair. *Frontiers in Cell and Developmental Biology*, *10*. https://www.frontiersin.org/articles/10.3389/fcell.2022.887764

Harada, M., Qin, Y., Takano, H., Minamino, T., Zou, Y., Toko, H., Ohtsuka, M., Matsuura, K., Sano, M., Nishi, J., Iwanaga, K., Akazawa, H., Kunieda, T., Zhu, W., Hasegawa, H., Kunisada, K., Nagai, T., Nakaya, H., Yamauchi-Takihara, K., & Komuro, I. (2005). G-CSF prevents cardiac remodeling after myocardial infarction by activating the Jak-Stat pathway in cardiomyocytes. *Nature Medicine*, *11*(3), 305–311. https://doi.org/10.1038/nm1199

Harrer, N., Schindler, C. E. M., Bruetzel, L. K., Forné, I., Ludwigsen, J., Imhof, A., Zacharias, M., Lipfert, J., & Mueller-Planitz, F. (2018). Structural Architecture of the Nucleosome Remodeler ISWI Determined from Cross-Linking, Mass Spectrometry, SAXS, and Modeling. *Structure (London, England: 1993)*, *26*(2), 282-294.e6. https://doi.org/10.1016/j.str.2017.12.015

Heavner, W., & Pevny, L. (2012). Eye Development and Retinogenesis. *Cold Spring Harbor Perspectives in Biology*, *4*(12), a008391. https://doi.org/10.1101/cshperspect.a008391

Hendrich, B., & Bickmore, W. (2001). Human diseases with underlying defects in chromatin structure and modification. *Human Molecular Genetics*, *10*(20), 2233–2242. https://doi.org/10.1093/hmg/10.20.2233

Hergeth, S. P., & Schneider, R. (2015). The H1 linker histones: Multifunctional proteins beyond the nucleosomal core particle. *EMBO Reports*, *16*(11), 1439–1453. https://doi.org/10.15252/embr.201540749

Hoang, Q. V., Linsenmeier, R. A., Chung, C. K., & Curcio, C. A. (2002). Photoreceptor inner segments in monkey and human retina: Mitochondrial density, optics, and regional variation. *Visual Neuroscience*, *19*(4), 395–407. https://doi.org/10.1017/s0952523802194028

Hood, D. C. (2000). Assessing retinal function with the multifocal technique. *Progress in Retinal and Eye Research*, *19*(5), 607–646. https://doi.org/10.1016/S1350-9462(00)00013-6

Hota, S. K., Bhardwaj, S. K., Deindl, S., Lin, Y., Zhuang, X., & Bartholomew, B. (2013). Nucleosome mobilization by ISW2 requires the concerted action of the ATPase and SLIDE domains. *Nature Structural & Molecular Biology*, *20*(2), Article 2. https://doi.org/10.1038/nsmb.2486

Huang, C., Sloan, E. A., & Boerkoel, C. F. (2003). Chromatin remodeling and human disease. *Current Opinion in Genetics & Development*, *13*(3), 246–252. https://doi.org/10.1016/S0959-437X(03)00054-6

Huberman, A. D., & Niell, C. M. (2011). What can mice tell us about how vision works? *Trends in Neurosciences*, *34*(9), 464–473. https://doi.org/10.1016/j.tins.2011.07.002

Inoue, T., Hojo, M., Bessho, Y., Tano, Y., Lee, J. E., & Kageyama, R. (2002). Math3 and NeuroD regulate amacrine cell fate specification in the retina. *Development*, *129*(4), 831–842. https://doi.org/10.1242/dev.129.4.831

International Human Genome Sequencing Consortium. (2004). Finishing the euchromatic sequence of the human genome. *Nature*, *431*(7011), Article 7011. https://doi.org/10.1038/nature03001

Jeon, C.-J., Strettoi, E., & Masland, R. H. (1998). The major cell populations of the mouse retina. *Journal of Neuroscience*, *18*(21), 8936–8946.

Jiang, Y., Ding, Q., Xie, X., Libby, R. T., Lefebvre, V., & Gan, L. (2013). Transcription Factors SOX4 and SOX11 Function Redundantly to Regulate the Development of Mouse Retinal Ganglion Cells *. *Journal of Biological Chemistry*, *288*(25), 18429–18438. https://doi.org/10.1074/jbc.M113.478503

Jones, B. W., & Marc, R. E. (2005). Retinal remodeling during retinal degeneration. *Experimental Eye Research*, *81*(2), 123–137. https://doi.org/10.1016/j.exer.2005.03.006

Jones, B. W., Watt, C. B., Frederick, J. M., Baehr, W., Chen, C.-K., Levine, E. M., Milam, A. H., Lavail, M. M., & Marc, R. E. (2003). Retinal remodeling triggered by photoreceptor degenerations. *Journal of Comparative Neurology*, *464*(1), 1–16. https://doi.org/10.1002/cne.10703

Katoh, K., Omori, Y., Onishi, A., Sato, S., Kondo, M., & Furukawa, T. (2010). Blimp1 Suppresses Chx10 Expression in Differentiating Retinal Photoreceptor Precursors to Ensure Proper Photoreceptor Development. *Journal of Neuroscience*, *30*(19), 6515–6526. https://doi.org/10.1523/JNEUROSCI.0771-10.2010

Kiser, A. K., Mladenovich, D., Eshraghi, F., Bourdeau, D., & Dagnelie, G. (2005). Reliability and Consistency of Visual Acuity and Contrast Sensitivity Measures in Advanced Eye Disease. *Optometry and Vision Science*, *82*(11), 946–954. https://doi.org/10.1097/01.opx.0000187863.12609.7b

Klimova, L., Lachova, J., Machon, O., Sedlacek, R., & Kozmik, Z. (2013). Generation of mRx-Cre Transgenic Mouse Line for Efficient Conditional Gene Deletion in Early Retinal Progenitors. *PLOS ONE*, *8*(5), e63029. https://doi.org/10.1371/journal.pone.0063029

Klinker, H., Mueller-Planitz, F., Yang, R., Forné, I., Liu, C.-F., Nordenskiöld, L., & Becker, P. B. (2014). ISWI Remodelling of Physiological Chromatin Fibres Acetylated at Lysine 16 of Histone H4. *PLOS ONE*, *9*(2), e88411. https://doi.org/10.1371/journal.pone.0088411

Kocaoglu, O. P., Liu, Z., Zhang, F., Kurokawa, K., Jonnal, R. S., & Miller, D. T. (2016). Photoreceptor disc shedding in the living human eye. *Biomedical Optics Express*, *7*(11), 4554–4568. https://doi.org/10.1364/BOE.7.004554

Kokavec, J., Majumdar, R., Kapalova, M., Curik, N., Savvulidi, F., Necas, E., Skoultchi, A. I., & Stopka, T. (2010). *ISWI Chromatin Remodeling ATPase Smarca5 (Snf2h) Is Required for Murine Erythroid Development and Globin Gene Regulation*. American Society of Hematology.

Kretschmer, F., Sajgo, S., Kretschmer, V., & Badea, T. C. (2015). A system to measure the Optokinetic and Optomotor response in mice. *Journal of Neuroscience Methods*, *256*, 91–105. https://doi.org/10.1016/j.jneumeth.2015.08.007

Kretschmer, F., Tariq, M., Chatila, W., Wu, B., & Badea, T. C. (2017). Comparison of optomotor and optokinetic reflexes in mice. *Journal of Neurophysiology*, *118*(1), 300–316. https://doi.org/10.1152/jn.00055.2017

Kuzelova, A., Dupacova, N., Antosova, B., Sunny, S. S., Kozmik, Z., Paces, J., Skoultchi, A. I., Stopka, T., & Kozmik, Z. (2023). Chromatin Remodeling Enzyme Snf2h Is Essential for Retinal Cell Proliferation and Photoreceptor Maintenance. *Cells*, *12*(7), Article 7. https://doi.org/10.3390/cells12071035

LaVail, M. M. (1976). Rod Outer Segment Disk Shedding in Rat Retina: Relationship to Cyclic Lighting. *Science*, *194*(4269), 1071–1074. https://doi.org/10.1126/science.982063

Lazzaro, M. A., & Picketts, D. J. (2001). Cloning and characterization of the murine Imitation Switch (ISWI) genes: Differential expression patterns suggest distinct developmental roles for Snf2h and Snf2l. *Journal of Neurochemistry*, *77*(4), 1145–1156.

Ledford, J. K., & Hoffman, J. (2005). *Quick Reference Dictionary of Eyecare Terminology*. SLACK.

Leinonen, H., & Tanila, H. (2018). Vision in laboratory rodents—Tools to measure it and implications for behavioral research. *Behavioural Brain Research*, *352*, 172–182. https://doi.org/10.1016/j.bbr.2017.07.040

Levenson, J. H., & Kozarsky, A. (1990). *Visual Acuit*. https://www.ncbi.nlm.nih.gov/books/NBK219

Levin, L. A., Nilsson, S. F. E., Hoeve, J. V., Wu, S., Kaufman, P. L., & Alm, A. (2011). *Adler's Physiology of the Eye: Expert Consult - Online and Print*. Elsevier Health Sciences.

Levine, M. W. (2011). VISION | Inner Retina and Ganglion Cells. In A. P. Farrell (Ed.), *Encyclopedia of Fish Physiology* (pp. 123–130). Academic Press. https://doi.org/10.1016/B978-0-12-374553-8.00092-7

Li, D., Wang, Q., Gong, N. N., Kurolap, A., Feldman, H. B., Boy, N., Brugger, M., Grand, K., McWalter, K., & Sacoto, M. J. G. (2021). Pathogenic variants in SMARCA5, a chromatin remodeler, cause a range of syndromic neurodevelopmental features. *Science Advances*, *7*(20), eabf2066.

Li, S., Mo, Z., Yang, X., Price, S. M., Shen, M. M., & Xiang, M. (2004). Foxn4 Controls the Genesis of Amacrine and Horizontal Cells by Retinal Progenitors. *Neuron*, *43*(6), 795–807. https://doi.org/10.1016/j.neuron.2004.08.041

Lieleg, C., Ketterer, P., Nuebler, J., Ludwigsen, J., Gerland, U., Dietz, H., Mueller-Planitz, F., & Korber, P. (2015). Nucleosome Spacing Generated by ISWI and CHD1 Remodelers Is Constant Regardless of Nucleosome Density. *Molecular and Cellular Biology*, *35*(9), 1588–1605. https://doi.org/10.1128/MCB.01070-14

Livne-bar, I., Pacal, M., Cheung, M. C., Hankin, M., Trogadis, J., Chen, D., Dorval, K. M., & Bremner, R. (2006). Chx10 is required to block photoreceptor differentiation but is dispensable for progenitor proliferation in the postnatal retina. *Proceedings of the National Academy of Sciences*, *103*(13), 4988–4993. https://doi.org/10.1073/pnas.0600083103

Madisen, L., Zwingman, T. A., Sunkin, S. M., Oh, S. W., Zariwala, H. A., Gu, H., Ng, L. L., Palmiter, R. D., Hawrylycz, M. J., Jones, A. R., Lein, E. S., & Zeng, H. (2010). A robust

and high-throughput Cre reporting and characterization system for the whole mouse brain. *Nature Neuroscience*, *13*(1), 133–140. https://doi.org/10.1038/nn.2467

Makałowski, W., Zhang, J., & Boguski, M. S. (1996). Comparative analysis of 1196 orthologous mouse and human full-length mRNA and protein sequences. *Genome Research*, *6*(9), 846–857. https://doi.org/10.1101/gr.6.9.846

Manelyte, L., Längst, G., Manelyte, L., & Längst, G. (2013). Chromatin Remodelers and Their Way of Action. In *Chromatin Remodelling*. IntechOpen. https://doi.org/10.5772/55683

Marc, R. E., Jones, B. W., Watt, C. B., & Strettoi, E. (2003). Neural remodeling in retinal degeneration. *Progress in Retinal and Eye Research*, *22*(5), 607–655. https://doi.org/10.1016/S1350-9462(03)00039-9

Marieb, E. N., & Hoehn, K. N. (2012). *Human Anatomy & Physiology*. Pearson Higher Ed.

Mears, A. J., Kondo, M., Swain, P. K., Takada, Y., Bush, R. A., Saunders, T. L., Sieving, P. A., & Swaroop, A. (2001). Nrl is required for rod photoreceptor development. *Nature Genetics*, *29*(4), Article 4. https://doi.org/10.1038/ng774

Mellor, J. (2006). Imitation Switch Complexes. In S. L. Berger, O. Nakanishi, & B. Haendler (Eds.), *The Histone Code and Beyond* (pp. 61–87). Springer. https://doi.org/10.1007/3-540-37633-X_4

Mirabella, A. C., Foster, B. M., & Bartke, T. (2016). Chromatin deregulation in disease. *Chromosoma*, *125*(1), 75–93. https://doi.org/10.1007/s00412-015-0530-0

Morrison, O., & Thakur, J. (2021). Molecular Complexes at Euchromatin, Heterochromatin and Centromeric Chromatin. *International Journal of Molecular Sciences*, *22*(13), 6922. https://doi.org/10.3390/ijms22136922

Nagy, A. (2000). Cre recombinase: The universal reagent for genome tailoring. *Genesis*, *26*(2), 99–109. https://doi.org/10.1002/(SICI)1526-968X(200002)26:2<99::AID-GENE1>3.0.CO;2-B

Naylor, A., Hopkins, A., Hudson, N., & Campbell, M. (2019). Tight Junctions of the Outer Blood Retina Barrier. *International Journal of Molecular Sciences*, *21*(1), 211. https://doi.org/10.3390/ijms21010211

Nelson, R., & Connaughton, V. (1995). Bipolar Cell Pathways in the Vertebrate Retina. In H. Kolb, E. Fernandez, & R. Nelson (Eds.), *Webvision: The Organization of the Retina and Visual System*. University of Utah Health Sciences Center. http://www.ncbi.nlm.nih.gov/books/NBK11521/

Nikonov, S. S., Kholodenko, R., Lem, J., & Pugh Jr, E. N. (2006). Physiological features of the S-and M-cone photoreceptors of wild-type mice from single-cell recordings. *The Journal of General Physiology*, *127*(4), 359–374.

Ohsawa, R., & Kageyama, R. (2008). Regulation of retinal cell fate specification by multiple transcription factors. *Brain Research*, *1192*, 90–98. https://doi.org/10.1016/j.brainres.2007.04.014

Okunuki, Y., Mukai, R., Nakao, T., Tabor, S. J., Butovsky, O., Dana, R., Ksander, B. R., & Connor, K. M. (2019). Retinal microglia initiate neuroinflammation in ocular autoimmunity. *Proceedings of the National Academy of Sciences*, *116*(20), 9989–9998. https://doi.org/10.1073/pnas.1820387116

Olmsted, J. M. D. (1944). The role of the autonomic nervous system in accommodation for far and near vision. *The Journal of Nervous and Mental Disease*, *99*(5), 794.

Pei, Y. F., & Rhodin, J. a. G. (1970). The prenatal development of the mouse eye. *The Anatomical Record*, *168*(1), 105–125. https://doi.org/10.1002/ar.1091680109

Peng, G.-H., Ahmad, O., Ahmad, F., Liu, J., & Chen, S. (2005). The photoreceptor-specific nuclear receptor Nr2e3 interacts with Crx and exerts opposing effects on the transcription of rod versus cone genes. *Human Molecular Genetics*, *14*(6), 747–764. https://doi.org/10.1093/hmg/ddi070

Pennesi, M. E., Bramblett, D. E., Cho, J.-H., Tsai, M.-J., & Wu, S. M. (2006). A Role for bHLH Transcription Factors in Retinal Degeneration and Dysfunction. In J. G. Hollyfield, R. E. Anderson, & M. M. LaVail (Eds.), *Retinal Degenerative Diseases* (pp. 155–161). Springer US. https://doi.org/10.1007/0-387-32442-9_23

Perlman, I. (1983). Relationship between the amplitudes of the b wave and the a wave as a useful index for evaluating the electroretinogram. *British Journal of Ophthalmology*, *67*(7), 443–448. https://doi.org/10.1136/bjo.67.7.443

Peters, S., & Schraermeyer, U. (2001). [Characteristics and functions of melanin in retinal pigment epithelium]. *Der Ophthalmologe: Zeitschrift Der Deutschen Ophthalmologischen Gesellschaft*, *98*(12), 1181–1185. https://doi.org/10.1007/s003470170011

Pfeiffer, R. L., Marc, R. E., & Jones, B. W. (2020). Persistent remodeling and neurodegeneration in late-stage retinal degeneration. *Progress in Retinal and Eye Research*, *74*, 100771. https://doi.org/10.1016/j.preteyeres.2019.07.004

Pinto, L. H., & Enroth-Cugell, C. (2000). Tests of the mouse visual system. *Mammalian Genome*, *11*(7), 531–536. https://doi.org/10.1007/s003350010102

Priyadharscini, R. A., & Sabarinath, T. (2013). Barr bodies in sex determination. *Journal of Forensic Dental Sciences*, *5*(1), 64–67.

Prusky, G. T., Alam, N. M., Beekman, S., & Douglas, R. M. (2004). Rapid Quantification of Adult and Developing Mouse Spatial Vision Using a Virtual Optomotor System. *Investigative Ophthalmology & Visual Science*, *45*(12), 4611–4616. https://doi.org/10.1167/iovs.04-0541

Reese, B. E. (2011). Development of the retina and optic pathway. *Vision Research*, *51*(7), 613–632. https://doi.org/10.1016/j.visres.2010.07.010

Reichenbach, A., & Bringmann, A. (2010). Müller Cells in the Healthy Retina. In A. Reichenbach & A. Bringmann (Eds.), *Müller Cells in the Healthy and Diseased Retina* (pp. 35–214). Springer. https://doi.org/10.1007/978-1-4419-1672-3_2

Reichenbach, A., & Bringmann, A. (2020). Glia of the human retina. *Glia*, *68*(4), 768–796. https://doi.org/10.1002/glia.23727

Remington, L. A. (2012). *Clinical Anatomy and Physiology of the Visual System*. Elsevier/Butterworth-Heinemann.

Rheaume, B. A., Jereen, A., Bolisetty, M., Sajid, M. S., Yang, Y., Renna, K., Sun, L., Robson, P., & Trakhtenberg, E. F. (2018). Single cell transcriptome profiling of retinal ganglion cells identifies cellular subtypes. *Nature Communications*, *9*(1), Article 1. https://doi.org/10.1038/s41467-018-05134-3

Rieke, F., & Baylor, D. A. (1998). Single-photon detection by rod cells of the retina. *Reviews of Modern Physics*, *70*(3), 1027–1036. https://doi.org/10.1103/RevModPhys.70.1027

Rippe, K., Schrader, A., Riede, P., Strohner, R., Lehmann, E., & Längst, G. (2007). DNA sequence- and conformation-directed positioning of nucleosomes by chromatin-

remodeling complexes. *Proceedings of the National Academy of Sciences*, *104*(40), 15635–15640. https://doi.org/10.1073/pnas.0702430104

Rossant, J., & Tam, P. P. L. (2002). *Mouse Development: Patterning, Morphogenesis, and Organogenesis*. Gulf Professional Publishing.

Rowan, S., & Cepko, C. L. (2004). Genetic analysis of the homeodomain transcription factor Chx10 in the retina using a novel multifunctional BAC transgenic mouse reporter. *Developmental Biology*, *271*(2), 388–402.

Salmon, J. F. (2019). *Kanski's Clinical Ophthalmology E-Book: A Systematic Approach*. Elsevier Health Sciences.

Samanta, A., Mauntana, S., Barsi, Z., Yarlagadda, B., & Nelson, P. C. (2023). Is your vision blurry? A systematic review of home-based visual acuity for telemedicine. *Journal of Telemedicine and Telecare*, *29*(2), 81–90. https://doi.org/10.1177/1357633X20970398

Selhorst, J. B., Madge, G., & Ghatak, N. R. (1984). The neuropathology of the Holmes-Adie syndrome. *Annals of Neurology*, *16*(1), 138–138.

Shi, C., Yuan, X., Chang, K., Cho, K.-S., Xie, X. S., Chen, D. F., & Luo, G. (2018). Optimization of Optomotor Response-based Visual Function Assessment in Mice. *Scientific Reports*, *8*, 9708. https://doi.org/10.1038/s41598-018-27329-w

Smith, R. S., John, S. W. M., Nishina, P. M., & Sundberg, J. P. (2001). *Systematic Evaluation of the Mouse Eye: Anatomy, Pathology, and Biomethods*. CRC Press.

Spencer, W. J., Lewis, T. R., Pearring, J. N., & Arshavsky, V. Y. (2020). Photoreceptor Discs: Built Like Ectosomes. *Trends in Cell Biology*, *30*(11), 904–915. https://doi.org/10.1016/j.tcb.2020.08.005

Stone, J., Maslim, J., Valter-Kocsi, K., Kyle Mervin, Bowers, F., Chu, Y., Barnett, N., Provis, J., Lewis, G., Fisher, S. K., Bisti, S., Gargini, C., Cervetto, L., Merin, S., & Pe'er, J. (1999). Mechanisms of photoreceptor death and survival in mammalian retina. *Progress in Retinal and Eye Research*, *18*(6), 689–735. https://doi.org/10.1016/S1350-9462(98)00032-9

Stopka, T., & Skoultchi, A. I. (2003). The ISWI ATPase Snf2h is required for early mouse development. *Proceedings of the National Academy of Sciences*, *100*(24), 14097–14102.

Strahl, B. D., & Allis, C. D. (2000). The language of covalent histone modifications. *Nature*, *403*(6765), Article 6765. https://doi.org/10.1038/47412

Struhl, K. (1998). Histone acetylation and transcriptional regulatory mechanisms. *Genes & Development*, *12*(5), 599–606.

Sun, H. B., Shen, J., & Yokota, H. (2000). Size-Dependent Positioning of Human Chromosomes in Interphase Nuclei. *Biophysical Journal*, *79*(1), 184–190. https://doi.org/10.1016/S0006-3495(00)76282-5

Sundin, O. H. (2005). The Mouse's Eye and *Mfrp*: Not Quite Human. *Ophthalmic Genetics*, *26*(4), 153–155. https://doi.org/10.1080/13816810500374359

Szél, Á., Röhlich, P., Caffé, A. R., & van Veen, T. (1996). Distribution of cone photoreceptors in the mammalian retina. *Microscopy Research and Technique*, *35*(6), 445–462. https://doi.org/10.1002/(SICI)1097-0029(19961215)35:6<445::AID-JEMT4>3.0.CO;2-H

*The Senses: A Comprehensive Reference : Vision*. (2008). Academic.

Tran, N. M., Shekhar, K., Whitney, I. E., Jacobi, A., Benhar, I., Hong, G., Yan, W., Adiconis, X., Arnold, M. E., Lee, J. M., Levin, J. Z., Lin, D., Wang, C., Lieber, C. M., Regev, A., He, Z., & Sanes, J. R. (2019). Single-Cell Profiles of Retinal Ganglion Cells Differing in

Resilience to Injury Reveal Neuroprotective Genes. *Neuron*, *104*(6), 1039-1055.e12. https://doi.org/10.1016/j.neuron.2019.11.006

Truett, G. e., Heeger, P., Mynatt, R. l., Truett, A. a., Walker, J. a., & Warman, M. l. (2000). Preparation of PCR-Quality Mouse Genomic DNA with Hot Sodium Hydroxide and Tris (HotSHOT). *BioTechniques*, *29*(1), 52–54. https://doi.org/10.2144/00291bm09

Tsukiyama, T., Daniel, C., Tamkun, J., & Wu, C. (1995). ISWI, a member of the SWI2/SNF2 ATPase family, encodes the 140 kDa subunit of the nucleosome remodeling factor. *Cell*, *83*(6), 1021–1026.

Tsukiyama, T., & Wu, C. (1995). Purification and properties of an ATP-dependent nucleosome remodeling factor. *Cell*, *83*(6), 1011–1020.

van der Zouwen, C. I., & Ryczko, D. (2020). Motor Control: Swim Harder, Faster, Stronger. *Current Biology: CB*, *30*(5), R229–R232. https://doi.org/10.1016/j.cub.2020.01.008

Vandamme, T. F. (2014). Use of rodents as models of human diseases. *Journal of Pharmacy & Bioallied Sciences*, *6*(1), 2. https://doi.org/10.4103/0975-7406.124301

Veselov, A. E., Kazakov, R. V., Sysoyeva, M. I., & Bahmet, I. N. (1998). Ontogenesis of rheotactic and optomotor responses of juvenile Atlantic salmon. *Aquaculture*, *168*(1), 17–26. https://doi.org/10.1016/S0044-8486(98)00362-7

Vissers, L. E. L. M., van Ravenswaaij, C. M. A., Admiraal, R., Hurst, J. A., de Vries, B. B. A., Janssen, I. M., van der Vliet, W. A., Huys, E. H. L. P. G., de Jong, P. J., Hamel, B. C. J., Schoenmakers, E. F. P. M., Brunner, H. G., Veltman, J. A., & van Kessel, A. G. (2004). Mutations in a new member of the chromodomain gene family cause CHARGE syndrome. *Nature Genetics*, *36*(9), Article 9. https://doi.org/10.1038/ng1407

Wang, M., Ma, W., Zhao, L., Fariss, R. N., & Wong, W. T. (2011). Adaptive Müller cell responses to microglial activation mediate neuroprotection and coordinate inflammation in the retina. *Journal of Neuroinflammation*, *8*(1), 173. https://doi.org/10.1186/1742-2094-8-173

Wang, S. W., Gan, L., Martin, S. E., & Klein, W. H. (2000). Abnormal Polarization and Axon Outgrowth in Retinal Ganglion Cells Lacking the POU-Domain Transcription Factor Brn-3b. *Molecular and Cellular Neuroscience*, *16*(2), 141–156. https://doi.org/10.1006/mcne.2000.0860

Wang, S. W., Kim, B. S., Ding, K., Wang, H., Sun, D., Johnson, R. L., Klein, W. H., & Gan, L. (2001). Requirement for math5 in the development of retinal ganglion cells. *Genes & Development*, *15*(1), 24–29. https://doi.org/10.1101/gad.855301

Watts, G. (2007). Nobel prize is awarded for work leading to "knockout mouse." *BMJ : British Medical Journal*, *335*(7623), 740. https://doi.org/10.1136/bmj.39364.367361.DB

Wensel, T. G., Potter, V. L., Moye, A., Zhang, Z., & Robichaux, M. A. (2021). Structure and dynamics of photoreceptor sensory cilia. *Pflügers Archiv - European Journal of Physiology*, *473*(9), 1517–1537. https://doi.org/10.1007/s00424-021-02564-9

Wolffe, A. P. (2012). *Chromatin: Structure and Function*. Academic Press.

Wolffe, A. P., & Hayes, J. J. (1999). Chromatin disruption and modification. *Nucleic Acids Research*, *27*(3), 711–720. https://doi.org/10.1093/nar/27.3.711

Wu, S., Zheng, Y., Xu, C., Fu, J., Xiong, F., & Yang, F. (2022). A Novel Mutation in ATRX Causes Alpha-Thalassemia X-Linked Intellectual Disability Syndrome in a Han Chinese Family. *Frontiers in Pediatrics*, *9*. https://www.frontiersin.org/articles/10.3389/fped.2021.811812

Xiao, J., Adil, M. Y., Chang, K., Yu, Z., Yang, L., Utheim, T. P., Chen, D. F., & Cho, K.-S. (2019). Visual contrast sensitivity correlates to the retinal degeneration in rhodopsin knockout mice. *Investigative Ophthalmology & Visual Science*, *60*(13), 4196–4204.

Yadon, A. N., & Tsukiyama, T. (2011). SnapShot: Chromatin remodeling: ISWI. *Cell*, *144*(3), 453-453.e1. https://doi.org/10.1016/j.cell.2011.01.019

Yan, R.-T., Ma, W., Liang, L., & Wang, S.-Z. (2005). BHLH Genes and Retinal Cell Fate Specification. *Molecular Neurobiology*, *32*(2), 157–171.

Yip, D. J., Corcoran, C. P., Alvarez-Saavedra, M., DeMaria, A., Rennick, S., Mears, A. J., Rudnicki, M. A., Messier, C., & Picketts, D. J. (2012). Snf2l regulates Foxg1-dependent progenitor cell expansion in the developing brain. *Developmental Cell*, *22*(4), 871–878. https://doi.org/10.1016/j.devcel.2012.01.020

Young, R. W. (1971). The renewal of rod and cone outer segments in the rhesus monkey. *Journal of Cell Biology*, *49*(2), 303–318. https://doi.org/10.1083/jcb.49.2.303

Young, R. W., & Bok, D. (1969). Participation of the retinal pigment epithelium in the rod outer segment renewal process. *Journal of Cell Biology*, *42*(2), 392–403. https://doi.org/10.1083/jcb.42.2.392

Zhang, X., Serb, J., & Greenlee, M. H. (2011). Mouse Retinal Development: A Dark Horse Model for Systems Biology Research. *Bioinformatics and Biology Insights*, *5*, 99–113. https://doi.org/10.4137/BBI.S6930

Zhang, X.-M., Ng, A. H.-L., Tanner, J. A., Wu, W.-T., Copeland, N. G., Jenkins, N. A., & Huang, J.-D. (2004). Highly restricted expression of Cre recombinase in cerebellar Purkinje cells. *Genesis (New York, N.Y.: 2000)*, *40*(1), 45–51. https://doi.org/10.1002/gene.20062